Polarimetrie compton

TAMAZIRT juba (IJCLab Orsay)

Polarimétrie pour FCC-ee

Energie du centre de mass au pole du Z^0
soit 45.6 Gev par faisceau

Première phase : sonder le secteur électrofaible avec des processus couplant les bosons de jauge au Higgs avec une précision sur les paramètres électrofaibles <1ppm

→ Calibration de l'énergie au centre de masse en temps réel en utilisant la dépolarisation résonnante: incertitude < Mev sur l'énergie

Dépolarisation résonnante :

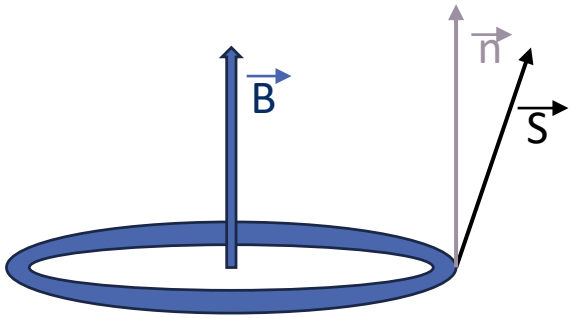

tune of closed orbit:
$k = a\gamma + Q^y m^y + Q^x m^x + Q^L m^L$

spin tune — transverse planes — Longitudinal plane (synchrotron)

La polarisation des électrons précesse Grace au champ magnétique oscillant de l'anneau de stockage.

Quand la fréquence de précession des électron et des spins sont en résonnance induit une ***Dépolarisation*** du faisceau

polarimètre Compton

- Calibration de l'énergie au centre de masse à l'aide de la dépolarisation résonante Monitoring de
- l'énergie du faisceau à partir de la géométrie dans le plan de mesure → utile lorsque les paquets pilotes ne peuvent pas être polarisés ?

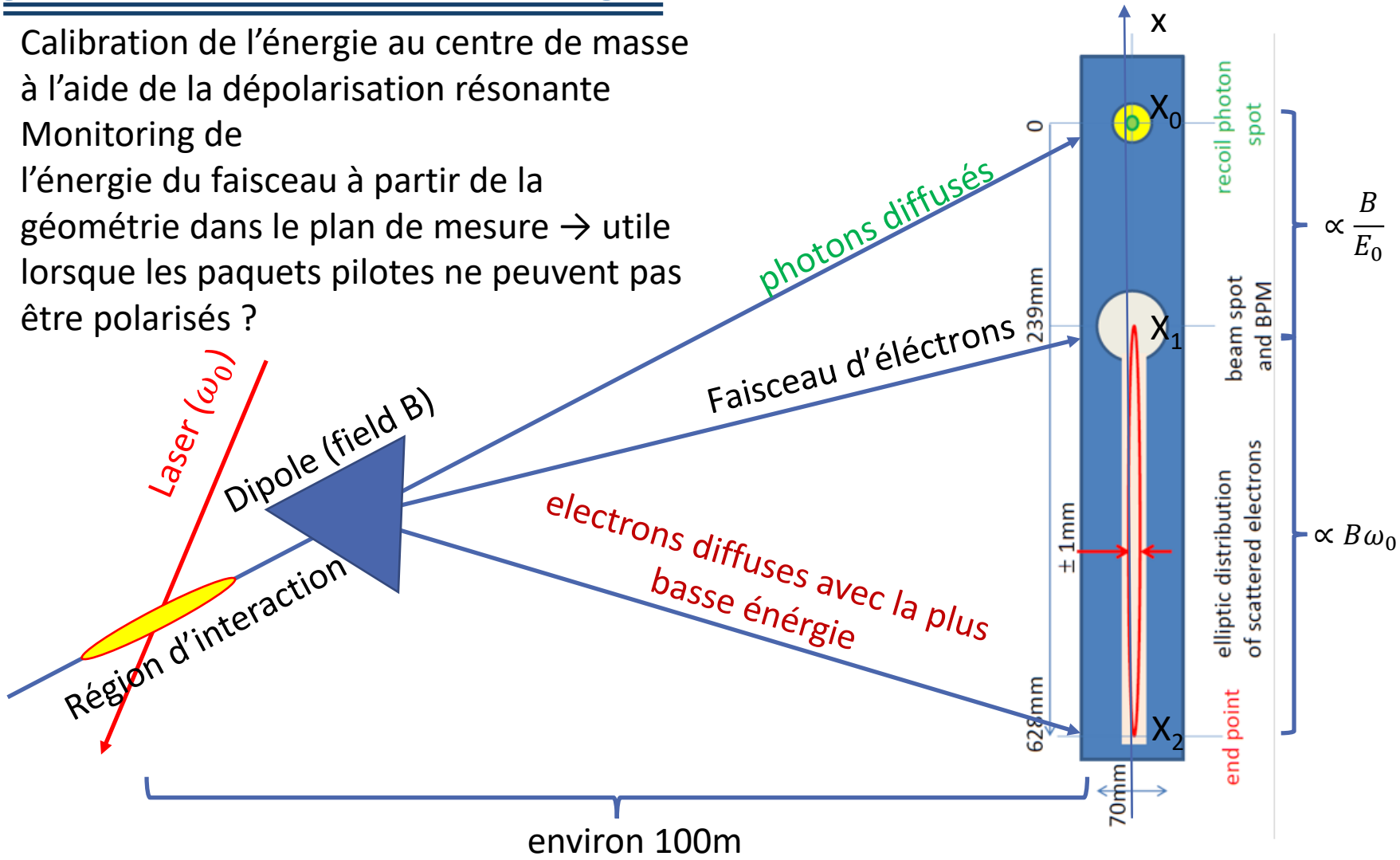

Nouveau concept (N. Yu Muchnoi) pour mesurer tous les parametres de polarisation → polarimetre 3D

Blondel et al., arXiv:1909.12245; Muchnoi, INST 17 P10014 (2022)

Section efficace differentielle

Outre la conception et la validation réalistes du détecteur et du système, une extraction précise des paramètres est nécessaire

Les électrons sont situés sur une surface ellipsoïdale dont la paramétrisation peut être transformée en un disque unité, sur lequel l'expression de la section efficace différentielle est plus commode

$$\frac{1}{r_e^2}\frac{d\sigma_0}{dxdy}\bigg|_\pm = \frac{1+(1+u_\pm)^2-(1+u_\pm)(1-\Delta_\pm^2)}{2(1+u_\pm)^3\sqrt{1-x^2-y^2}},$$

$$\frac{1}{r_e^2}\frac{d\sigma_{\xi_1}}{dxdy}\bigg|_\pm = \xi_1\frac{\delta_\pm^2-y^2}{2(1+u_\pm)^2\sqrt{1-x^2-y^2}},$$

$$\frac{1}{r_e^2}\frac{d\sigma_{\xi_2}}{dxdy}\bigg|_\pm = \xi_2\frac{-\delta_\pm y}{(1+u_\pm)^2\sqrt{1-x^2-y^2}},$$

$$\frac{1}{r_e^2}\frac{d\sigma_x}{dxdy}\bigg|_\pm = \xi_3\zeta_x\frac{-u_\pm\delta_\pm}{2(1+u_\pm)^3\sqrt{1-x^2-y^2}},$$

$$\frac{1}{r_e^2}\frac{d\sigma_y}{dxdy}\bigg|_\pm = \xi_3\zeta_y\frac{u_\pm y}{2(1+u_\pm)^3\sqrt{1-x^2-y^2}},$$

$$\frac{1}{r_e^2}\frac{d\sigma_z}{dxdy}\bigg|_\pm = \xi_3\zeta_z\frac{-u_\pm(u_\pm+2)\Delta_\pm}{2(1+u_\pm)^3\sqrt{1-x^2-y^2}}.$$

NB: $1/\sqrt{1-x^2-y^2}$ devient >> aux limites du cercle

Example electron distribution

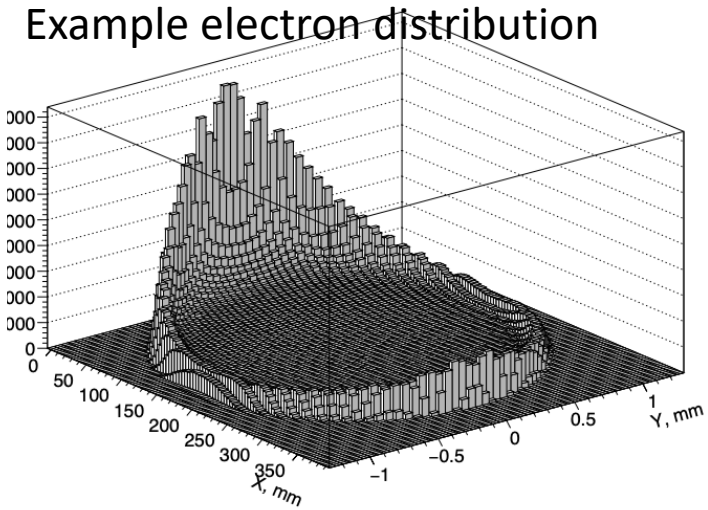

$u_\pm$, $\Delta_\pm$ et $\delta_\pm$ sont des fonctions de (x, y)

$\delta_\pm$ est negligeable

$\zeta_{x,y,z}$: parametres de polarisation du faisceau d'e$^-$

$\xi_{1,2,3}$: parametres de stokes

NB: $\xi_3 = \pm 1 \Leftrightarrow$ polarisation circulaire gauche/droite

Muchnoi, INST 17 P10014 (2022)

Obtenu en 30s pour un seul bunch

Resultat– fit des Distributions

$$\frac{d\sigma}{dud\varphi} = \frac{d\sigma_0}{dud\varphi} + \xi_1 \frac{d\sigma_1}{dud\varphi} + \xi_2 \frac{d\sigma_2}{dud\varphi} + \xi_3 \left(\zeta_x \frac{d\sigma_x}{dud\varphi} + \zeta_y \frac{d\sigma_y}{dud\varphi} + \zeta_z \frac{d\sigma_z}{dud\varphi} \right)$$

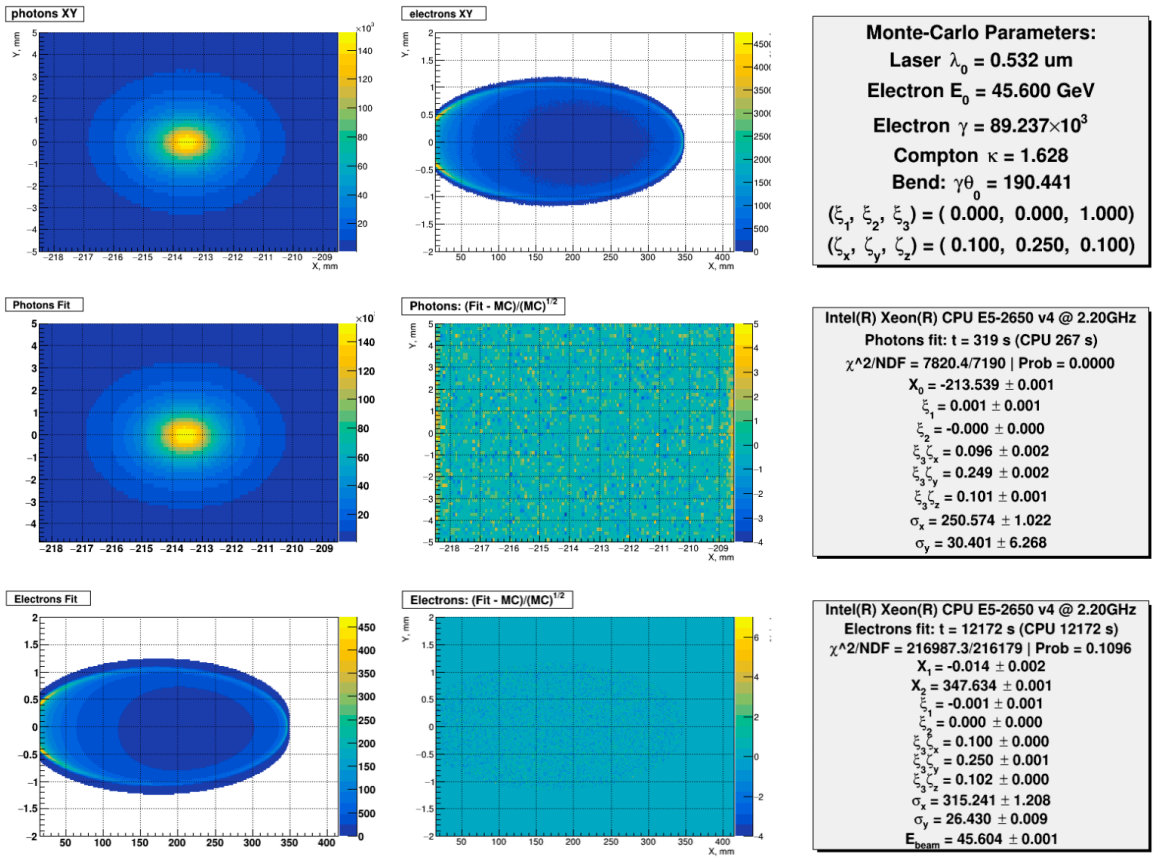

Tous les parametres sont extrait avec une precision de ~0.001 en quelques seconds

En plus de la DPR l'energie est aussi extraite de ce fit

Blondel et al., arXiv:1909.12245; Muchnoi, INST 17 P10014 (2022)

Conclusion

- Dépolarisation résonnante permet la calibration en temps réel de l'énergie du faisceau
- Le polarimètre sera basé sur l'interaction Compton qui dépend de tous les paramètres de polarisation
- Il sera possible d'aussi bien de mesurer directement l'énergie, que de l'extraire grâce à la dépolarisation résonnante par les mesures d'asymérie (Voir Poster)

cnrs GDR SCIPAC
SCIences of Particle ACcelerators

IJCLab Irène Joliot-Curie
Laboratoire de Physique des 2 Infinis

Merci pour votre attention

cnrs GDR SCiPAC
SCIences of Particle ACcelerators

IJCLab
Irène Joliot-Curie
Laboratoire de Physique des 2 Infinis

AI based anomaly detection of Turn-by-turn Beam Position Monitors

Doctorant:

Quentin BRUANT

Sous la supervision de:

- Barbara DALENA (Dir)(CEA)
- Francesca BUGIOTTI (CNRS/CentraleSupélec)
- Valérie GAUTARD (CEA)

Context

FCC collaboration: FUTURE CIRCULAR COLLIDER

EAJADE Europe-America-Japan Accelerator Development Exchange Programme

KEK

FSR published in European Physical Journal C and ST

Accessible on https://cds.cern.ch/record/2928793

- **Largest existing e+/e- collider**
  - **small-scale FCCee**
- **Provides proof of principle of several concepts and design choices.**

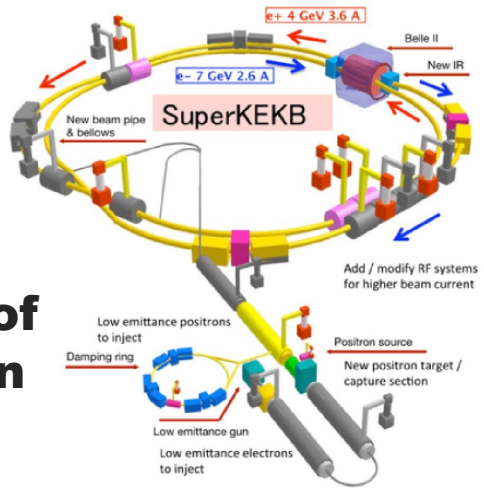

ADVANCED NUMERICAL TECHNIQUES AND AI TO MITIGATE IMPERFECTIONS IN FUTURE CIRCULAR COLLIDER

- **Optimisation** du design du booster haute énergie pour le FCCee
- **Étude et évaluation** des techniques d'IA pour améliorer les mesures d'optique par amélioration des rapports signal sur bruit des BPM tour-par-tour (TbT-BPMs)
- **Implémentation** de techniques IA pour la prédiction de l'ouverture dynamique des futurs collisionneurs.

Context

FCC collaboration: FUTURE CIRCULAR COLLIDER

EAJADE Europe-America-Japan Accelerator Development Exchange Programme

KEK

FSR published in European Physical Journal C and ST

Accessible on https://cds.cern.ch/record/2928793

- **Largest existing e+/e- collider**
  - **small-scale FCCee**
- **Provides proof of principle of several concepts and design choices.**

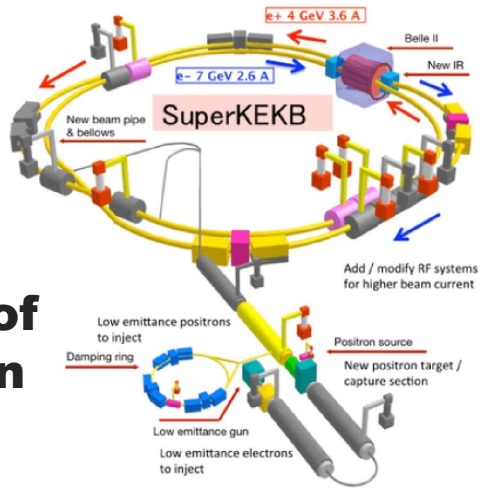

ADVANCED NUMERICAL TECHNIQUES AND AI TO MITIGATE IMPERFECTIONS IN FUTURE CIRCULAR COLLIDER

- **Optimisation** du design du booster haute énergie pour le FCCee
- **Étude et évaluation** des techniques d'IA pour améliorer les mesures d'optique par amélioration des rapports signal sur bruit des BPM tour-par-tour (TbT-BPMs)
- **Implémentation** de techniques IA pour la prédiction de l'ouverture dynamique des futurs collisionneurs.

TbT BPM data

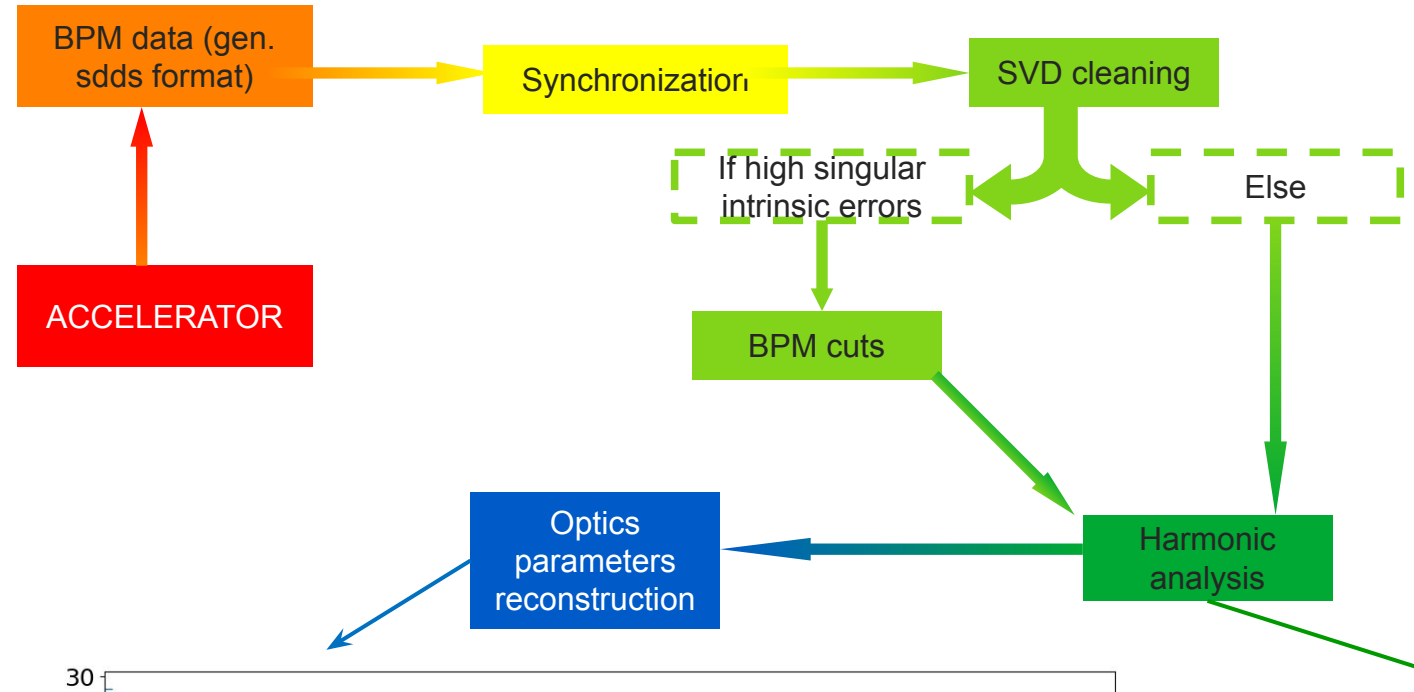
BPM data (gen. sdds format)
Synchronization
SVD cleaning
If high singular intrinsic errors
Else
ACCELERATOR
BPM cuts
Optics parameters reconstruction
Harmonic analysis

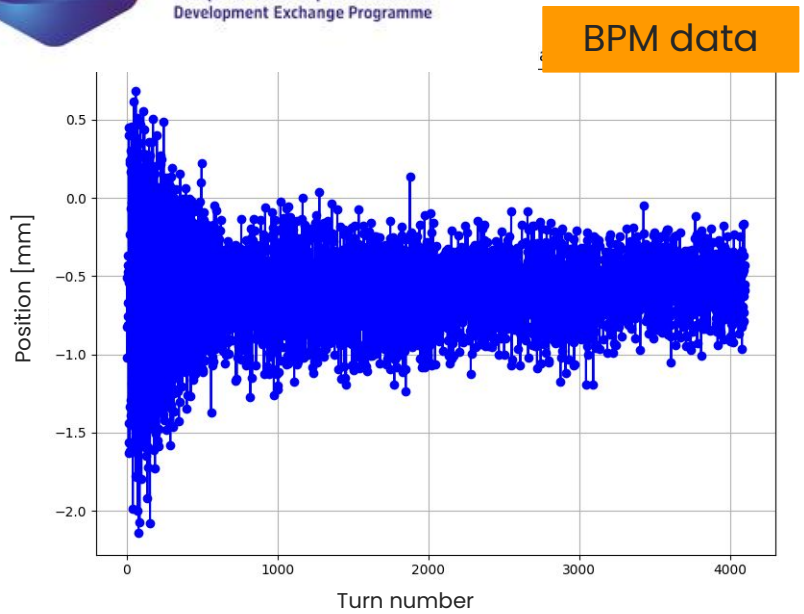
BPM data
Position [mm]
Turn number

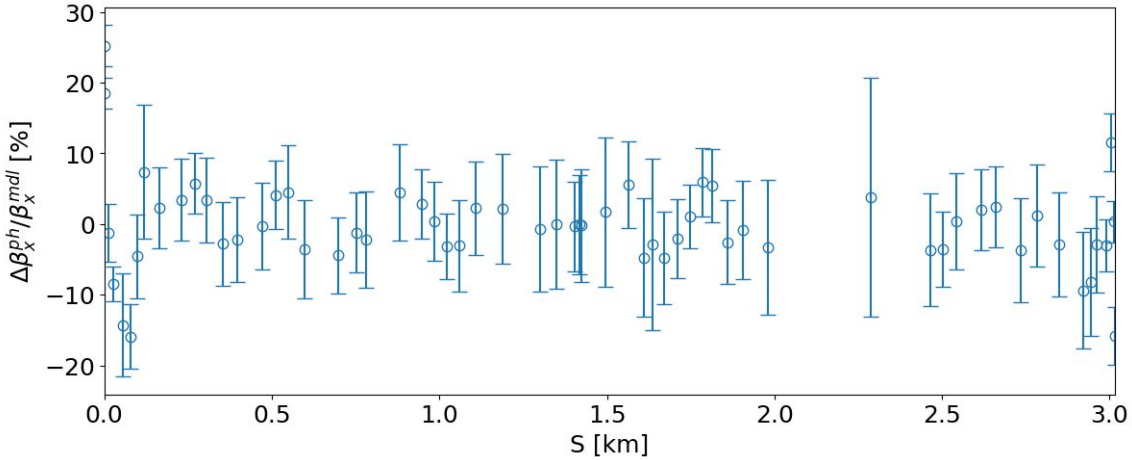
$\Delta\beta_x^{ph}/\beta_x^{mdl}$ [%]
S [km]

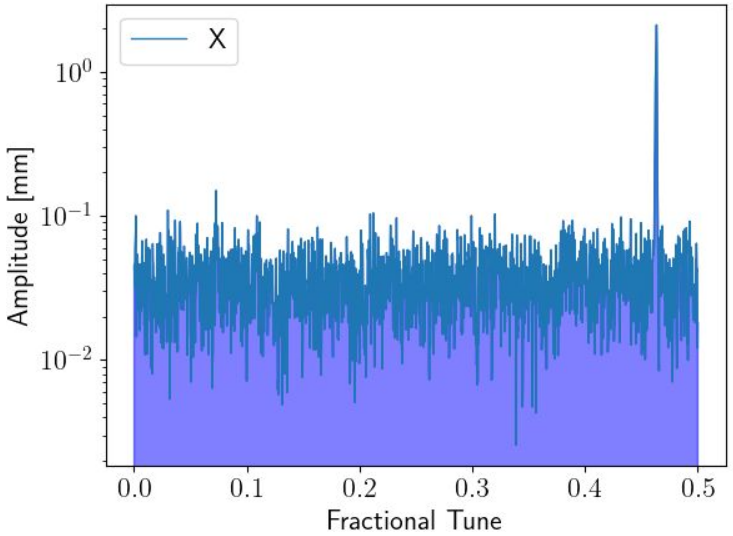
X
Amplitude [mm]
Fractional Tune

TbT BPM data

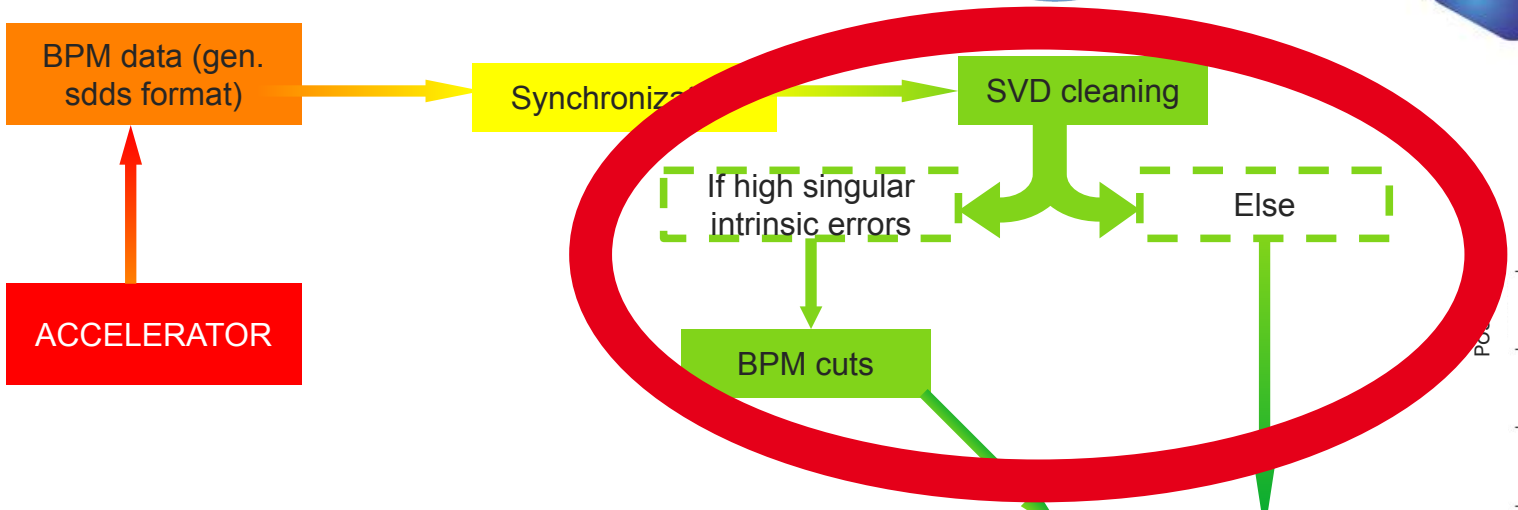
BPM data (gen. sdds format)
Synchroniza
SVD cleaning
If high singular intrinsic errors
Else
BPM cuts
ACCELERATOR

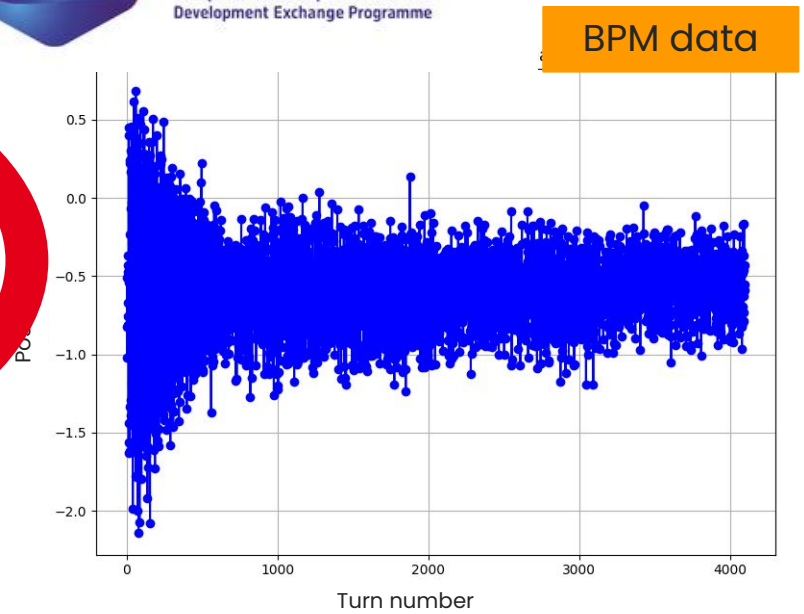
BPM data
0.5
0.0
−0.5
−1.0
−1.5
−2.0
0
1000
2000
3000
4000
Turn number

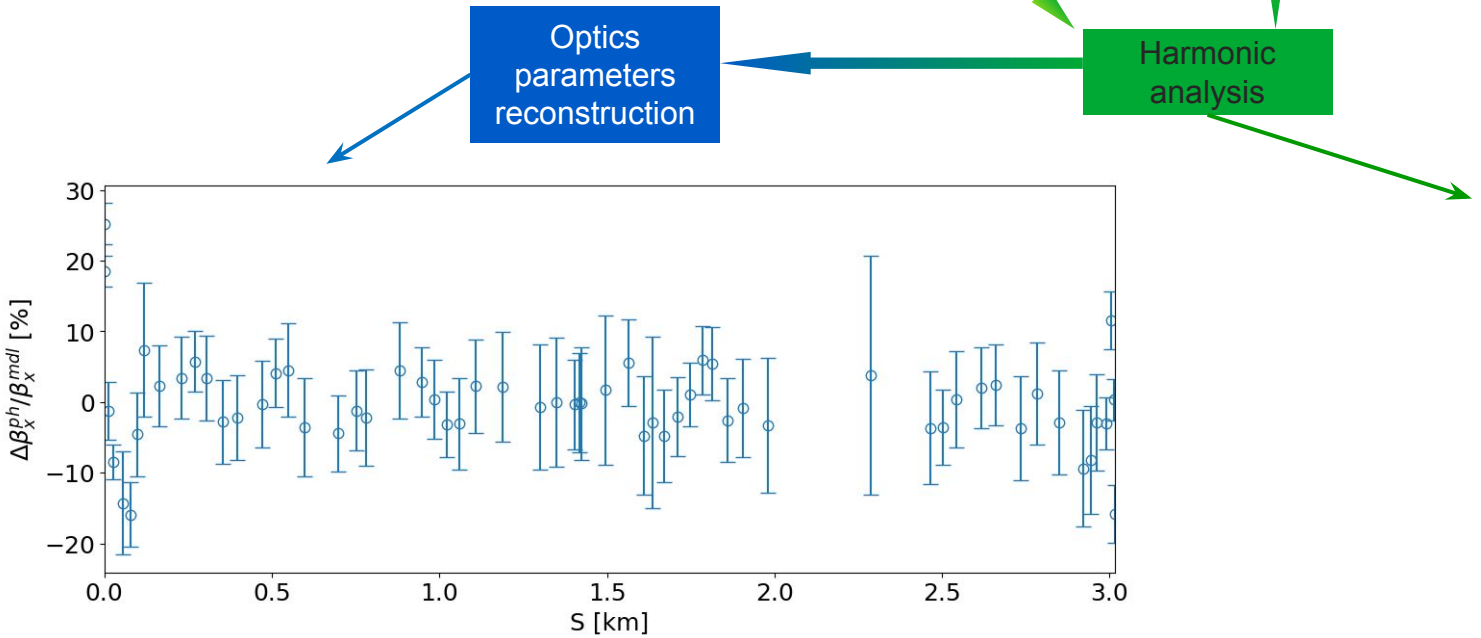
Optics parameters reconstruction
Harmonic analysis
30
20
10
0
−10
−20
0.0
0.5
1.0
1.5
2.0
2.5
3.0
S [km]
$\Delta\beta_x^{ph}/\beta_x^{mdl}$ [%]

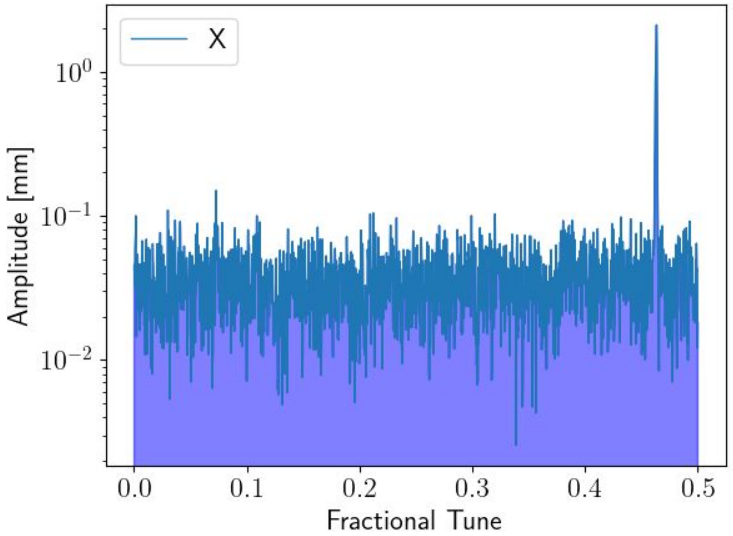
X
10^0
10^{-1}
10^{-2}
Amplitude [mm]
0.0
0.1
0.2
0.3
0.4
0.5
Fractional Tune

DBSCAN

- **Clustering algorithm : Density-Based Spectral Clustering Application w/ Noise**
  - **Hyperspace of the statistical features from Multivariate Time Series (MTS)**
- **1 vs All approach**
- **ε distance based algorithm**

Main approach:

- **One measurement, all tracks**

★ : outlier out of ε range from other points

★ : first point considered in the cluster

★ : point in the cluster

★ : point in the cluster w/ no neighbour

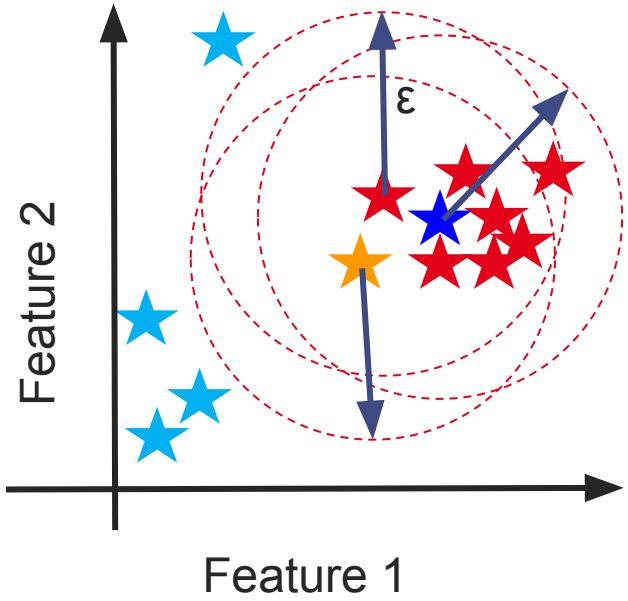

Main results

Faulty BPM HER (DBSCAN)	Expected faulty BPM HER	Faulty BPM LER (DBSCAN)	Expected faulty BPM LER
MQEAE35	MQEAE35		MQD3P23
MQD3E18	MQD3E18	MQEAP29	MQEAP29
MQR2ORE	MQR2ORE		MQD3P8
MQEAE20	MQEAE20		MQEAP10
MQEAE33		MQEAP35	MQEAP35
MQD3E29		MQW2ORP	MQW2ORP
	MQD3E23	MQEAP32	
MQEAE25		MQEAP33	
	MQD3E8	MQEAP44	
		MQD3P29	
		MQI6P	
		MQEAP38	

Résultats DBSCAN

Faulty BPM HER (DBSCAN)	Expected faulty BPM HER	Faulty BPM LER (DBSCAN)	Expected faulty BPM LER
MQEAE35	MQEAE35	MQD3P23	MQD3P23
MQD3E18	MQD3E18	MQEAP29	MQEAP29
MQR2ORE	MQR2ORE		MQD3P8
	MQD3E8		MQEAP10
MQD3E23	MQD3E23	MQEAP35	MQEAP35
	MQEAE20	MQW2ORP	MQW2ORP
MQC2RE			
MQLB1LE			

Results of an SVD & Isolation Forest algorithm built by CentraleSupelec students co-supervised by B.Dalena and F.Bugiotti (CentraleSupélec)

Pour plus d'infos, venez voir le poster !!

Design d'une cavité optique Fabry-Perot pour le stockage plusieurs centaines de kW et l'interaction avec des faisceaux de particules : application à l'ERL PERLE

Alice RENAUX
CNRS/IN2P3/IJLab

Journée "Accélérateurs" de la Société Française de Physique

Interaction Compton inverse

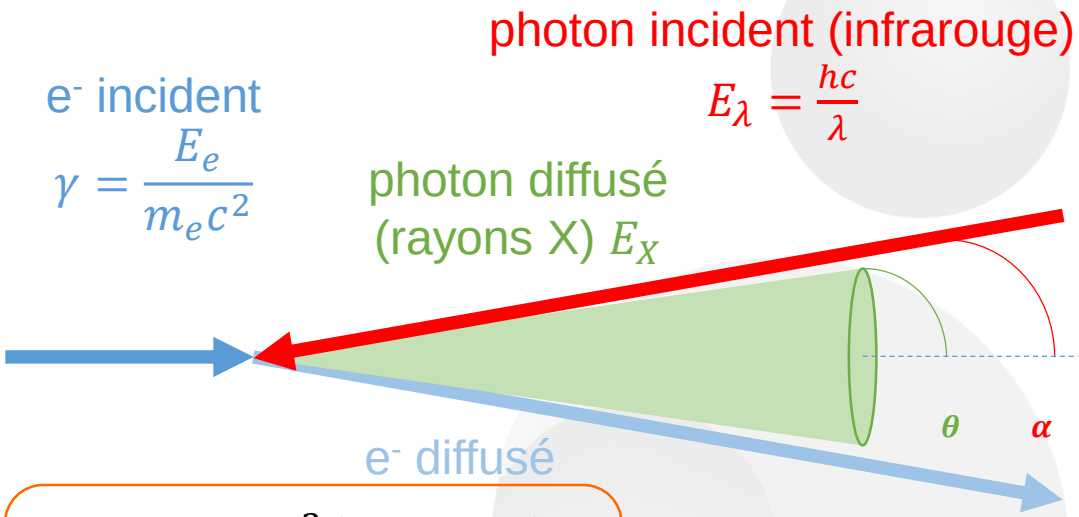

$$E_X \simeq E_\lambda \frac{2\gamma^2(1-\cos\alpha)}{1+\gamma^2\theta^2}$$

$$E_{X,max} \simeq E_\lambda \times 4\gamma^2$$

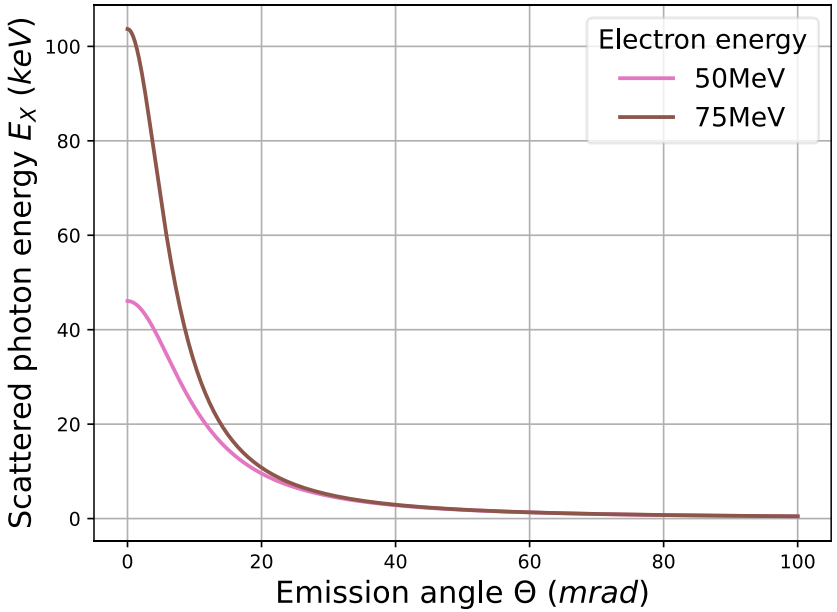

$$\lambda = 1030nm \rightarrow E_\lambda = 1.2eV$$

Sources Compton compactes

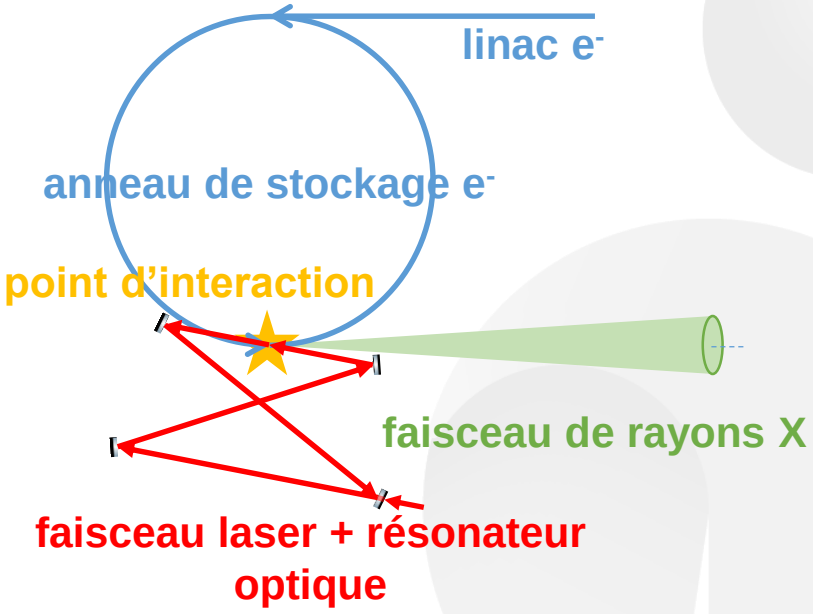

- Section efficace de l'interaction Compton inverse très faible ($\simeq 0.6 barn$)
- Maximisation du flux de rayons X
- Paramètres du faisceau d'e$^-$ fixés

➢ **Très forte puissance laser moyenne nécessaire : $\geq 100 kW$**

ThomX @ IJCLab

- Énergie des rayons X : **45-90 keV**
- Flux de rayons X : **10^{11}-10^{13} ph.s^{-1}**

Design d'une cavité à $515nm$ pour l'ERL PERLE

- Caractéristiques de PERLE :
  - Contraintes d'encombrement

  → Choix de $f_{rep} \rightarrow L_{cav}$, d_1, d_2, h, $\theta_{Crossing}$

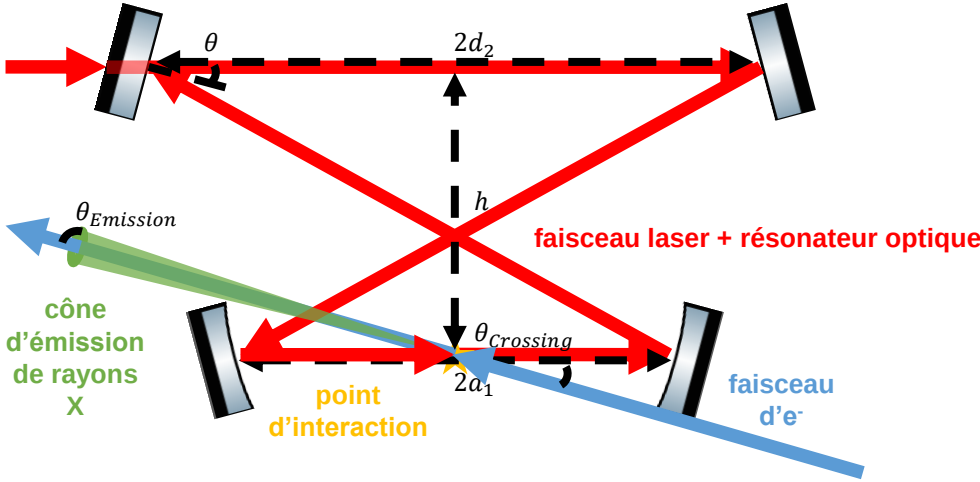

- Maximisation du flux de rayons X :
  - Maximisation du flux de rayons X sans couplage géométrique
  - Maximisation du couplage géométrique
  - Prise en compte des effets thermiques → minimisation de la perte de flux et de couplage dûe aux changements dans le mode propre fondamental de la cavité

  → Choix de R

  → *Design* d'un télescope

Design d'une cavité à $515nm$ pour l'ERL PERLE

- *Design* d'un télescope :

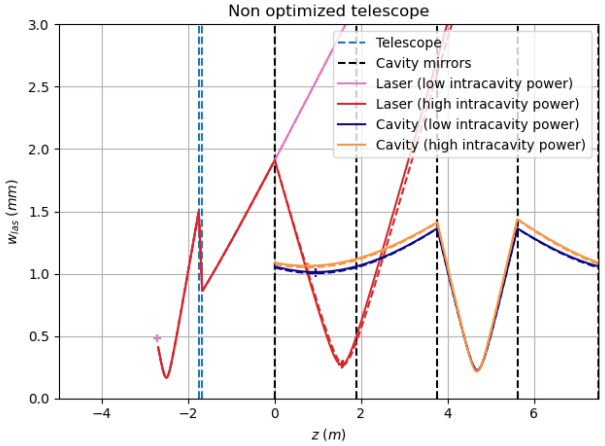

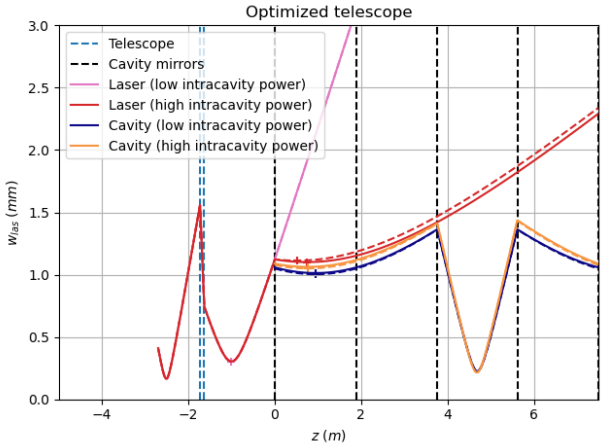

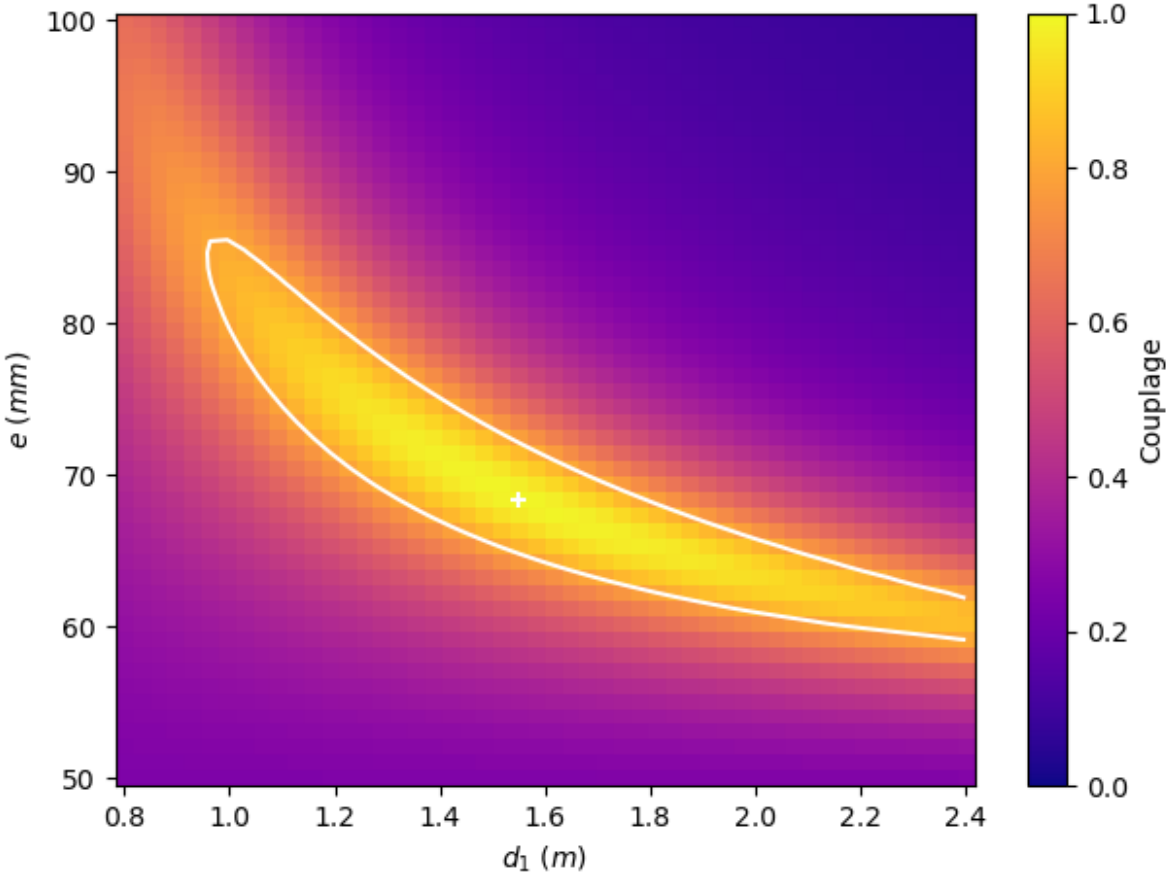

Conclusion

- *Design* d'une cavité pour la production de rayons X avec l'ERL PERLE :
  - Design d'une cavité
  - Design d'un télescope
  - Prise en compte d'effets thermiques présents à haute puissance intracavité

→ **Contribution au *Technical Design Report***

→ **R&D expérimentale autour des cavités**

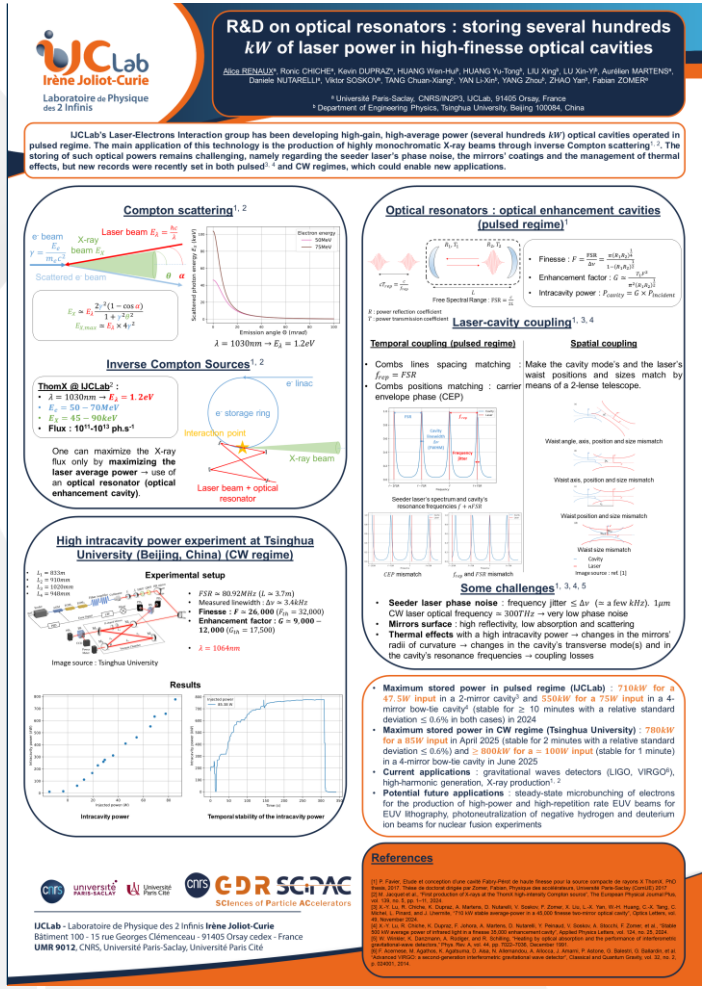

Merci pour votre attention

Des questions ?

Génération de sources de neutrons pilotées par le laser PETAL à partir de convertisseurs double-couche

Lucas Ribotte[1,2], R. Lelièvre[3], G. Boutoux[1], C. Rousseaux[1], X. Davoine[1,4], L. Gremillet[1,4], I. Lantuéjoul[1], B. Vauzour[1], V. Hénot[1], O. Landoas[1], T. Ferraro[1], V. Mary[1], P. Romain[1], N. Blanchot[5], C. Chappuis[5], R. du Jeu[5], B. Etchessahar[5], B. Mahieu[1], M. Bardon[2], D. Raffestin[2], P. Nicolaï[2], E. d'Humières[2], and J. Fuchs[3]

[1]*CEA, DAM, DIF, F-91297 Arpajon, France*

[2]*CELIA, Université de Bordeaux-CNRS-CEA, UMR 5107, 33405 Talence, France*

[3]*LULI, F-91128 Palaiseau, France*

[4]*Université Paris-Saclay, CEA, LMCE, 91680 Bruyères-le-Châtel, France*

[5]*CEA, DAM, CESTA, F-33116 Le Barp, France*

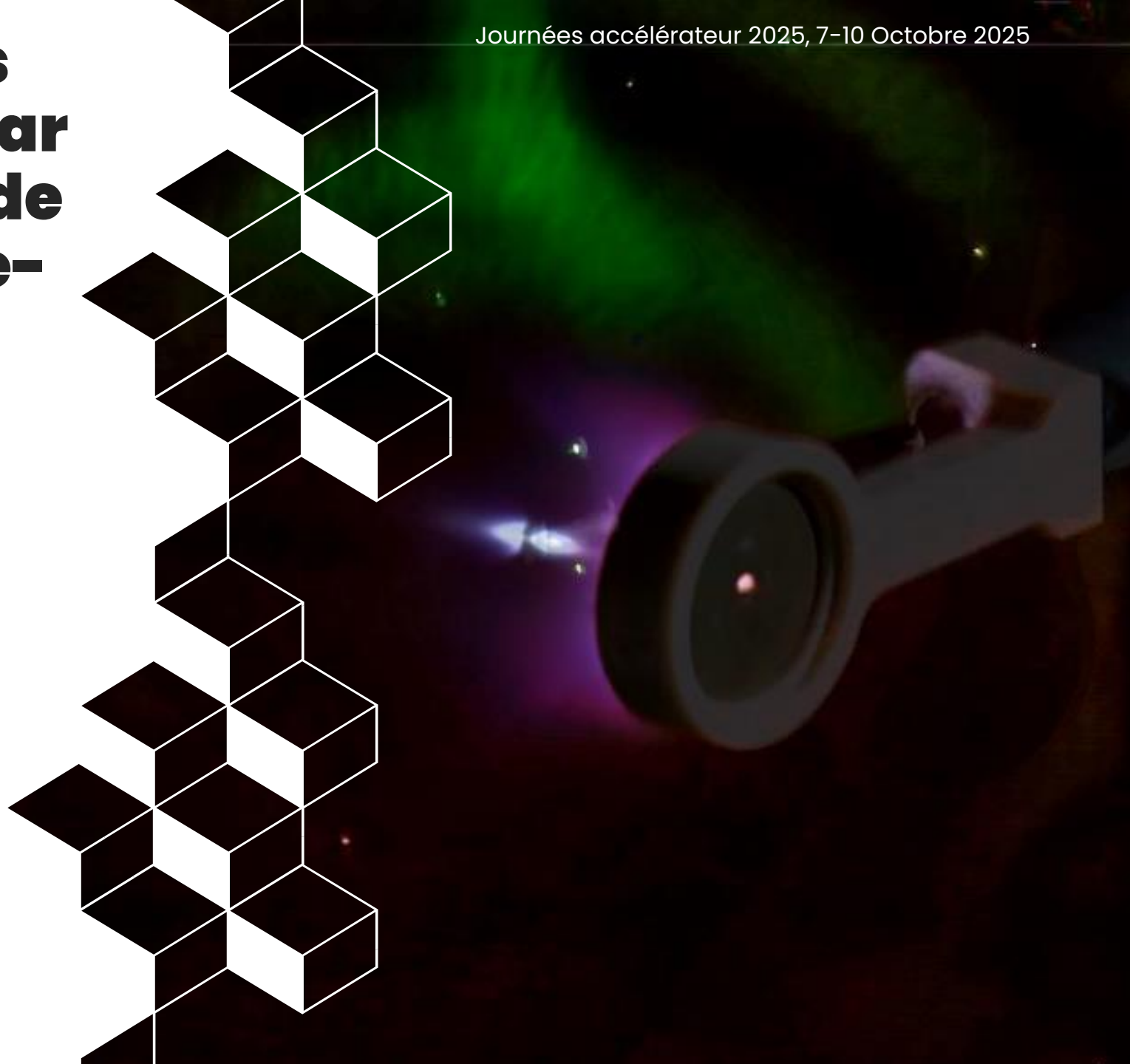

1. Introduction

Sources de neutrons pilotées par laser

Target Normal Sheath Acceleration (TNSA)

Cible fine (nm, µm)

Target Normal Sheath Acceleration (TNSA)

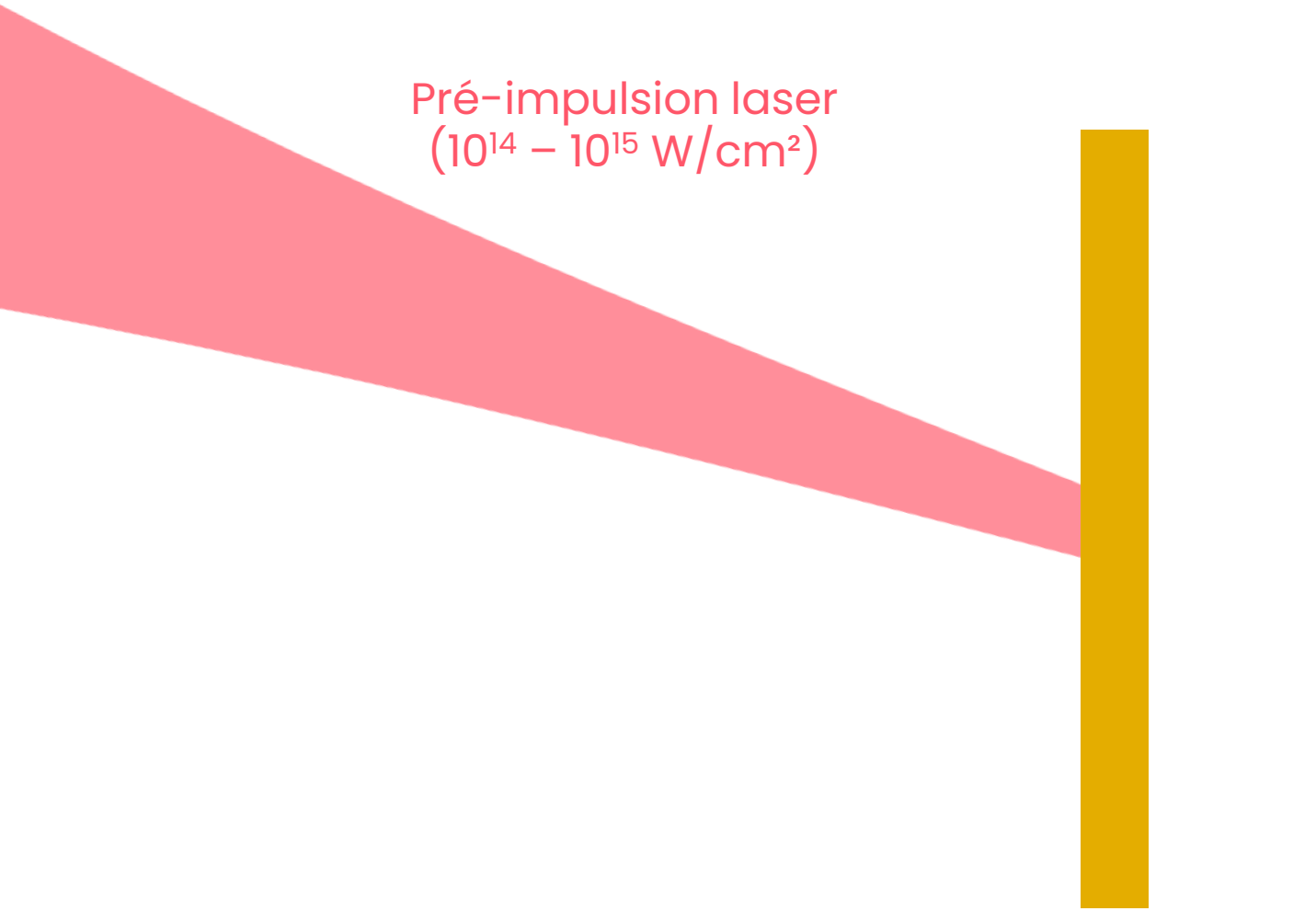

Cible fine (nm, µm)

Target Normal Sheath Acceleration (TNSA)

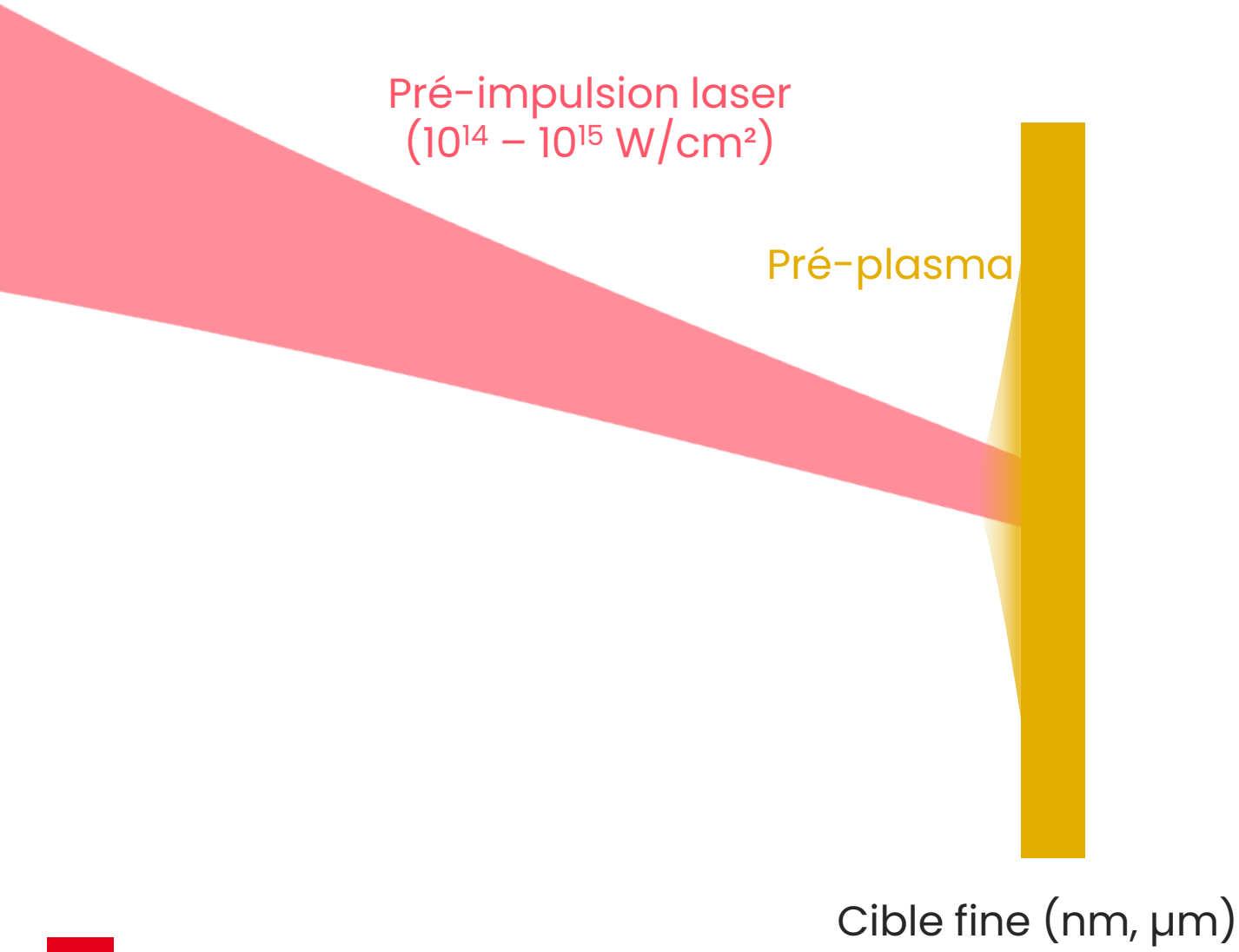

Target Normal Sheath Acceleration (TNSA)

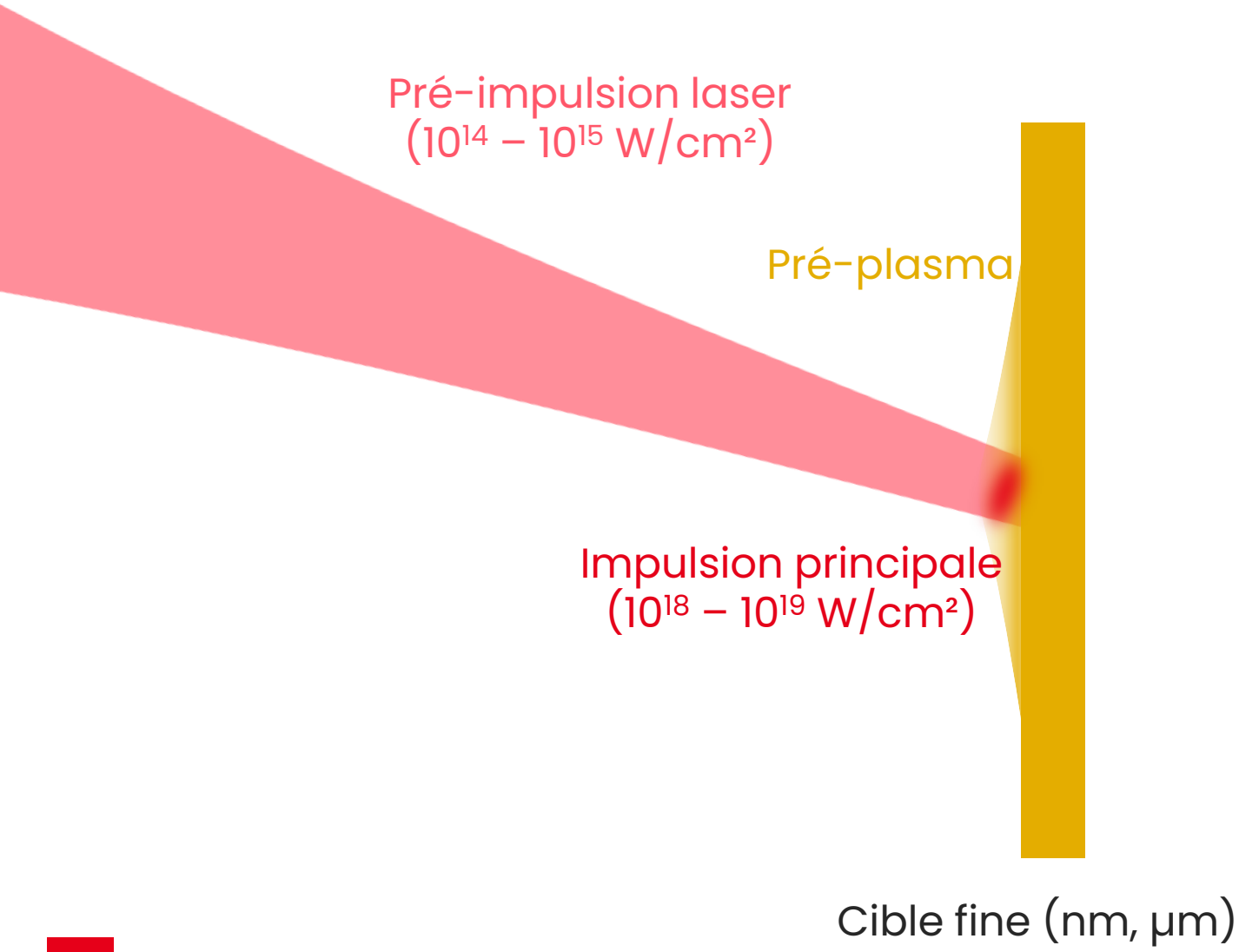

Target Normal Sheath Acceleration (TNSA)

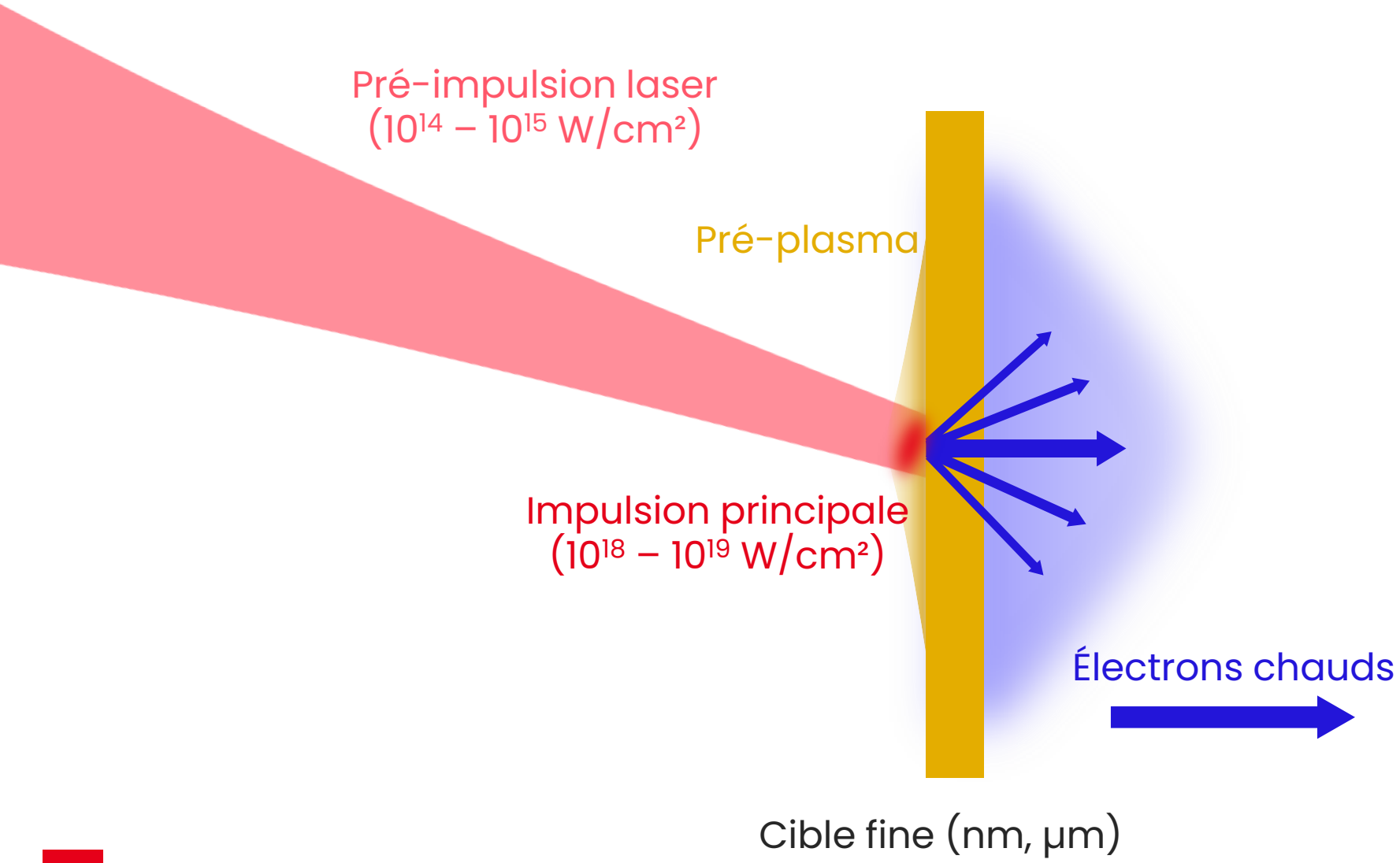

Target Normal Sheath Acceleration (TNSA)

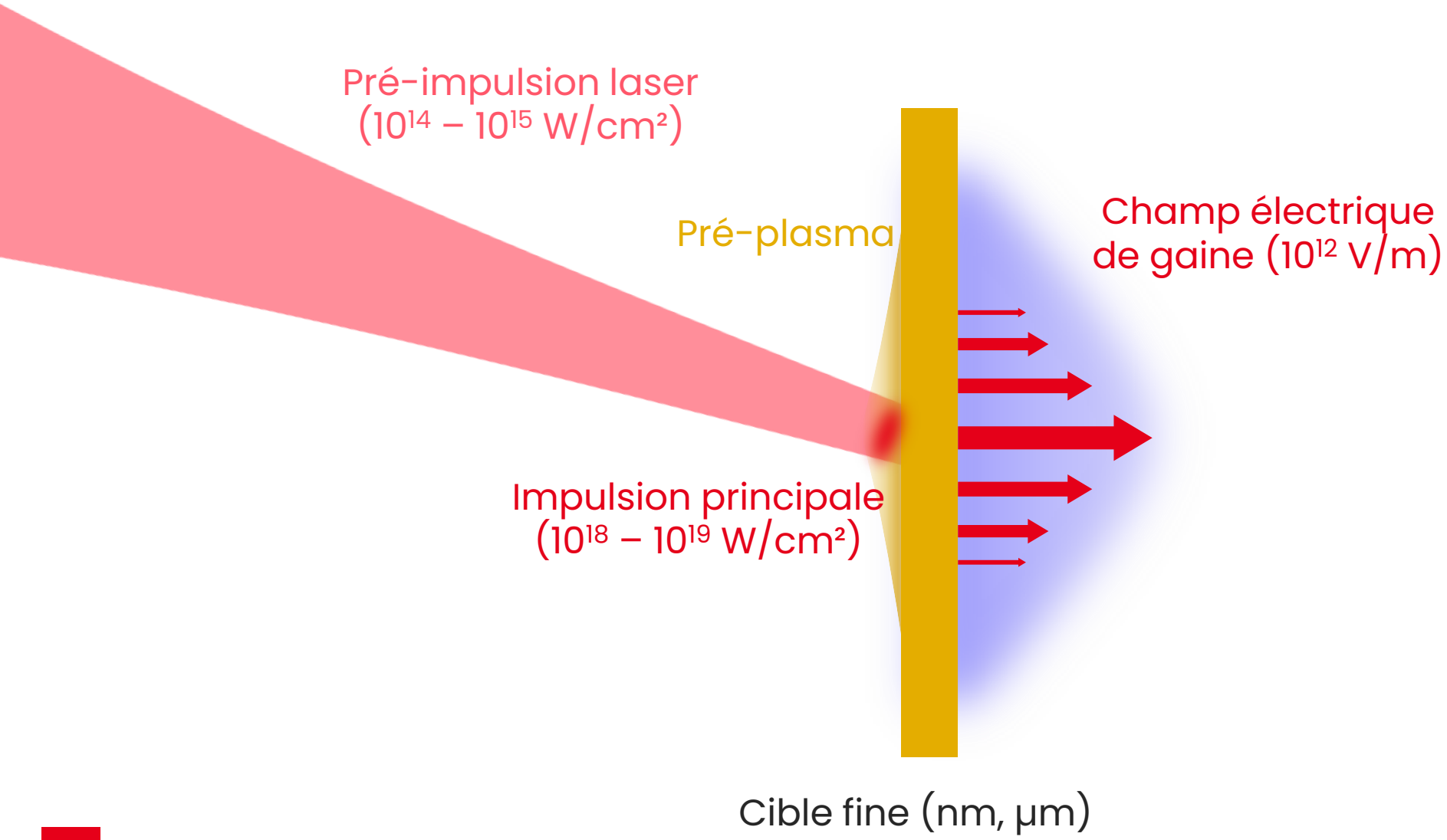

Target Normal Sheath Acceleration (TNSA)

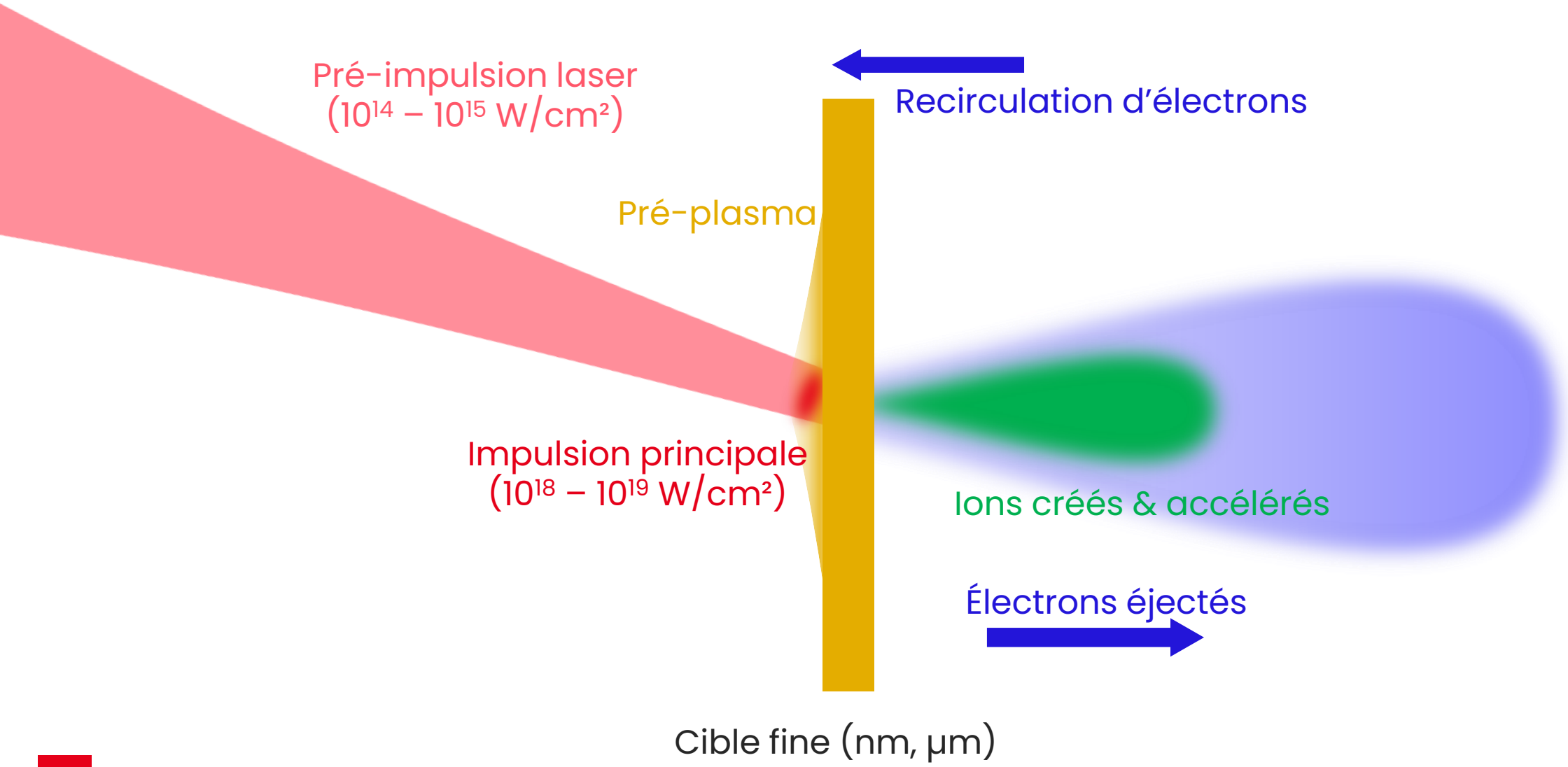

Sources de neutrons secondaires

Convertisseurs classiques: Be, LiF, Pb ou plastique deutéré

Spectres TNSA: 0 – ≈50 MeV

- Au-delà de ≈10 MeV, LiF/Be ne sont plus efficaces
- Au-delà de ≈10 MeV, Pb est efficace

→ **Convertisseurs double-couches (LiF + Pb)** pour augmenter le nombre de neutrons produits [2,3]

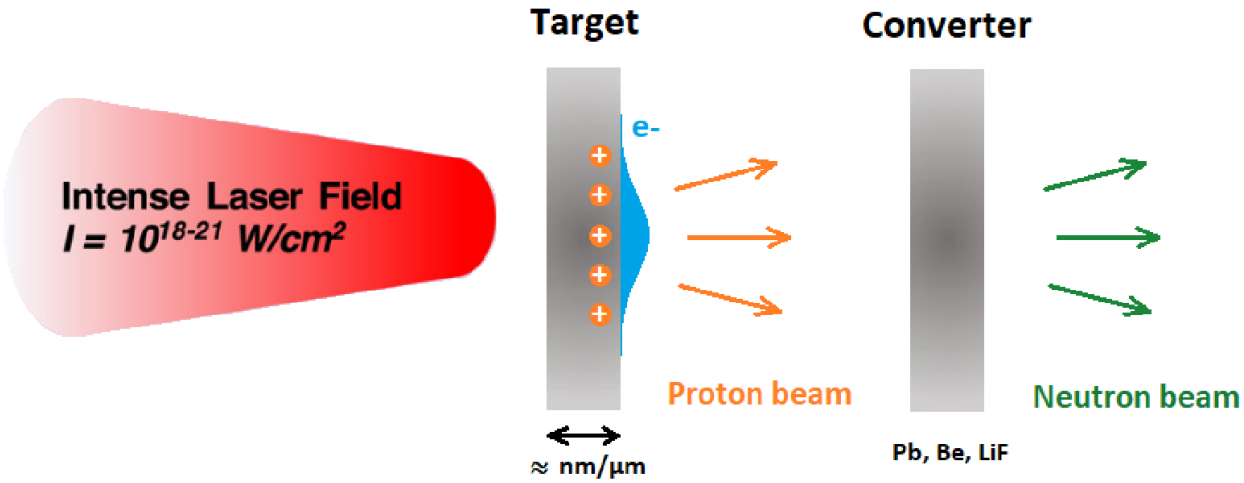

[2] M. Zimmer *et al*, « Demonstration of non-destructive and isotope-sensitive material analysis using a short-pulsed laser-driven epi-thermal neutron source », *Nature Communications* 13, 1173 (2022)
[3] B. Martinez *et al*, « Numerical investigation of spallation neutrons generated from petawatt-scale laser-driven proton beams », *Matter Radiat. Extremes* 7, 024404 (2022), doi: 10.1063/5.0060582

Sources de neutrons secondaires

<u>Convertisseurs classiques</u>: Be, LiF, Pb ou plastique deutéré

Spectres TNSA: 0 – ≈50 MeV

- Au-delà de ≈10 MeV, LiF/Be ne sont plus efficaces
- Au-delà de ≈10 MeV, Pb est efficace

→ **Convertisseurs double-couches (LiF + Pb)** pour augmenter le nombre de neutrons produits [2,3]

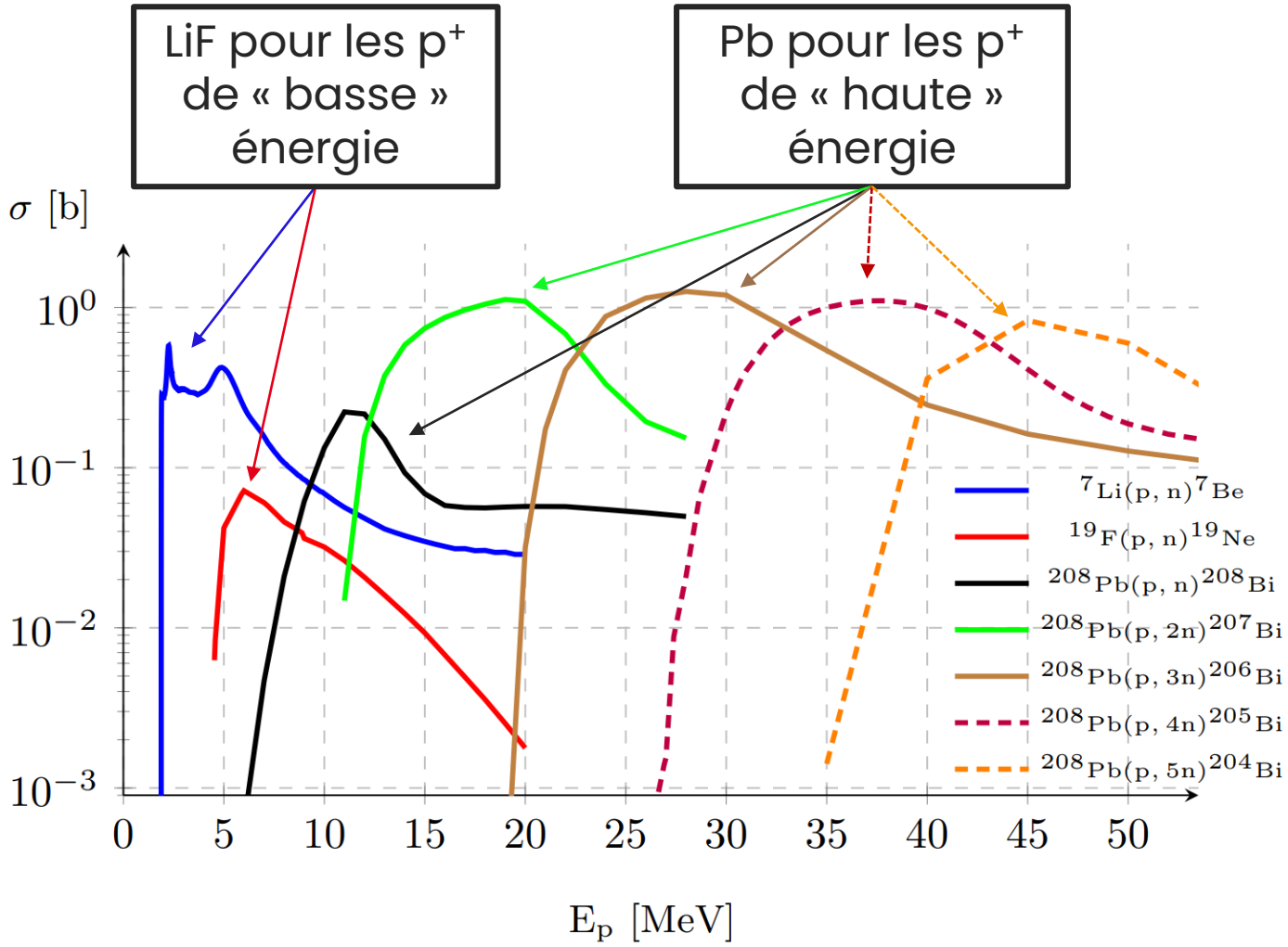

[2] M. Zimmer *et al*, « <u>Demonstration of non-destructive and isotope-sensitive material analysis using a short-pulsed laser-driven epi-thermal neutron source</u> », *Nature Communications* 13, 1173 (2022)
[3] B. Martinez *et al*, « <u>Numerical investigation of spallation neutrons generated from petawatt-scale laser-driven proton beams</u> », *Matter Radiat. Extremes* 7, 024404 (2022), doi: 10.1063/5.0060582

2. Implémentation

Sur l'installation LMJ-PETAL

Configuration expérimentale

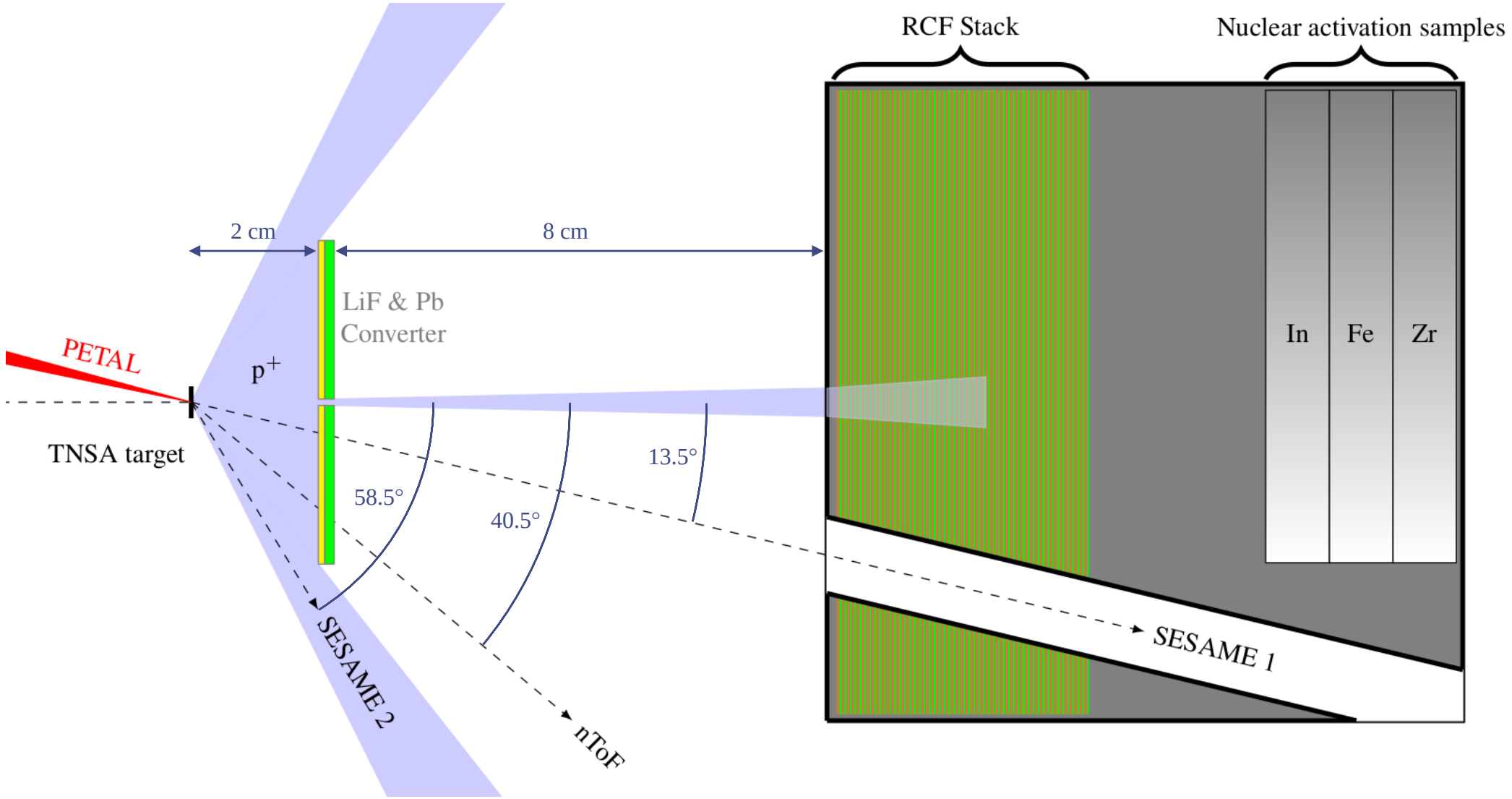

Configuration expérimentale

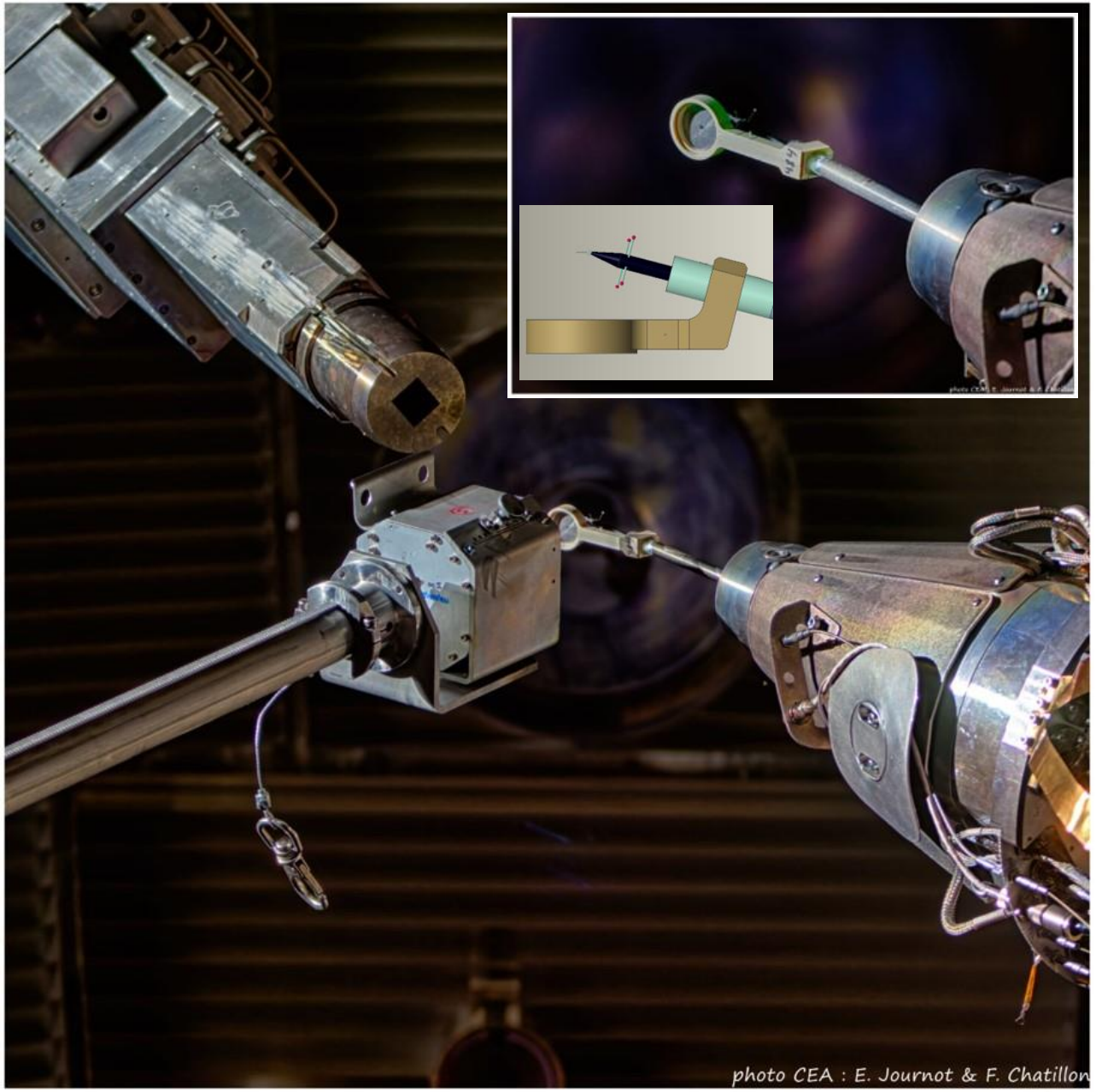

Configuration expérimentale

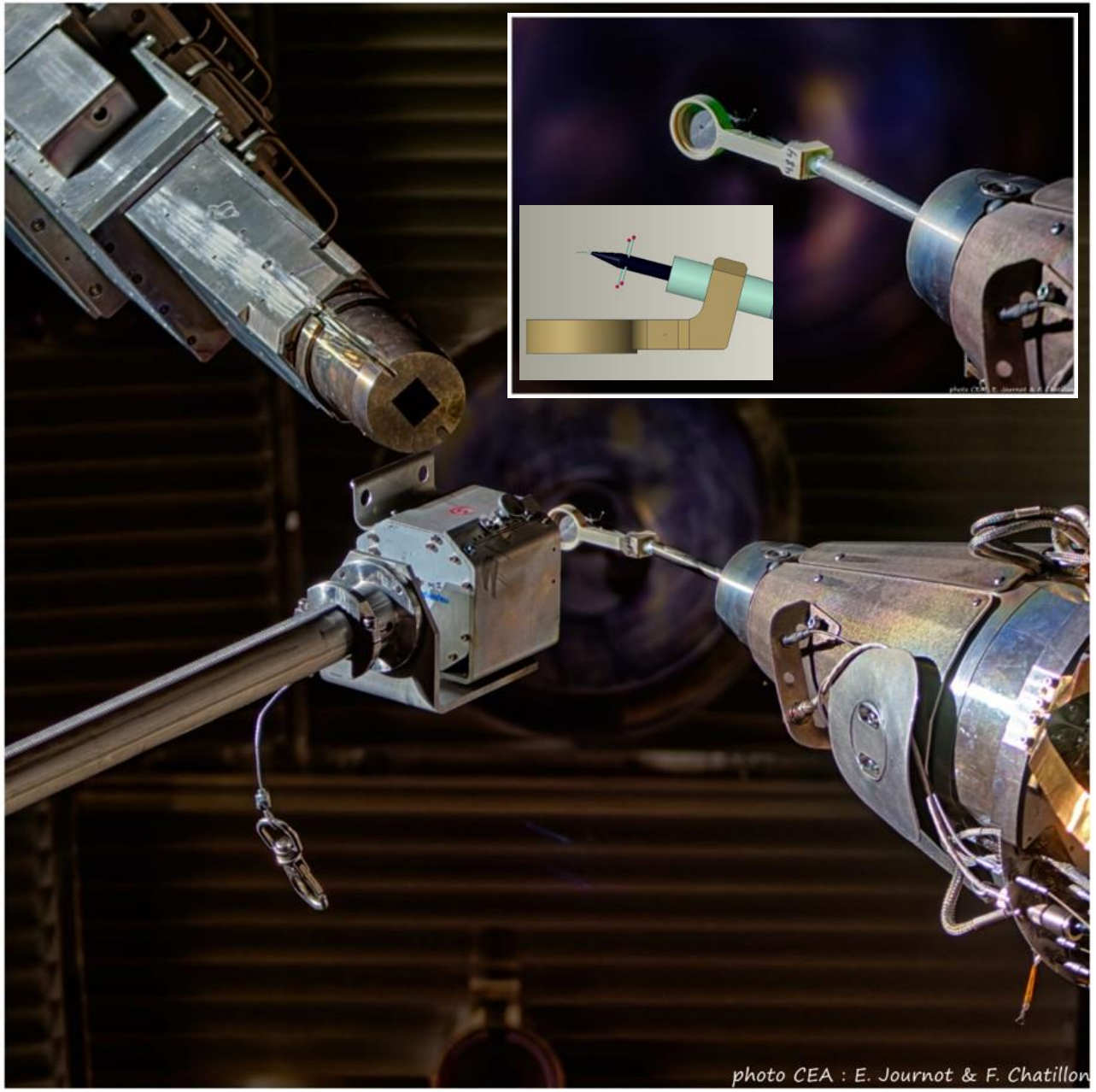

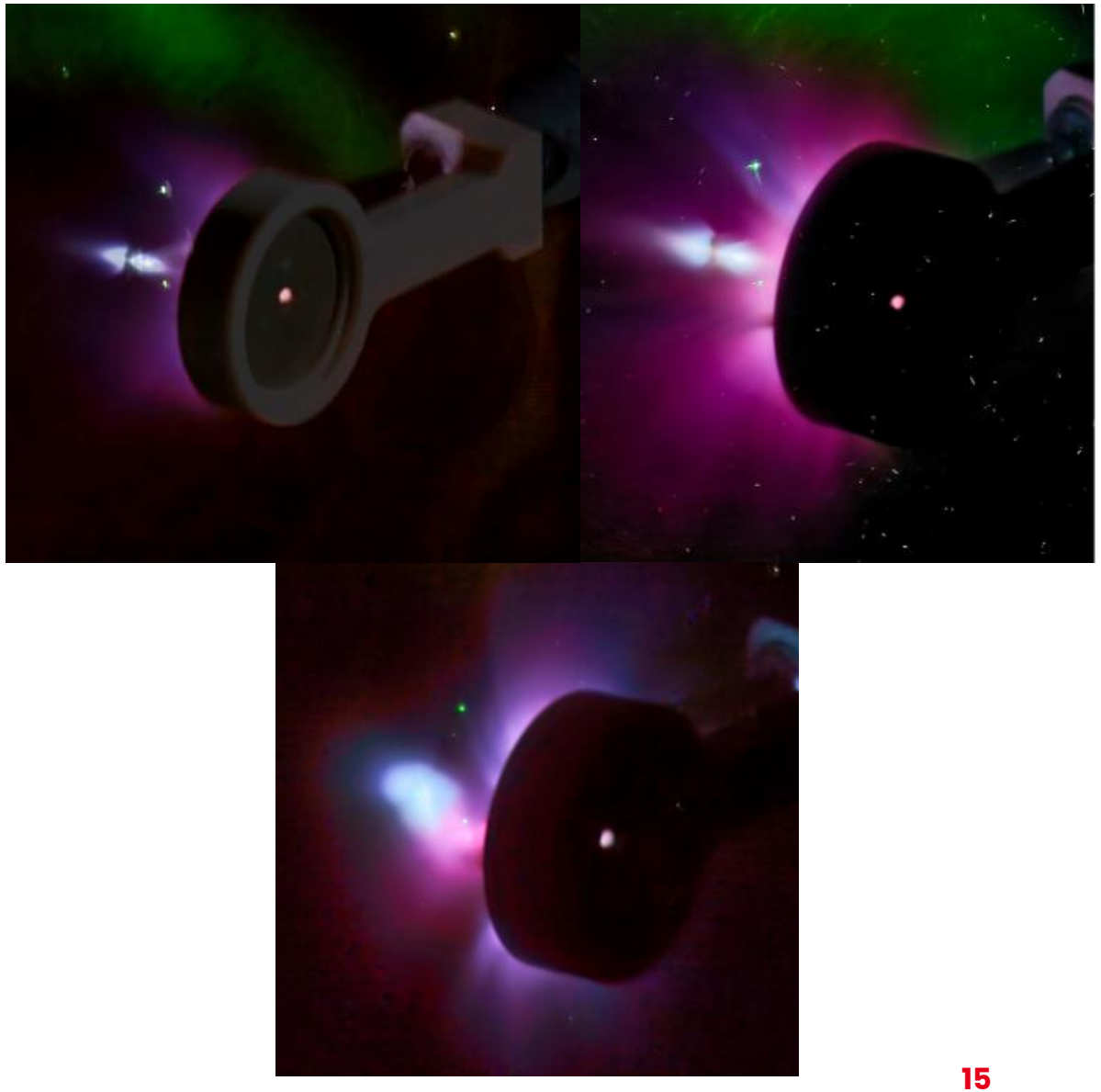

3. Résultats

Propriétés des termes sources générés

Paramètres laser

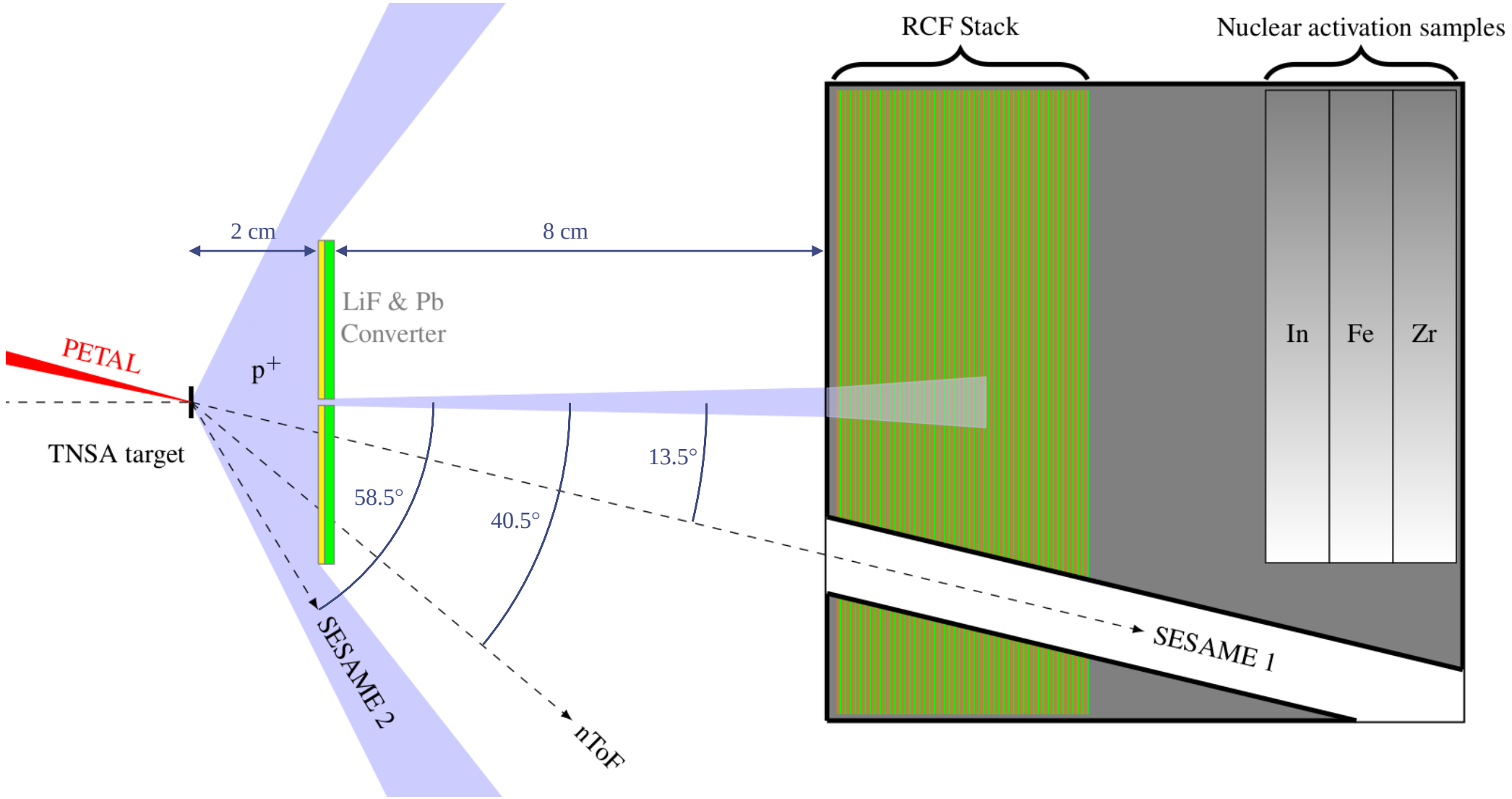

Paramètres laser

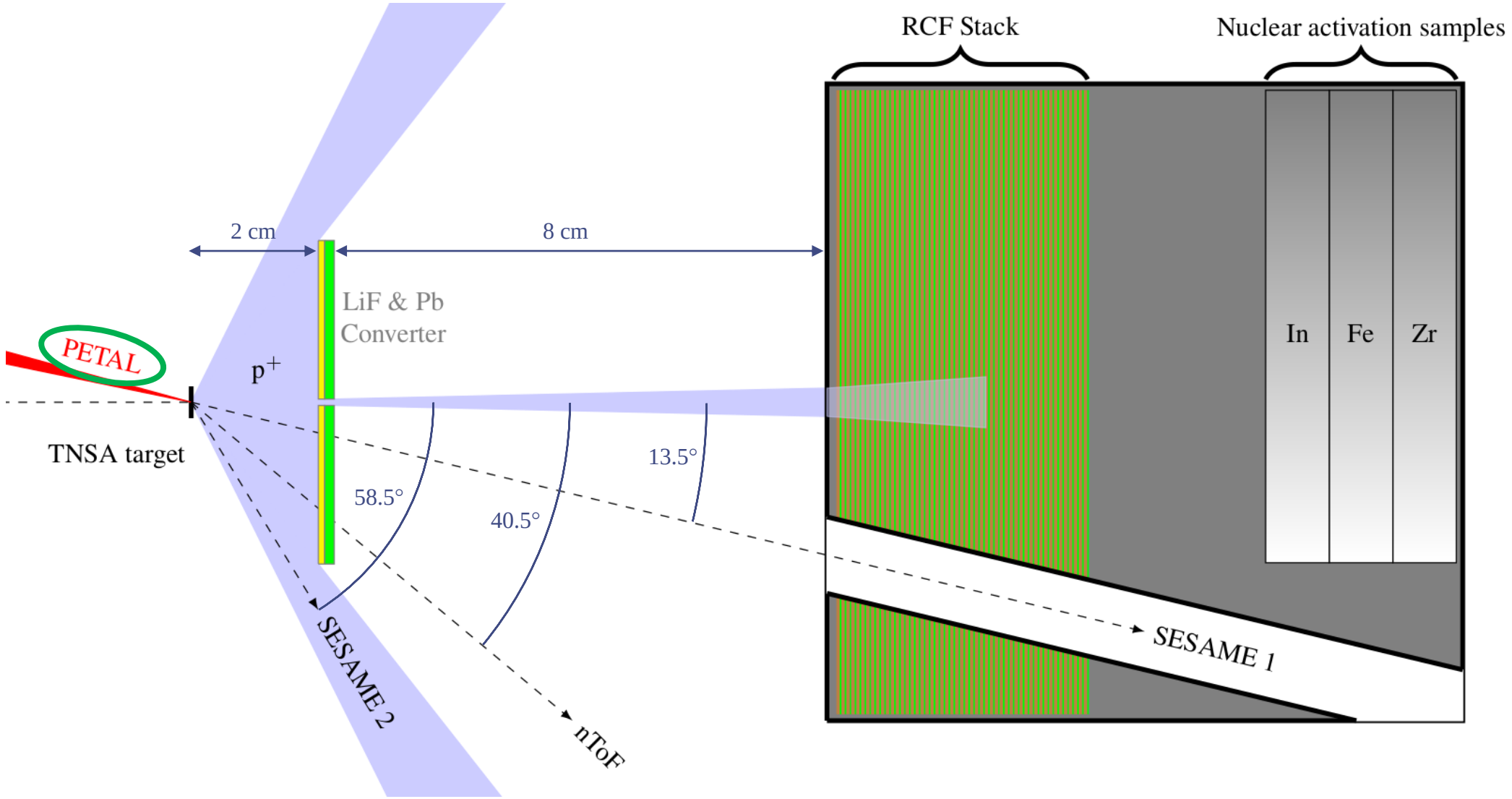

Paramètres laser

Énergie laser: 330J – 640J
Durée d'impulsion: 500fs – 1ps
Intensité sur cible: 10^{18}–10^{19} W/cm²

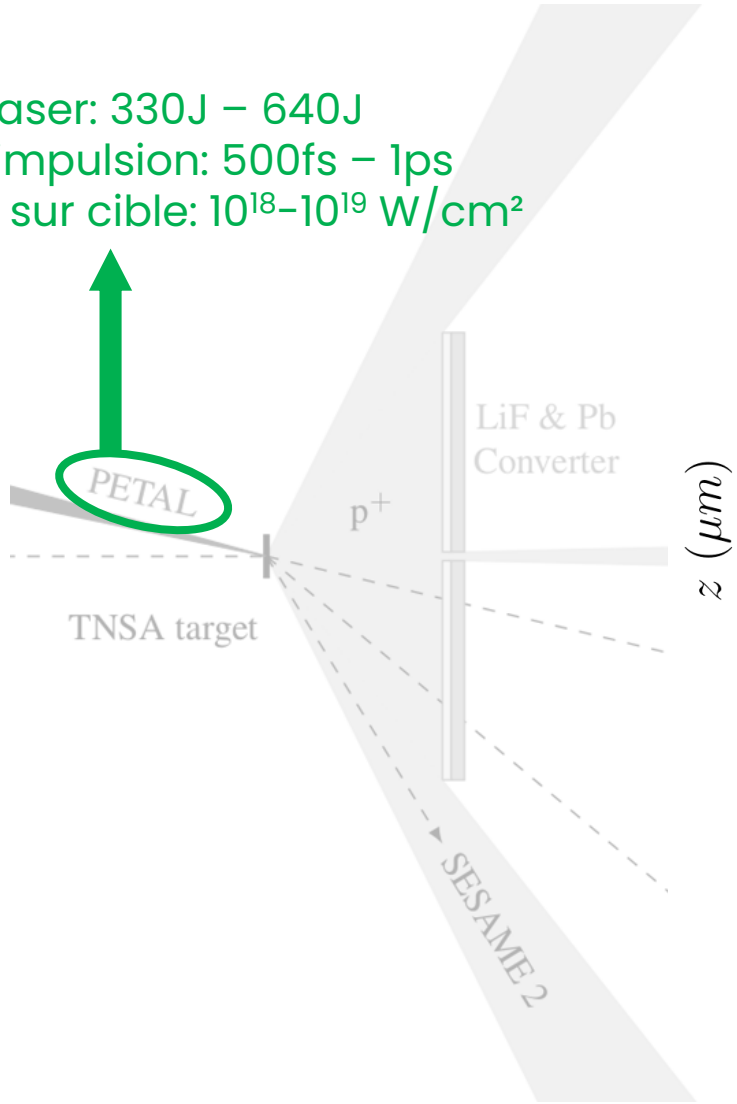

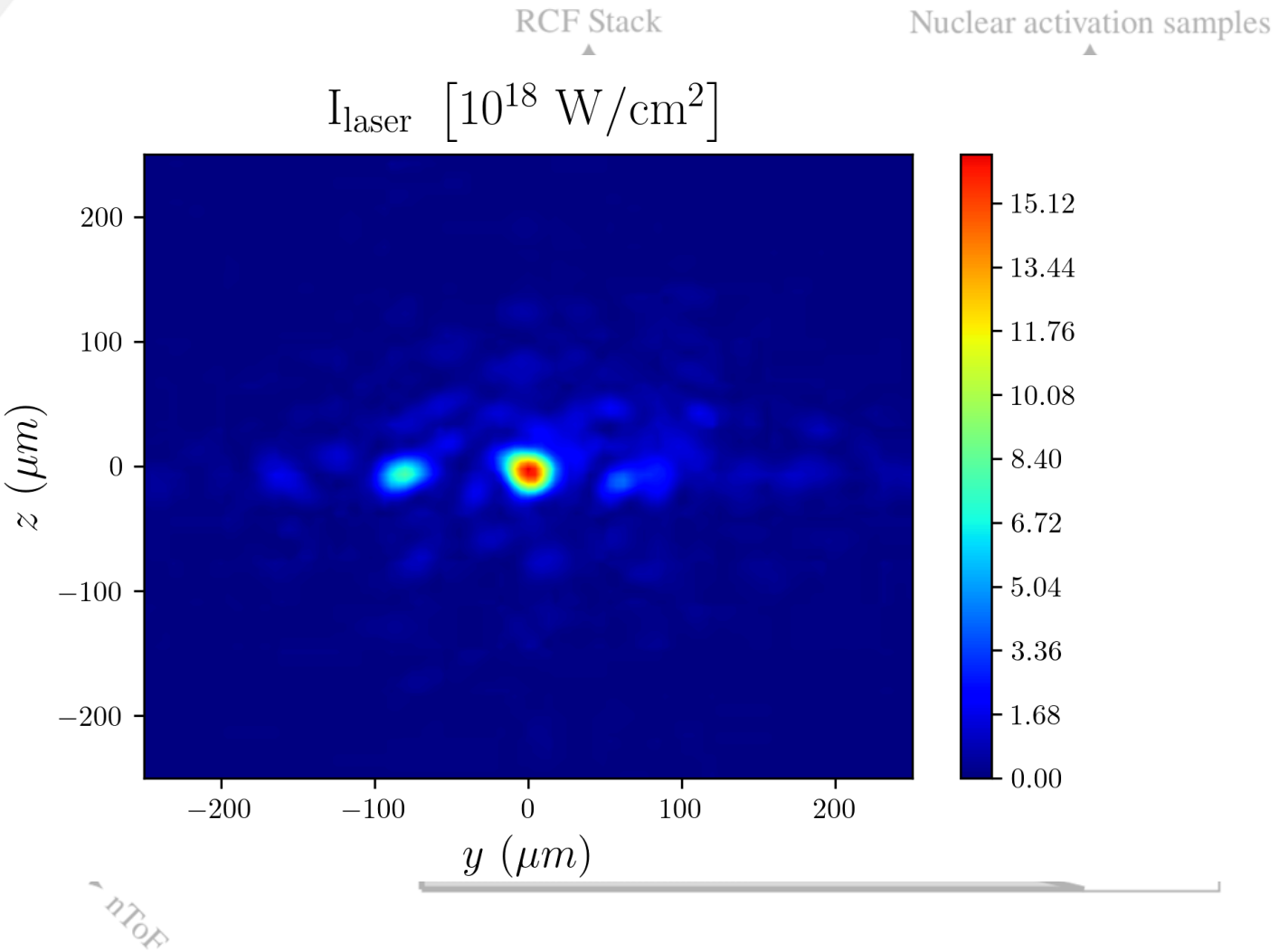

Spectromètres magnétiques

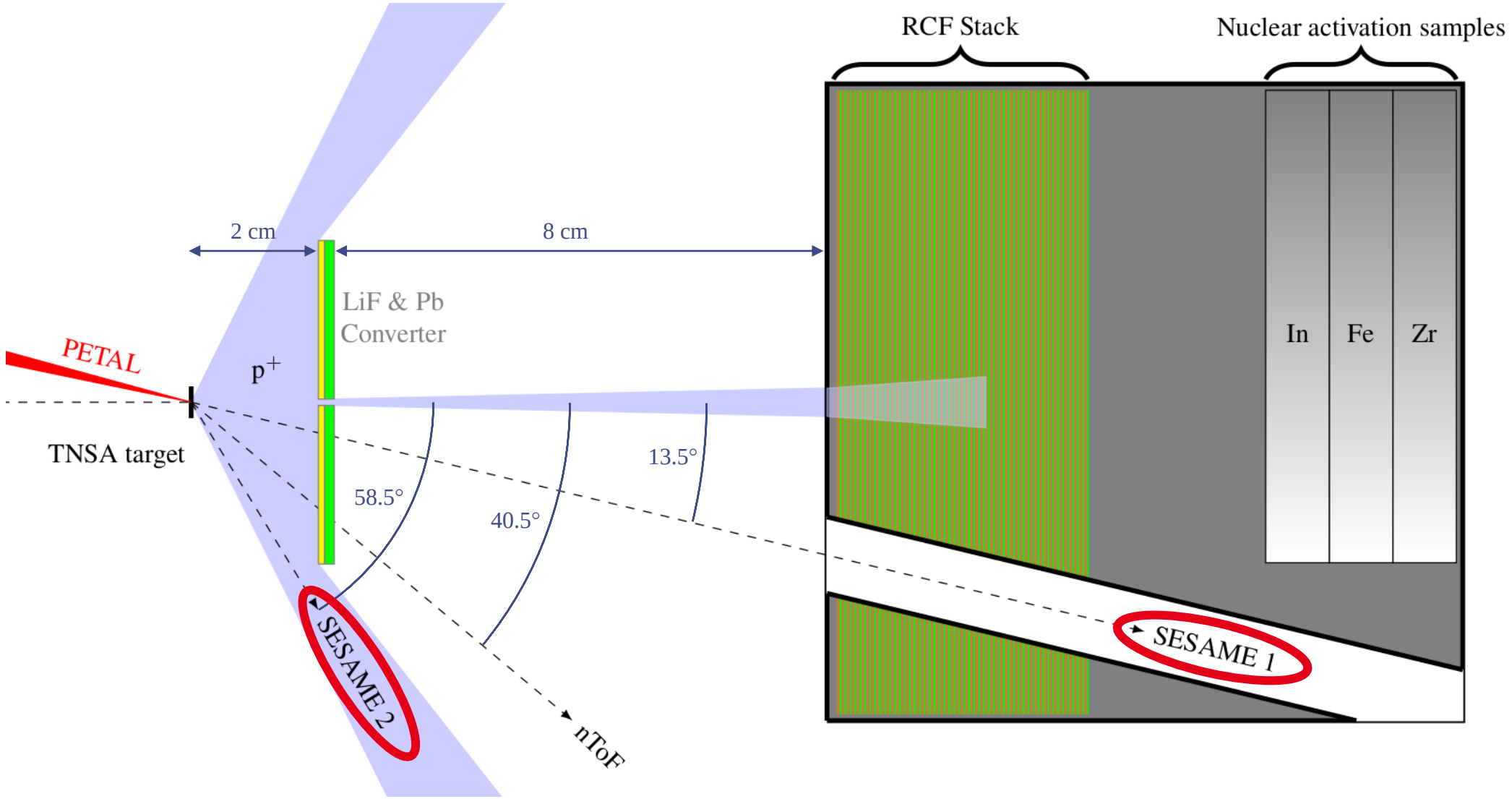

Spectromètres magnétiques

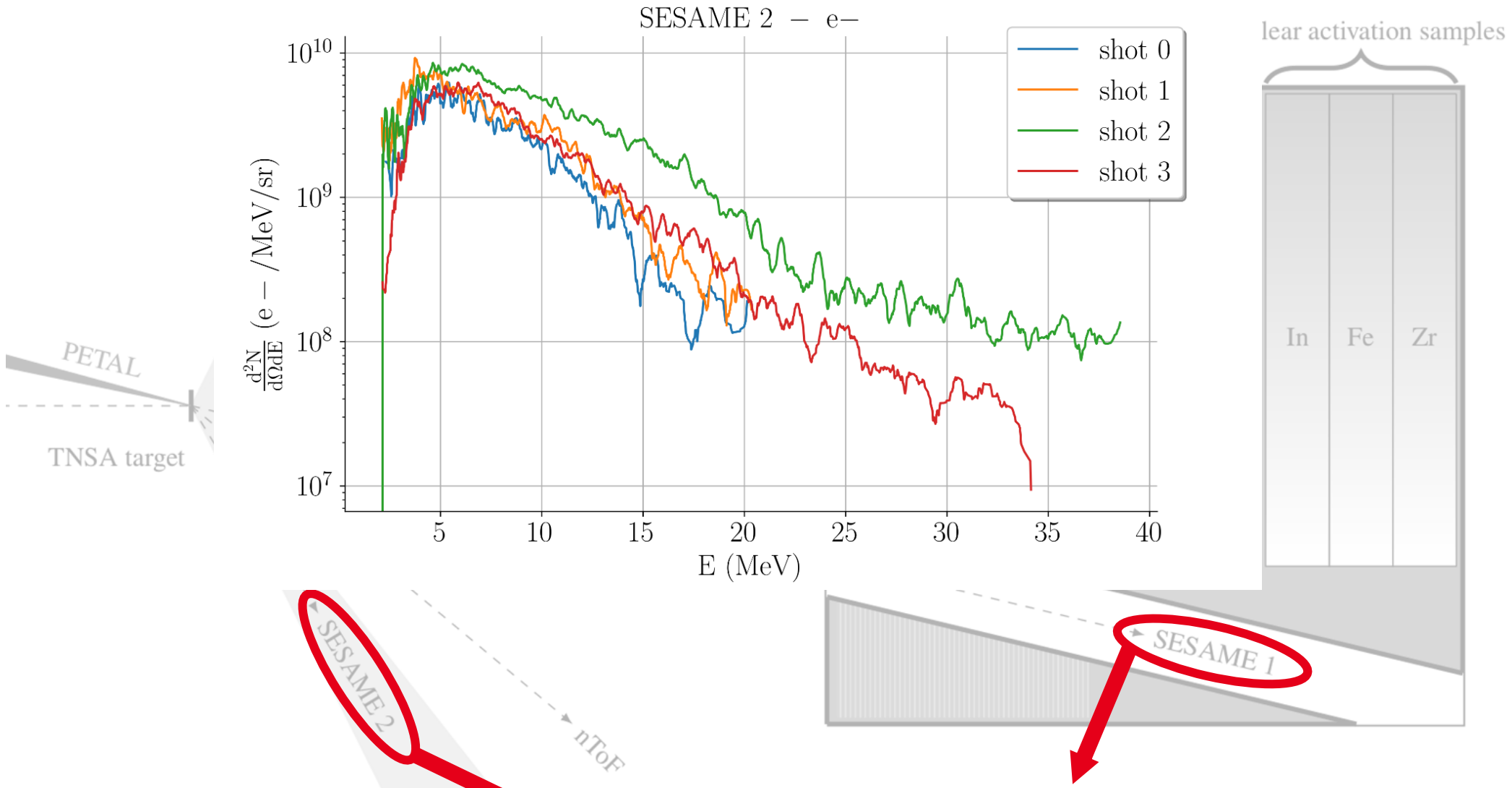

Électrons + Photons jusqu'à **40 MeV**

Empilements de films radiochromiques (RCFs)

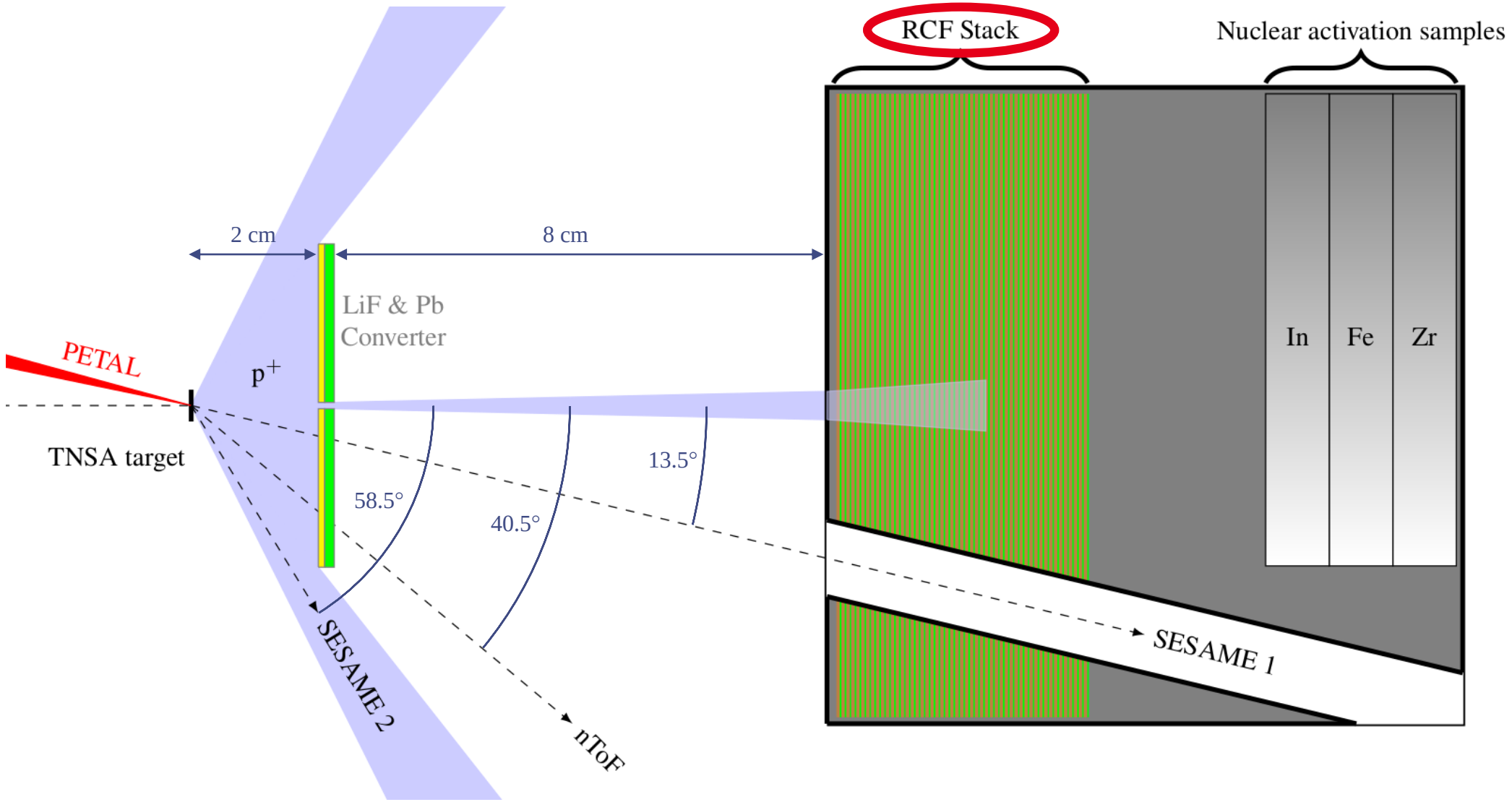

Empilements de films radiochromiques (RCFs)

Jusqu'à **10^{14}** protons(> 2 MeV)
Énergie maximale: **53 MeV**

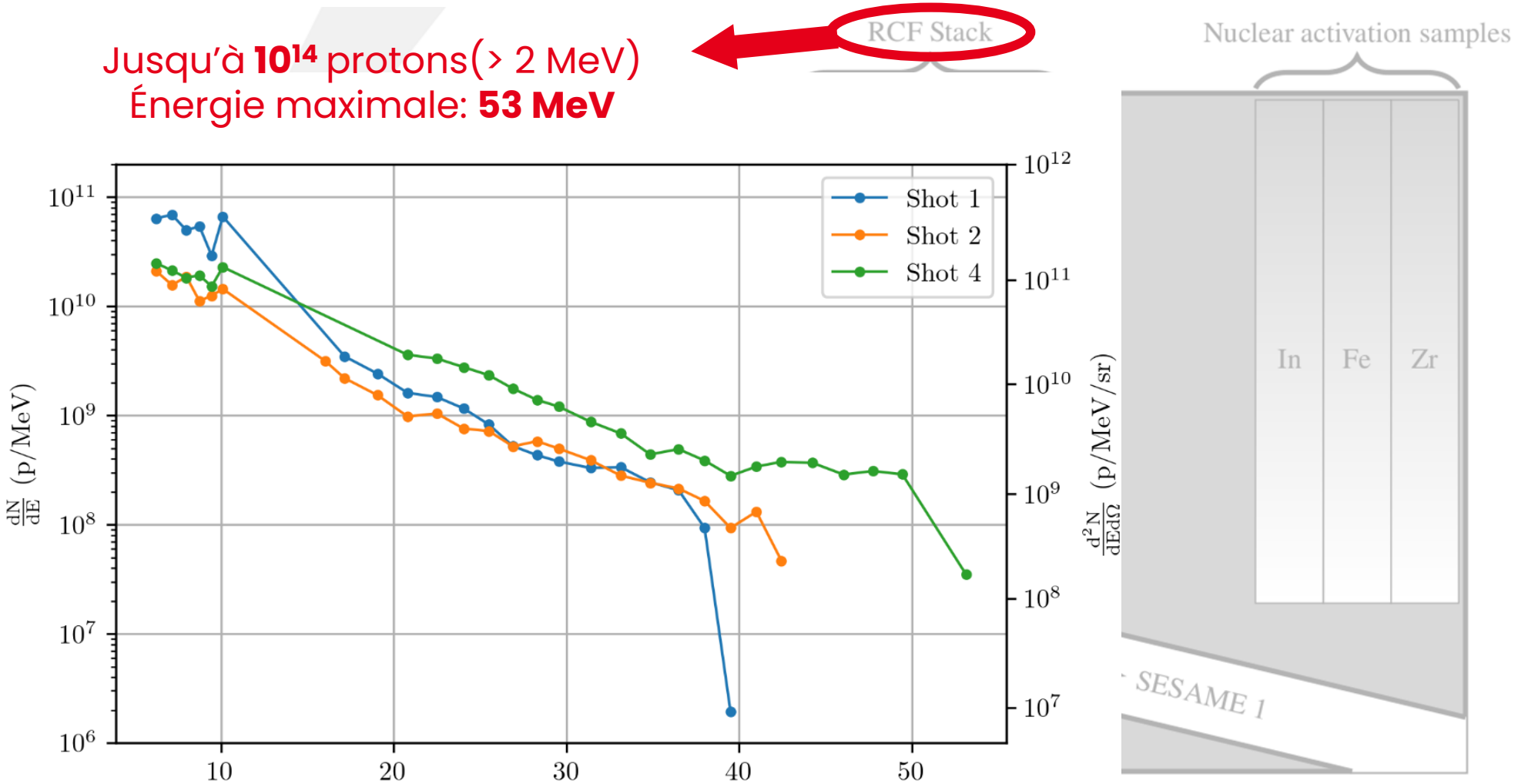

Détecteurs temps de vol neutrons (nToFs)

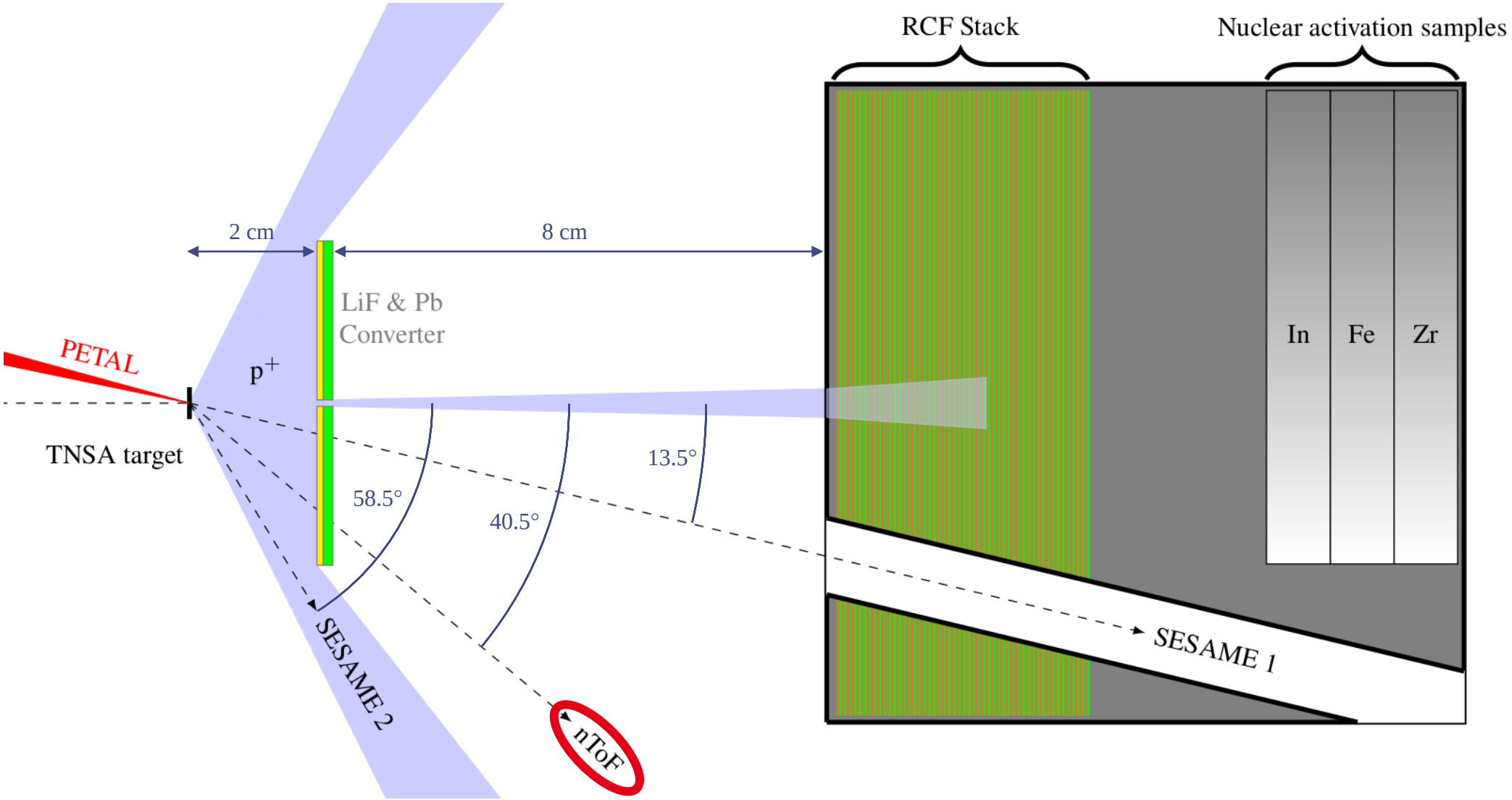

Détecteurs temps de vol neutrons (nToFs)

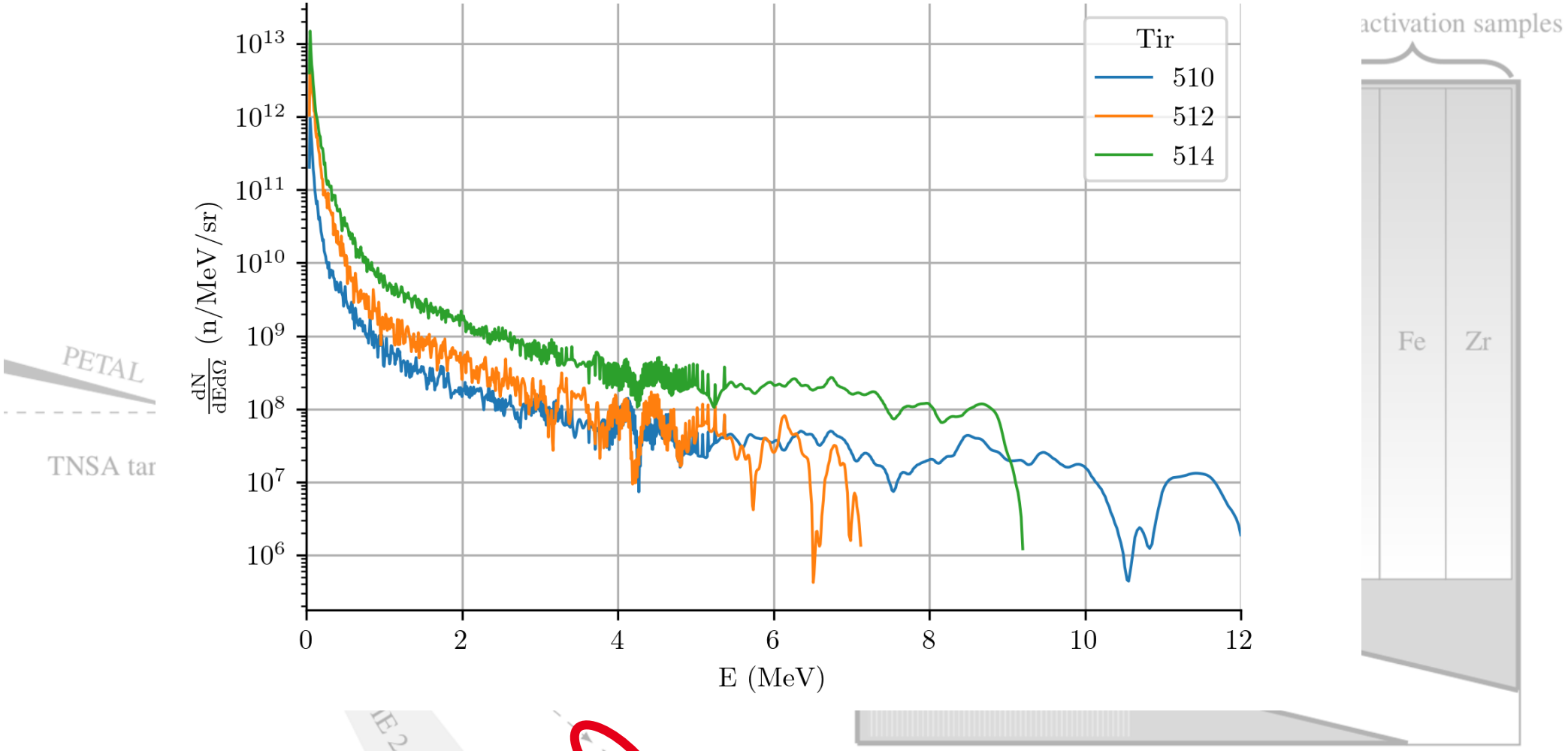

Jusqu'à **5.55×10¹⁰** neutrons rapides (> 1 MeV)
Énergie maximale: **30 MeV**

Pastilles d'activation nucléaire

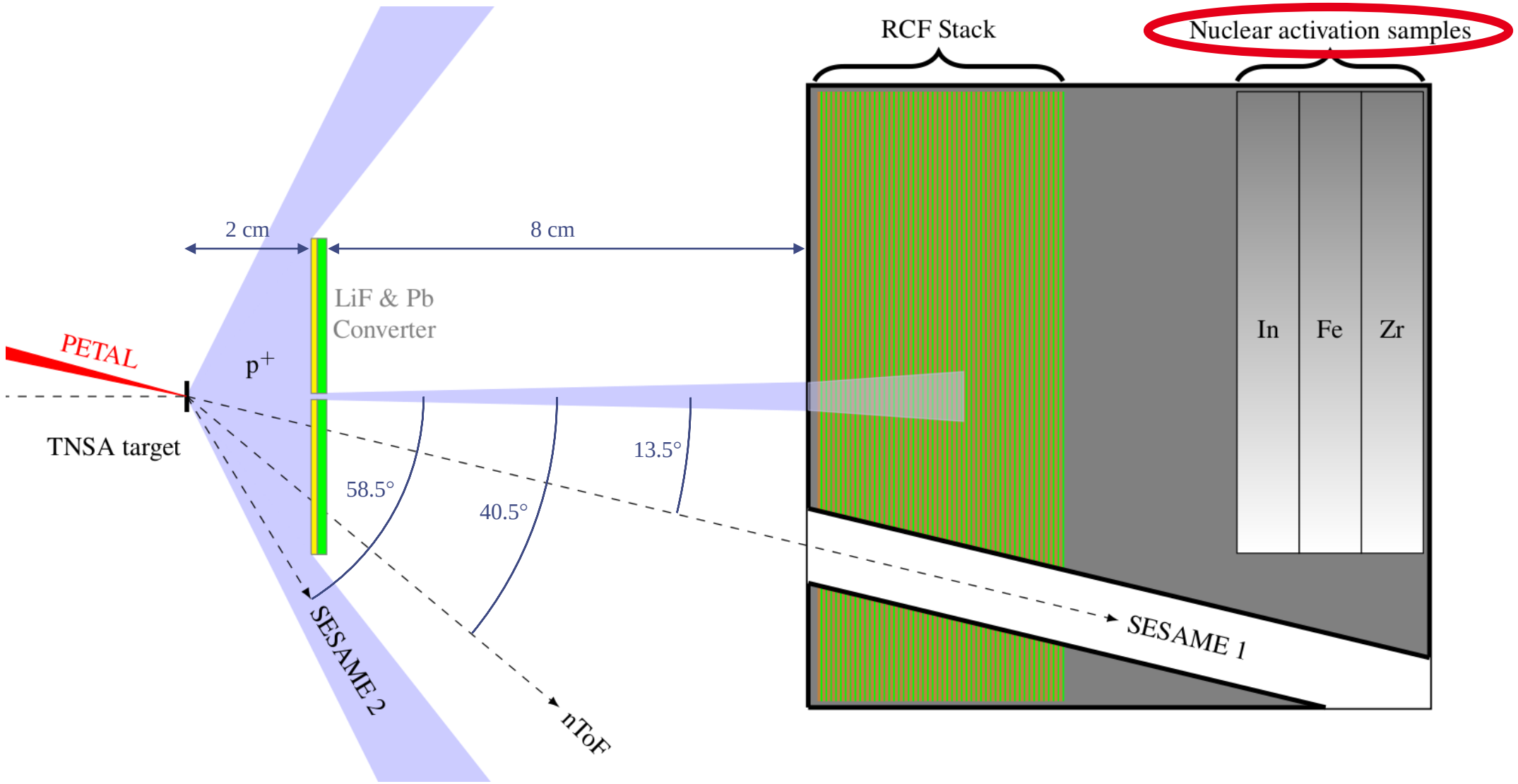

Pastilles d'activation nucléaire

Mesures p^+, e^-, n et γ et + Simulations Geant4
(activation neutronique + photonucléaire)

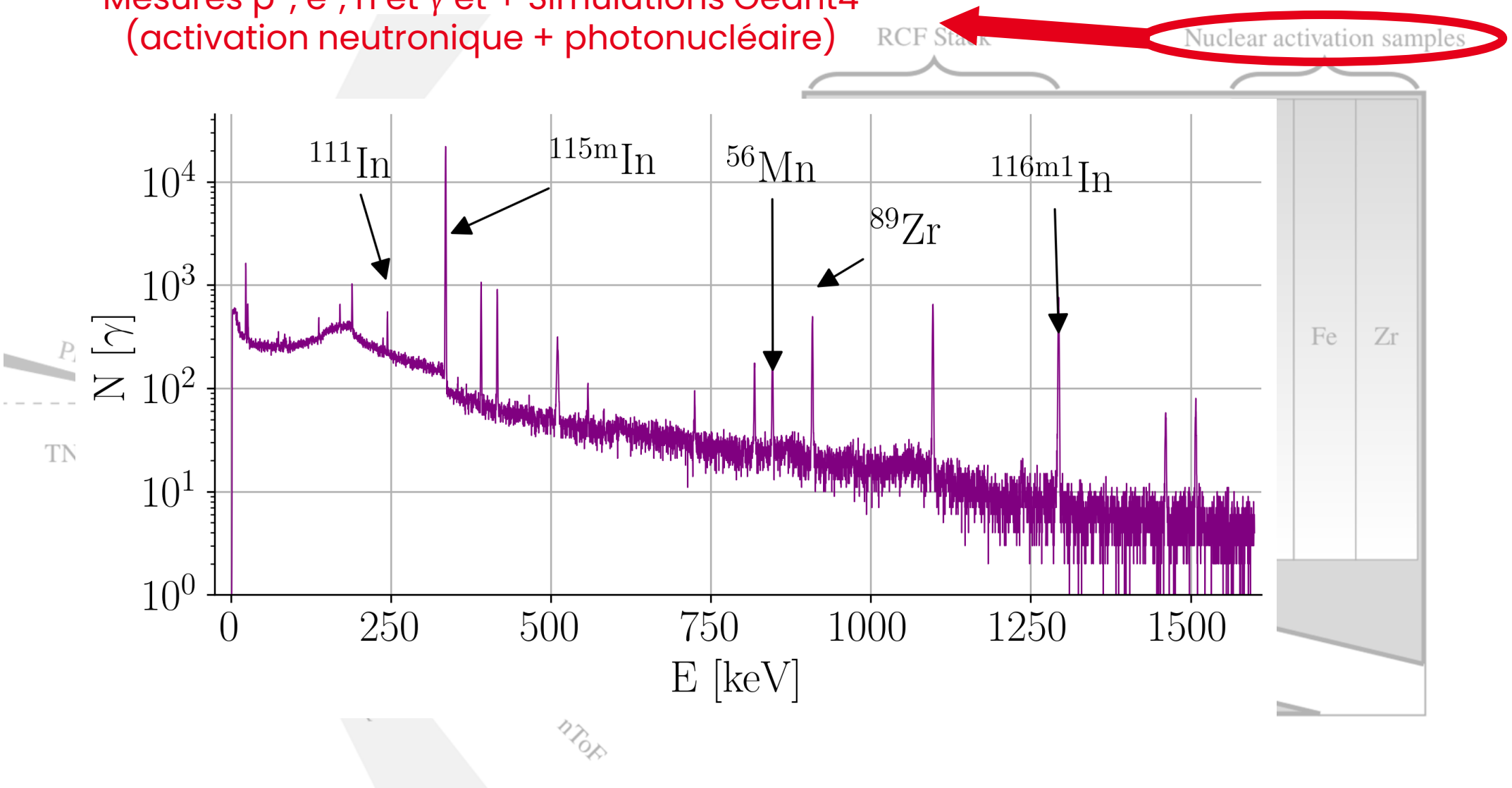

Merci de votre attention

Mail: lucas.ribotte@cea.fr

Soutiens PETAL:

Le projet PETAL a été mis en œuvre par le CEA grâce aux financements de la région Nouvelle-Aquitaine (maître d'ouvrage), du gouvernement français et de l'Union Européenne. Ce travail est soutenu par la région Nouvelle-Aquitaine dans le cadre du projet PETAL-Upgrade (contrats #13532820, #22577420 et #42979220).

Détection d'anomalies temporelles sur les données opérationnelles du cyclotron ARRONAX par l'approche hybride Autoencodeur-Forêt d'Isolation

Journées Accélérateurs 2025 de la SFP

Fatima BASBOUS
Dirigée par: Ferid HADDAD
Encadrée par: Diana MATEUS et Freddy POIRIER

GIP ARRONAX

1. **Production de radionucléides pour la médecine nucléaire**
   - Imagerie
   - Thérapie

2. **Recherche et Développement**
   - Radiochimie et radiobiologie
   - Physique et développement de détecteurs
   - Formation et enseignement

Pourquoi la détection d’anomalies dans les données opérationnelles du cyclotron C70XP?

01

Complexité du système

Des centaines de capteurs et dispositifs de contrôle, interactions entre sous-systèmes.

02

Risque élevé

La panne d’un seul sous-système peut compromettre l’expérience et perturber l’accélérateur.

Détection d’anomalies

- Assurer la fiabilité et la sécurité du cyclotron
- Garantir la continuité des expériences
- Identifier précocement les comportements inhabituels

Poirier et al. (2023)

Isolation Forest: Une approche de référence

Un des premiers algorithmes spécifiquement conçus pour la détection d'anomalies (*Liu et al. (2008)*)

Atouts

Efficacité, scalabilité, large utilisation dans des cas réels (*Chua et al. (2024), (Kumar et al., 2024), Zerkouk et al. (2023), Ahmed et al. (2019)*)

Limites

Difficultés avec les anomalies subtiles dues aux partitions parallèles aux axes.

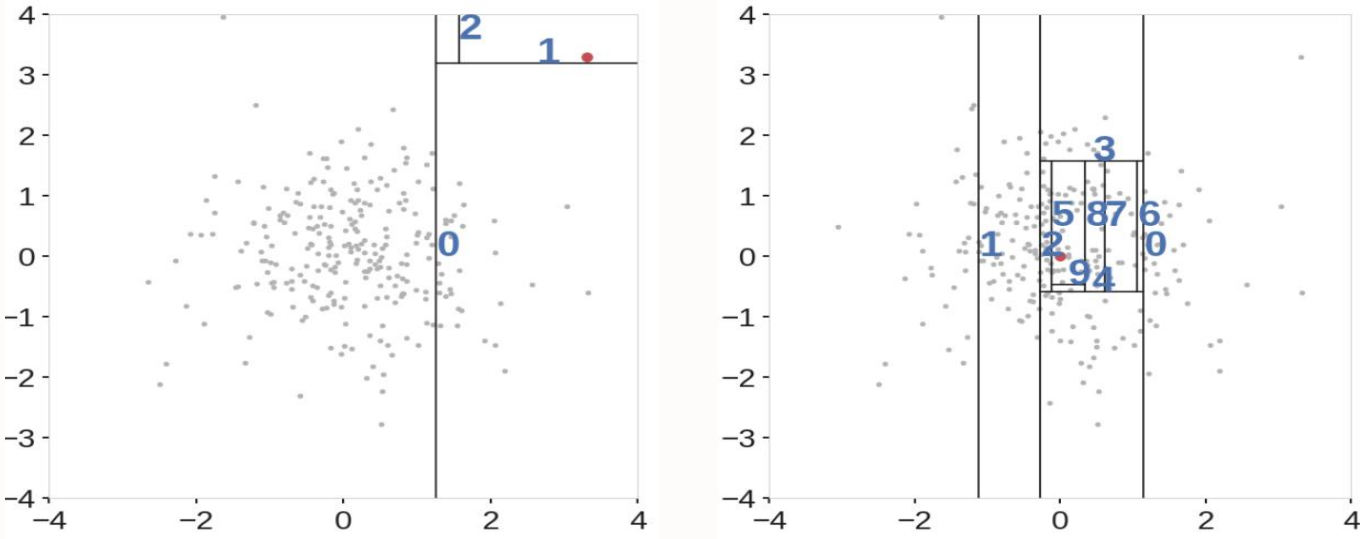

analyticsvidhya.com

Exemple d'isolement d'une anomalie globale (gauche) et d'une anomalie subtile (droite)

Anomalies globales et locales

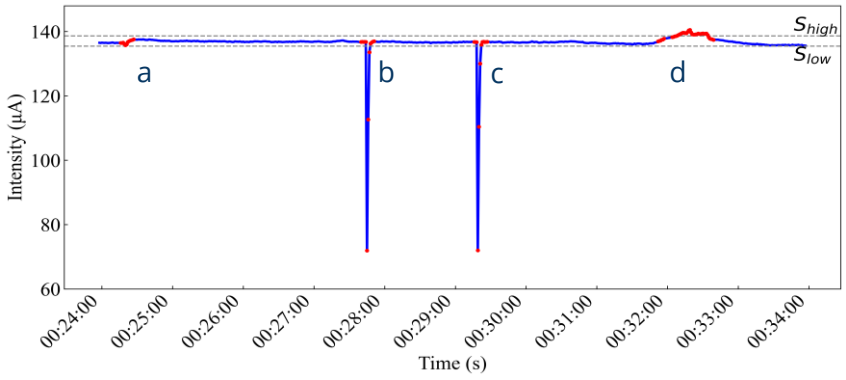

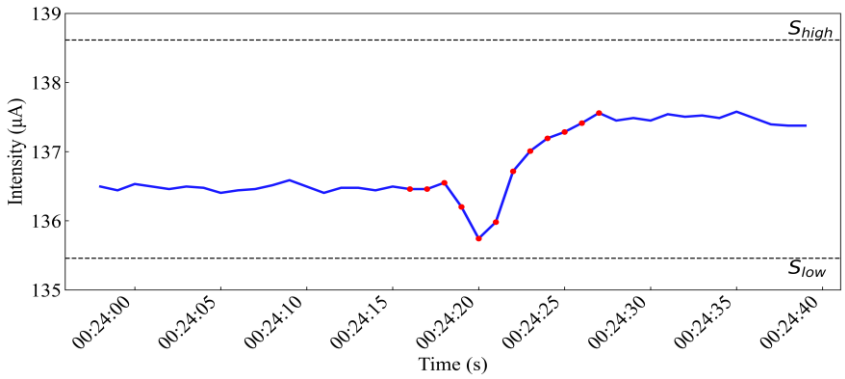

Les anomalies globales (b, c et d) sont visibles en figure (a), alors que un zoom de l'anomalie locale (a) est représentée en figure (b)

Anomalies globales
fortes déviations hors seuils → visibles à grande échelle

Anomalies locales
fluctuations internes importantes malgré des valeurs dans les seuils → visibles seulement en zoom

Surmonter les limites d'Isolation Forest : Trois axes explorés, un manque à combler

Trois axes de recherche dans la littérature

Amélioration de l'algorithme	Pré-traitement	Post traitement
Xu et al. (2023), Hariri et al. (2021), Lesouple et al. (2021), Ding & Xing (2020)	Chen et al. (2020), Puggini & McLoone (2018)	Alsini et al. (2021), Aminanto et al. (2020)

Gap identifié

- Peu d'études explorent la transformation de l'espace de caractéristiques.
- La représentation des données influence fortement la performance de IF.

Méthodologie proposée (AE-IF)

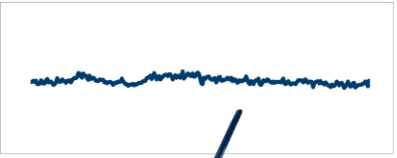

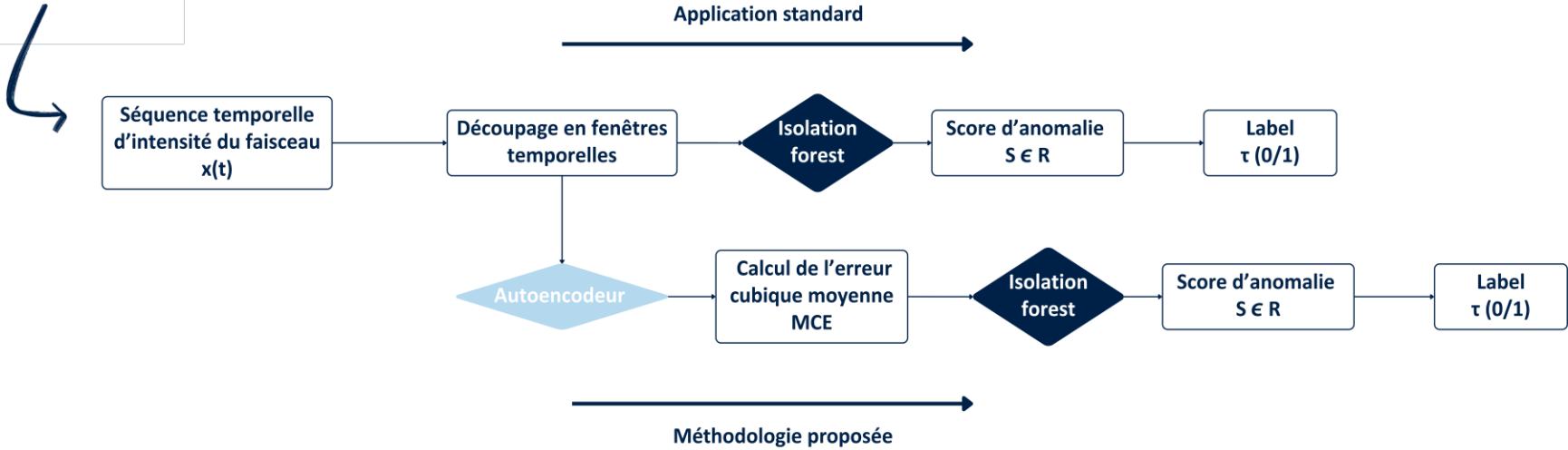

Comparaison entre l'application de l'Isolation Forest standard et la méthodologie hybride AE–IF où un autoencodeur transforme les données brutes et fournit les erreurs de reconstruction à Isolation Forest

De l'IF seul au modèle AE-IF: Résultats obtenus

IF (Standard)

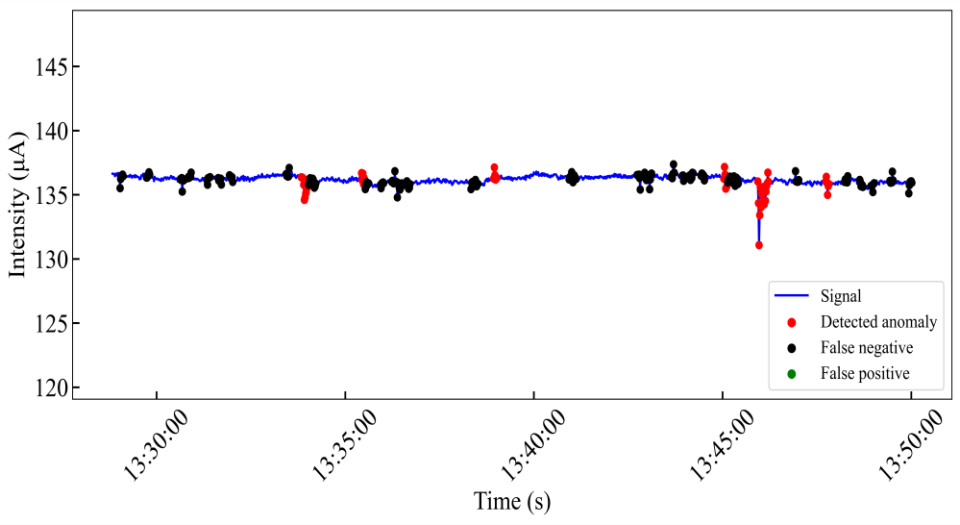

AE-IF (Proposé)

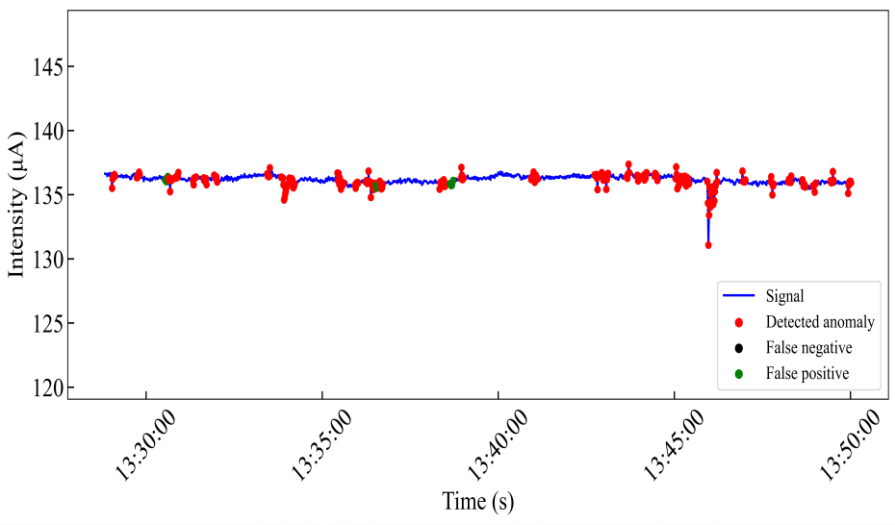

Figure de gauche : IF échoue à détecter certaines anomalies subtiles. Figure de droite : AE-IF les détecte efficacement.

Conclusion et perspectives

Apport de la méthode AE-IF

La méthode AE-IF améliore significativement la détection de toutes les anomalies, globales et locales.

Perspectives et applications

- Stabilisation des irradiations
- Réduction du temps d’irradiation pour la production des radionucléides
- Ouverture vers la flash-thérapie

MERCI!

STUDY OF LONGITUDINAL BUNCH-BY-BUNCH FEEDBACK IN AN ULTRA-LOW-EMITTANCE RING IN THE PRESENCE OF BUNCH LENGTHENING CAVITIES

Elene Kravishvili
Supervisor: Ryutaro Nagaoka

Upgrade of Soleil ring and aim of PhD thesis

The SOLEIL ring will be upgraded to SOLEIL II with much lower emittance, while keeping the same beam current.

- New main RF cavities will be installed
  - *This may introduce higher-order-mode (HOM) instabilities.*
- New harmonic cavities will also be added to lengthen the bunches and improve beam lifetime.
  - *However, these harmonic cavities can create additional instabilities, which may limit the achievable bunch lengthening.*

Developing a longitudinal feedback system could mitigate the HOM instabilities from the main cavities and also control the new instabilities from the harmonic cavities, thus relaxing their limitations.

- Longitudinal feedback for SOLEIL II must be developed from scratch (3 parts):
  - Detection → pick up beam signal.
  - Processing → filter & compute correction (FIR filter, etc.)
  - Kicker → apply correction kick to stabilize the beam
- Studies required for all three components: **detection, processing, kicker**
- **Kicker design** must suppress expected HOMs from main cavities
- PhD goal: develop a **complete FBL system** including a kicker able to cure HOMs and instabilities from harmonic cavities

FBL experiment - FBL test: Preliminary test

At Soleil, we have a transverse feedback system that could also be used for longitudinal studies by simple re-cabling. We took the opportunity to plan this experiment, with the main motivation being to gain experience for the whole group, since longitudinal feedback is a very new development at Soleil and has never been operated here before.

- During the session, we applied RF modulation with an amplitude of 0.3 V. The ADC data shows clear oscillations in the longitudinal plane, and the FFT reveals a peak at the synchrotron frequency (~4 kHz), confirming the excitation.

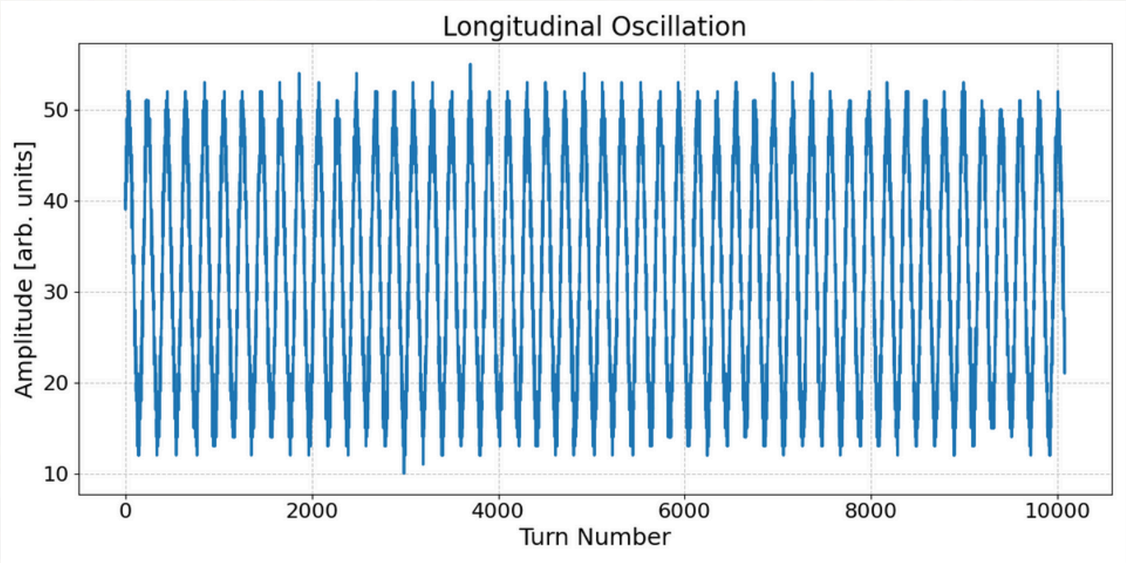

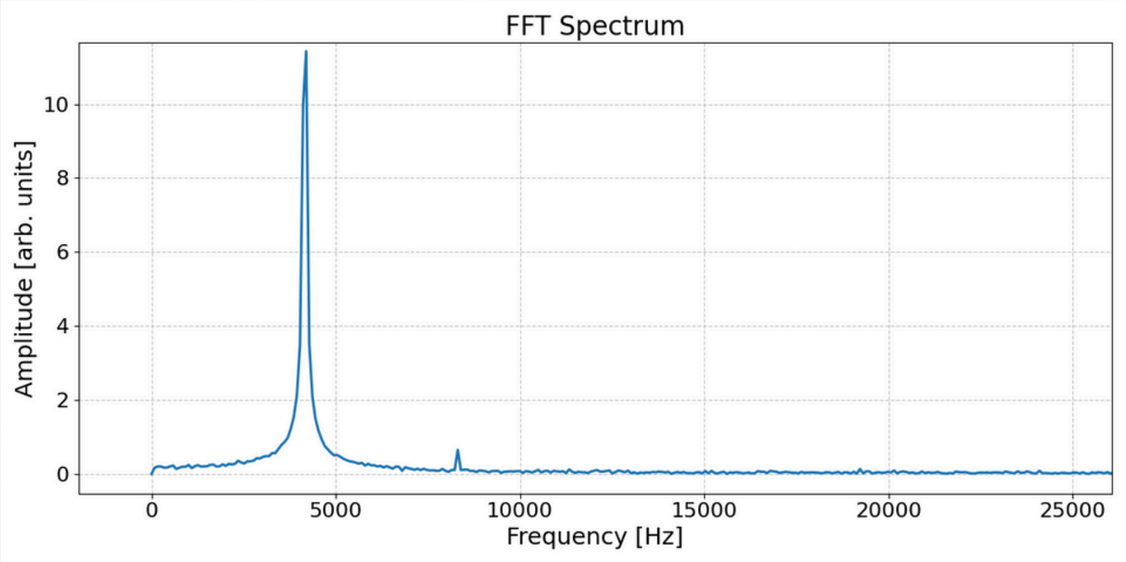

FBL test - preparation for the experiment

Front end

- Normally, BPMs are used in difference mode → detect betatron oscillations, which are relatively fast.
- To study synchrotron (longitudinal) oscillations, we switched to sum mode, which gives us the charge signal.
- Synchrotron oscillations are much slower, and the BPM signal is weak.
- To increase sensitivity, colleagues developed a comb filter

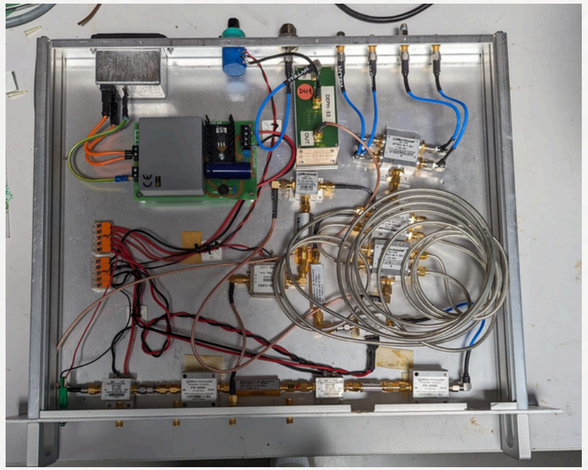

Stripline

- Electric field at the two electrodes in the beginning and in the end of stripline are not cancelling each other which gives us a longitudinal kick.
- We evaluated the strength of the kick that the stripline could apply to the beam using GdfidL, by calculating its shunt impedance.
- H Stripline

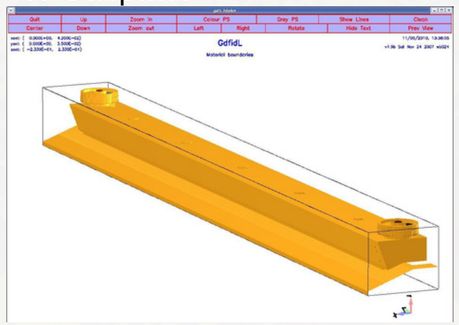

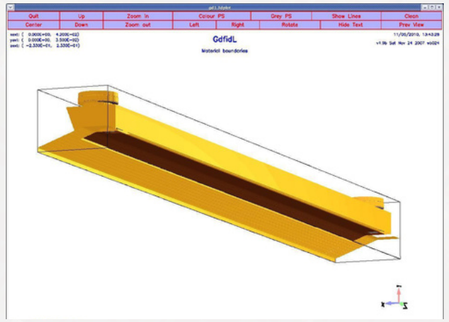

FIR filter

- For the stripline used to feedback the beam, we prepared the FIR filter coefficients. Since the synchrotron frequency is much lower than the betatron frequency, the filter required many more taps: while the transverse feedback uses only 5 taps, the longitudinal case required about 250.

- To verify that the implementation of FIR coefficients were correct, we used pulse generator via the processor, which was sending single pulse (like delta funtion) to the processor and time interval was higher then revolution time times the tap number, so that the output will be only one coefficient each time

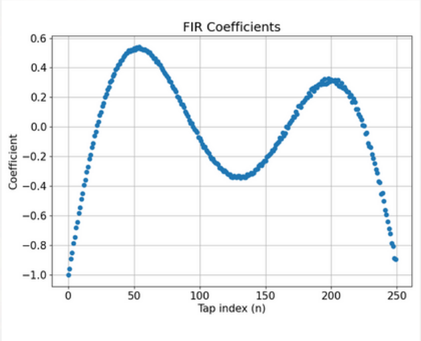

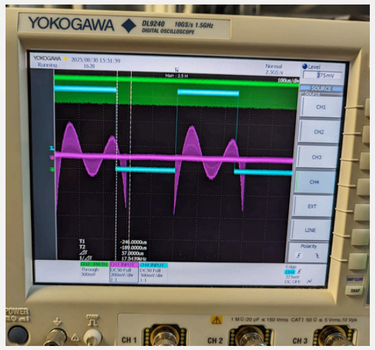

FBL test - experiment and results

Frequency applied to stripline kick: $f = nf_0 + f_s$

- The spectrum analyzer shows a peak at the applied frequency, confirming that the stripline is exciting the beam.
- The signals of the kick and the bunch pass in the stripline must be synchronized to ensure the beam is kicked at the correct location.

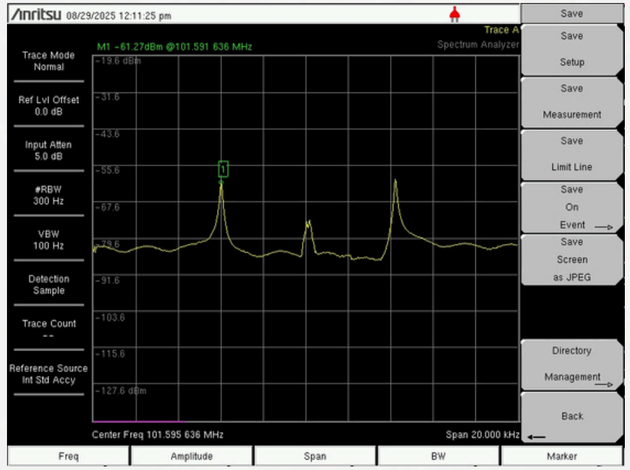

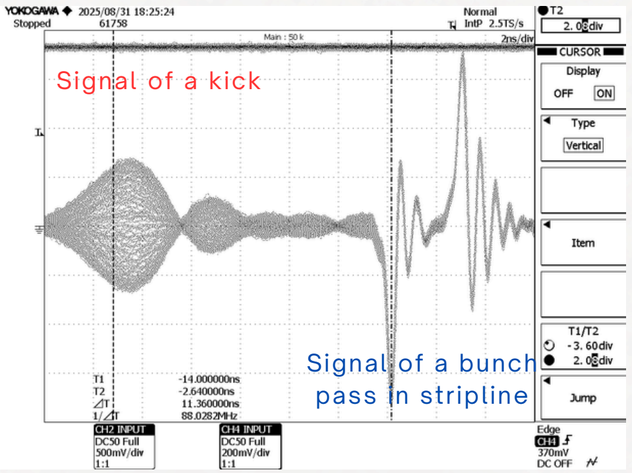

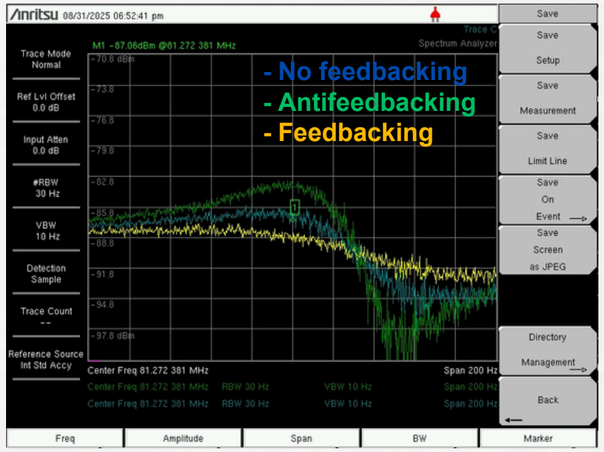

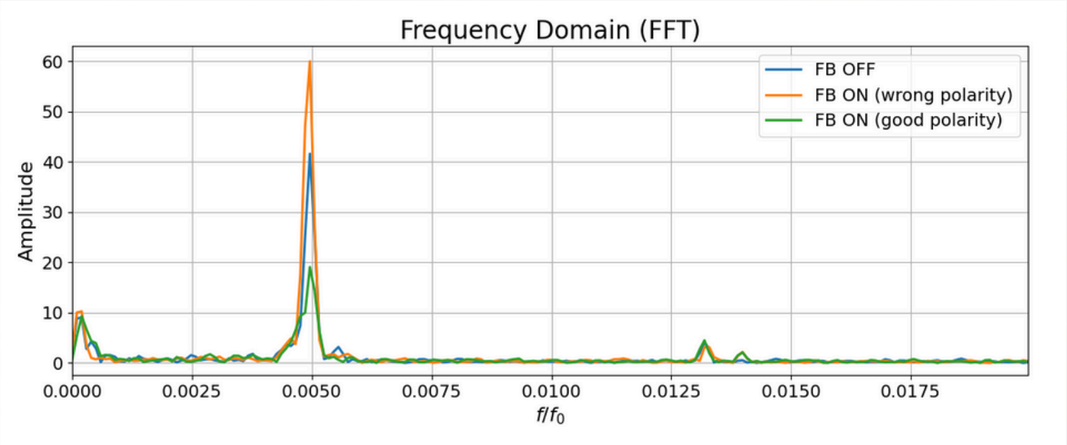

- The FFT peak decreases when feedback is applied with the correct polarity.
- Post-processing of ADC data reproduces the same results.

Merci de votre attention !

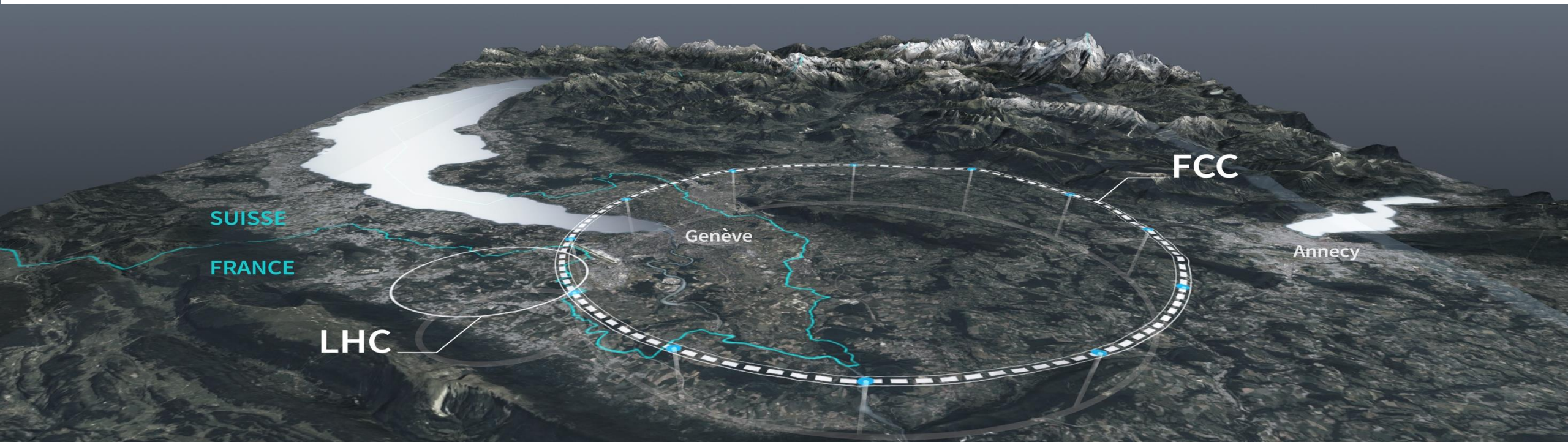

Updated monochromatization interaction region optics design based on FCC-ee GHC lattice

A. Korsun, A. Faus-Golfe, IJCLab, Orsay, France
Université Paris-Saclay

Outline

- Introduction and motivation
- Monochromatization Principle
- FCC-ee Monochromatization IR Optics Design
- Performance Check of FCC-ee MonochroM Optics
- Summary and outlook

Introduction: Physics Requirements

- **FCC-ee modes:**
  - The FCC-ee standard modes:
    - Four different energy operation modes:

      Z, $W^{\pm}$, Zh **and** $t\bar{t}$
  - The optional fifth mode: ***s***-channel Higgs production mode
    - The measurement of the electron Yukawa coupling, in dedicated runs at 125 GeV with center-of-mass (CM) energy spread (5-10 MeV). But the natural collision energy spread, due to the synchrotron radiation, is about 50 MeV.

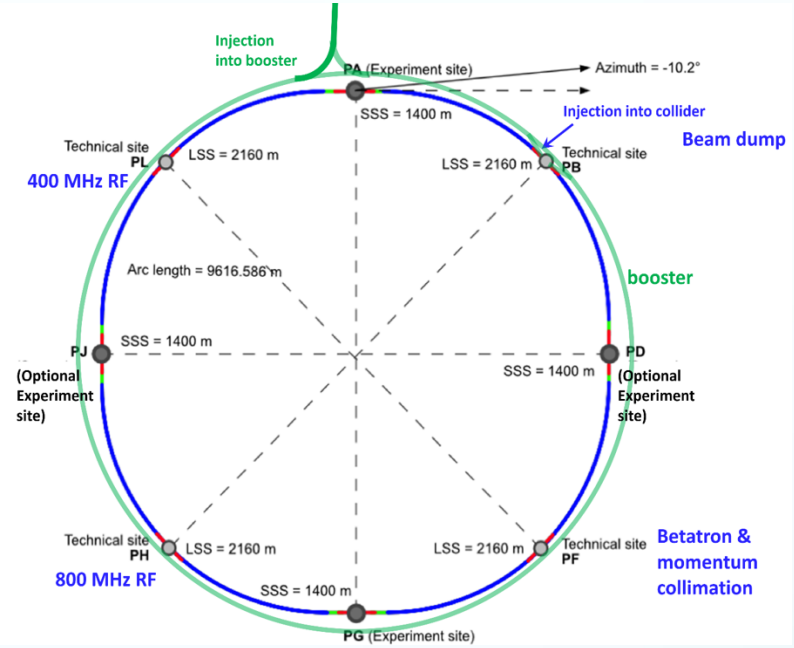

- **Requirements:**
  - Reduce the CM energy spread from 50 MeV to 5 MeV, which is comparable to the resonant width of the standard model Higgs Boson itself (4.2 MeV)

Monochromatization Principle

Standard

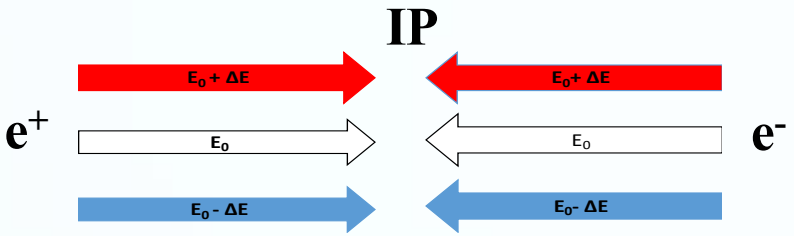

$D^*_{x,y}=0$

correlation between transverse spatial position and energy deviation

Monochromatization

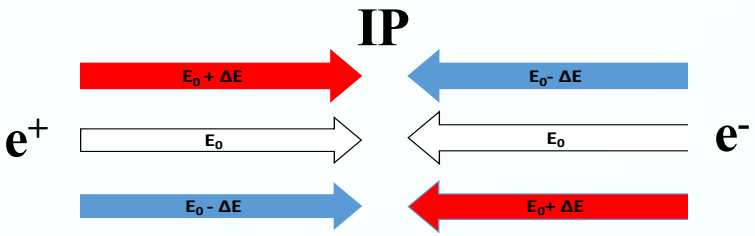

$D^*_{x+} = - D^*_{x-} = D^*_x$

$D^*_{y+} = - D^*_{y-} = D^*_y$

Opposite correlations between transverse spatial position and energy deviation

CM energy

$$w = 2(E_b + \Delta E)$$

$$w = 2E_b + O(\Delta E)^2$$

Spread of the CM energies

$$\sigma_w = \sqrt{2}E_b\sigma_\delta$$

$$\sigma_w = \frac{\sqrt{2}E_b\sigma_\delta}{\lambda}$$

Monochromatization factor

$$\lambda = 1$$

$$\lambda = \left(1 + \sigma_\delta^2\left(\frac{D_x^{*2}}{\sigma_{x\beta}^{*2}} + \frac{D_y^{*2}}{\sigma_{y\beta}^{*2}}\right)\right)^{1/2}$$

Luminosity

$$L_0 = \frac{k_b f_r N_+ N_-}{4\pi\sigma_{x\beta}^*\sigma_{y\beta}^*}$$

$$L = \frac{L_0}{\lambda}$$

betatronic beam sizes at the IP

$$\sigma^*_{x,y} = \sqrt{\beta^*_{x,y}\epsilon_{x,y} + \left(D^*_{x,y}\sigma_\delta\right)^2}$$

dispersive beam size at the IP

Enhancement of energy resolution, and sometimes increase of the relative frequency of the events at the center of of the distribution but **luminosity loss !!!!**

Monochromatization in High-energy Colliders

In the previous case for low-energy e^+e^- colliders, the **relative energy spread** is mainly given by **SR** in the colliders arcs ($\sigma_\delta = \sigma_{\delta,SR}$). Alternatively in **high-energy e^+e^-**, we have to take into account also the **SR** created by the strong opposing EM field during collision or "**beamstrahlung**"(**BS**) ($N\gamma \propto 1/\sigma_z(\sigma^*_x + \sigma^*_y)$, with σ_z the bunch length).

Standard BS

$D^*_{x,y}=0$

Energy spread

$$\sigma_{\delta,tot} = \sqrt{\frac{1}{2}\sigma^2_{\delta,SR} + \sqrt{\frac{1}{4}\sigma^4_{\delta,SR} + A\frac{\sigma^2_{\delta,SR}}{\sigma^2_{z,SR}}}}$$

$$A = \frac{275}{36\,\pi^{\frac{3}{2}}}\frac{n_{IP}\tau_E}{4T_{rev}}\frac{r_e{}^5 N_b{}^3\gamma^2}{\alpha\sigma^*_{x,SR}{}^3}$$

Horizontal emittance

$$\varepsilon_{x,tot} \approx \varepsilon_{x,SR}$$

Bunch length

$$\sigma_{z.tot} = \frac{\alpha_c C}{2\pi Q_s}\sigma_{\delta,tot}$$

BS at **high-energy** with $D_x^*=0$, has more **impact** on **energy spread** in standard mode than in monochromatization mode.

Monochromatization BS

$D^*_{x+} = -D^*_{x-} = D^*_x$
$D^*_{y+} = -D^*_{y-} = D^*_y$

Coupled system to be solved numerically

Energy spread

$$\sigma^2_{\delta,tot} = \sigma^2_{\delta,SR} + \frac{B}{D_x^{*3}\sigma^5_{\delta,tot}}$$

$$B \approx 50\frac{n_{IP}\tau_E}{T_{rev}}\frac{r_e^5 N_b^3\gamma^2}{(\alpha_c C/(2\pi Q_s))^2}$$

Horizontal emittance

$$\varepsilon_{x,tot} \approx \varepsilon_{x,SR} + \frac{2B}{D_x^*\beta_x^*\sigma^5_{\delta,tot}}$$

Bunch length

$$\sigma_{z.tot} = \frac{\alpha_c C}{2\pi Q_s}\sigma_{\delta,tot}$$

BS with **monochromatization** at **high-energy**, **avoids** the **blow up** of the relative beam energy spread, which is significant in standard mode with $D_x^*=0$.

M. A. Valdivia García, F. Zimmermann, Towards an optimized monochromatization for direct Higgs production in future circular e+ e- Colliders, in CERN-BINP Workshop for Young Scientists in e+e- Colliders, pp. 1–12 (2017)

Monochrom Implementation in FCC-ee GHC IR

Despite the **simplicity** of the **monochromatization concept**, the **creation** and the **control** of the necessary **H/V dispersion** function of opposite signs at the IP could be **rather difficult to implement**.

Monochromatization factor

$$\lambda = \sqrt{1 + \sigma_{\delta,SR}^2 \left(\frac{D_x^{*2}}{\sigma_{x\beta}^{*2}} + \frac{D_y^{*2}}{\sigma_{y\beta}^{*2}} \right)}$$

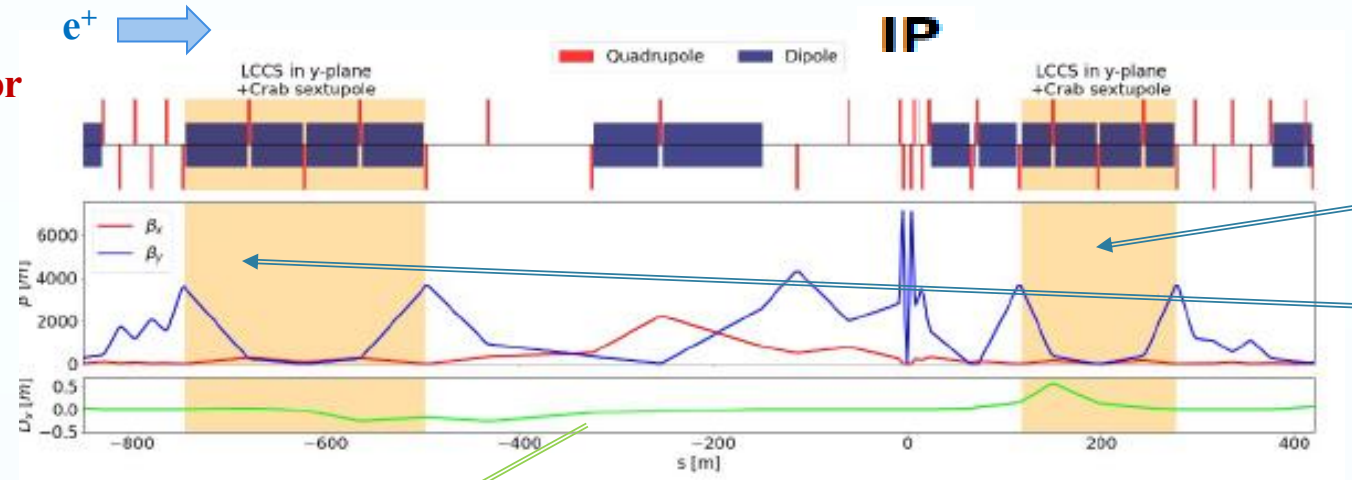

IR GHC: Local Chromaticity Correction Section (LCCS) with **Crab Sextupoles** (CS) in the vertical to produce a crab waist collision

➢ $D^*_x \neq 0$ generation at the IP

In FCC-ee IR region, the **large crossing angle of 30 mrad** in the H-plane and the **local chromaticity correction system (LCCS)** are achieved using **H-dipoles** at both sides of the IP, creating some **H-dispersion** D^*_x ($D_x \neq 0$ in the LCCS and $D_x = 0$ close to the IP for high-luminosity). $D^*_x \neq 0$ can be generated **(~10 cm)** by intentionally **mismatching D_x** in the LCCS.

➢ $D^*_y \neq 0$ generation at the IP

Because $\sigma^*_{y\beta} <<< \sigma^*_{x\beta}$, about **100 times smaller D^*_y (~mm)** is needed to get the same monochromatization factor. Therefore, **$D^*_y \neq 0$** could be generated by implementing **skew quadrupoles** around IP. These quadrupoles could be located where the chromatic sextupole (CS) pairs are located in the LCC system.

FCCee H Monochromatization optic design

- **Comparison between Standard Survey and Horizontal Monochromatization Survey**
  - Standard Survey Plot

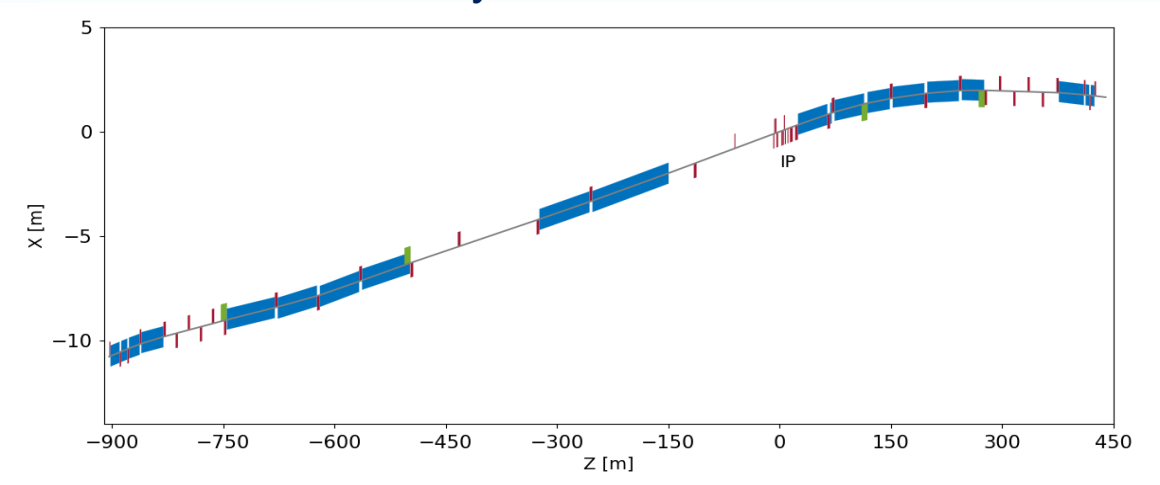

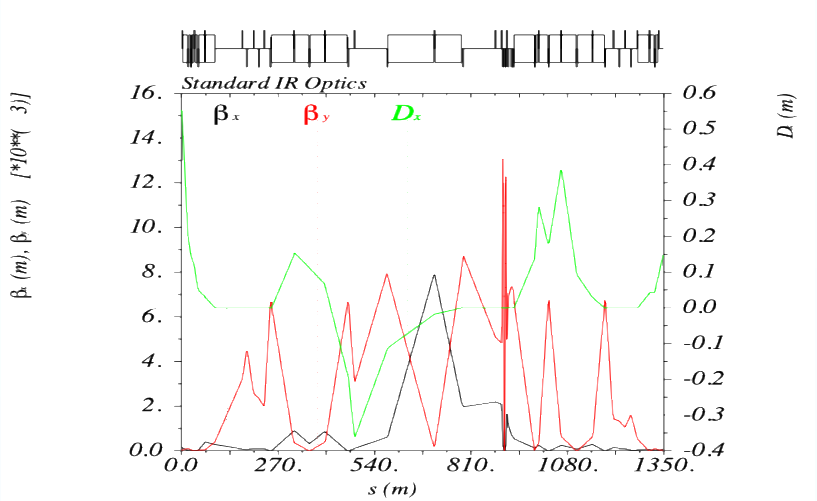

  - Monochromatization Survey Plot

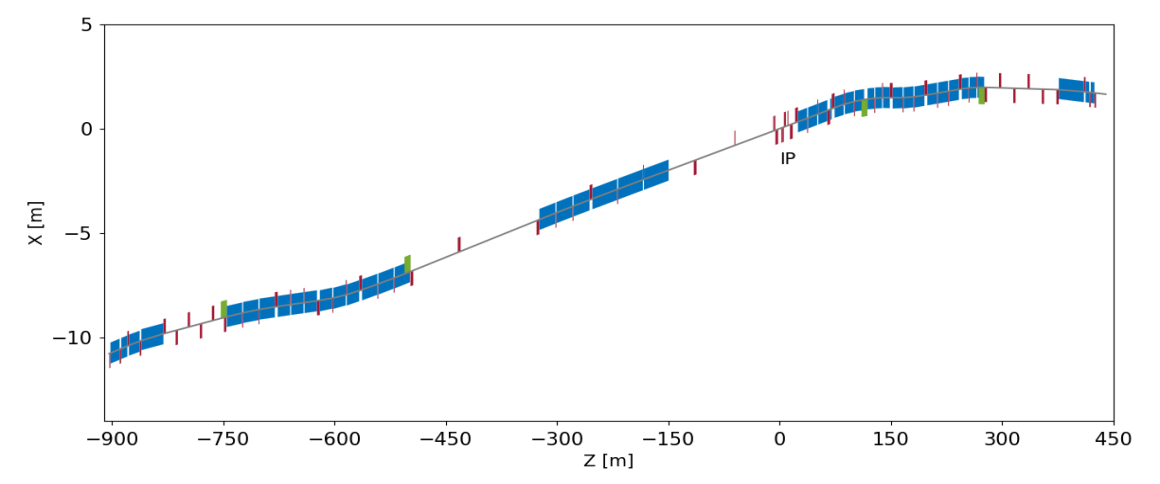

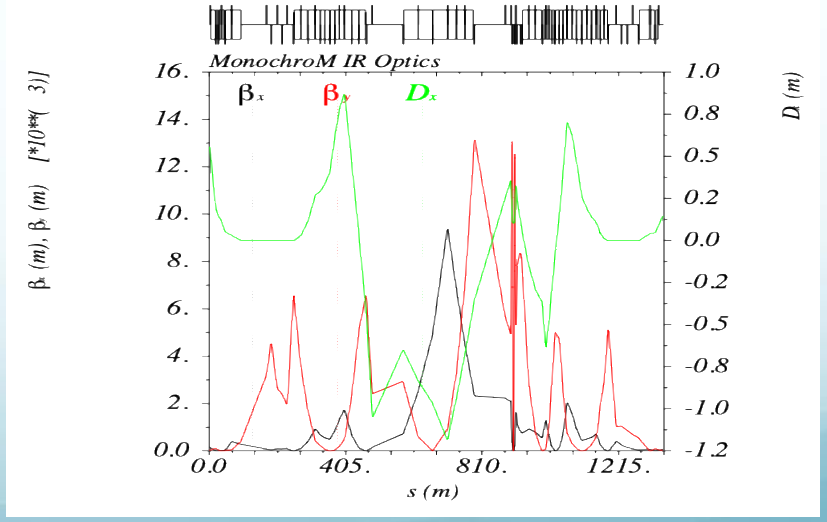

Parameters table for GHC Z V23 lattice

Parameters	Units	Standard	Standard_625	Monochrom_h_4ip	Monochrom_v_opt	Monochrom_v
Beam Energy E	GeV	45.6	62.5	62.5	62.5	62.5
# of IPs	/	4	4	4	4	4
Circumference	m	90658.816	90658.816	90658.816	90658.816	90658.816
Energy Loss/turn	MeV	39.4	138.1791153	143.0311645	137.1381791	138.1791153
SR power loss	MW	50.0	50.0	50.0	50.0	50.0
Beam current	mA	1270	360	350	360	360
Bunches/beam n_b	/	15880	12000	12000	12000	12000
Bunch population N_b	10^{11}	1.51	0.56	0.56	0.56	0.56
Horizontal emittance (SR/BS) ε_x	nm	0.71 / 0.71	1.317 / 1.317	1.68 / 4.12	1.32 / 1.32	1.31 / 1.31
Vertical emittance (SR/BS) ε_y	pm	1.4 / 1.4	2.64 / 2.64	3.32 / 3.32	4.8 / 85	4 / 533.9
Momentum compaction α_c	10^{-6}	28.6	28.0	27.4	27.9	27.9
$\beta^*_{x/y}$	mm	110 / 0.7	110 / 0.7	110 / 0.7	1500 / 0.7	110 / 0.7
$D^*_{x/y}$	m	0 / 0	0 / 0	0.105 / 0	0 / 0.001	0 / 0.001
Energy Spread (SR/BS) σ_δ	%	0.039 / 0.089	0.0537 / 0.074	0.0547 / 0.0558	0.0537 / 0.0564	0.0537 / 0.0689
MonochroM Factor (SR/BS) λ	/	1 / 1	1 / 1	2.7 / 1.96	9.31 / 2.51	10.23 / 1.5
CM energy spread (SR/BS) σ_W	MeV	25.3 / 57.4	47.47 / 65	17 / 27	5 / 29.9	4 / 40
Bunch length (SR/BS) σ_z	mm	5.6 / 13	5.4 / 7.25	5.32 / 5.34	5.4 / 5.5	5.4 / 6.8
Sychrotron tune Q_s	/	0.0288	0.041069085	0.041350116	0.041069108	0.041069085
Longitudinal damping time	turns	1158	452	437	456	452
Luminosity (SR/BS)	10^{34}cm^{-2} s^{-1}	360 / 140	28.9 / 18	20 / 9.35	2 / 1.35	2.3 / 0.9

Performance Check of FCC-ee MonochroM Optics

- **Luminosity and CM Energy Spread Calculations in Guinea-pig (with BS)**

- *FCC-ee Monochromatization Optics based on Z mode lattice*

Parameters		Standard ZES V23	MonochroM ZH V23	MonochroM ZV V23
RMS CM energy spread σ_w (with crab cavity)	[MeV]	64.90	27.17	29.90
Luminosity per IP (with crab cavity)	[10^{34}cm^{-2}s^{-1}]	18	9	1.35

- *FCC-ee Monochromatization Optics based on ttbar mode lattice*

Parameters		Standard TES V22	MonochroM TH V22	MonochroM TV V22
RMS CM energy spread σ_w (with crab cavity)	[MeV]	67.25	29.59	15.85
Luminosity per IP (with crab cavity)	[10^{34}cm^{-2}s^{-1}]	57.9	12.01	1.57

Summary and Outlook

- ✓ Parametric analysis for monochrome optimization (future optimization using ML)
- ✓ Design optics update of the monochromatization IR optics in the whole ring GHC lattice (future LCC lattice)
- ✓ Dynamic aperture and beam-beam studies in the case of the monochrom scheme with Xsuite tracking (brute force)
- ✓ Scanned beam-beam studies with the Circulant Matrix Model (semi-analytical)
- ➢ Exploration of possible experimental implementation on SuperKEKB, BEPC, and BEPCII

Thanks for you attention!

Impedance Modelling and Collective Effects in FCC-ee: Impact of Collimators and Optimization Strategies

Les Journées Accélérateurs de la Société Française de Physique (SFP), 7-10 October 2025

Dora Gibellieri[1,2,3], Carlo Zannini[1], Adnan Ghribi[2,3] and Mauro Migliorati[4,5]

[1]CERN [2]University of Caen Normandy [3]GANIL [4]Sapienza University of Rome [5]INFN

FCC-ee: impedance challenges

- **Model challenges:**
  - Necessity of a **highly flexible impedance/wake (I/W) model** in the development phase.
  - Improvement of devices' design after evaluation of impedance and impact on the machine.
  - Constant update of the FCC-ee impedance model.

- **Challenging simulation regime:**
  - Combination of **large beam** pipe dimension (30 mm radius) and **short bunch lengths** (5÷15 mm) ➔ computationally demanding simulations.
  - Very high number of mesh cells (~billions) in electromagnetic solvers ➔ CST.
  - Very high number of slices (~500) in tracking simulations ➔ Xsuite.

~ 95 B mesh cells

SIMULIA CST STUDIO SUITE

- **Beam pipe cut-off frequency:**
  - The beam **pipe cut-off** (~3 GHz) lies within the **relevant frequency spectrum** (up to ~20 GHz).
  - Modes above cut-off can be strongly excited ➔ leading to significant crosstalk between different devices.

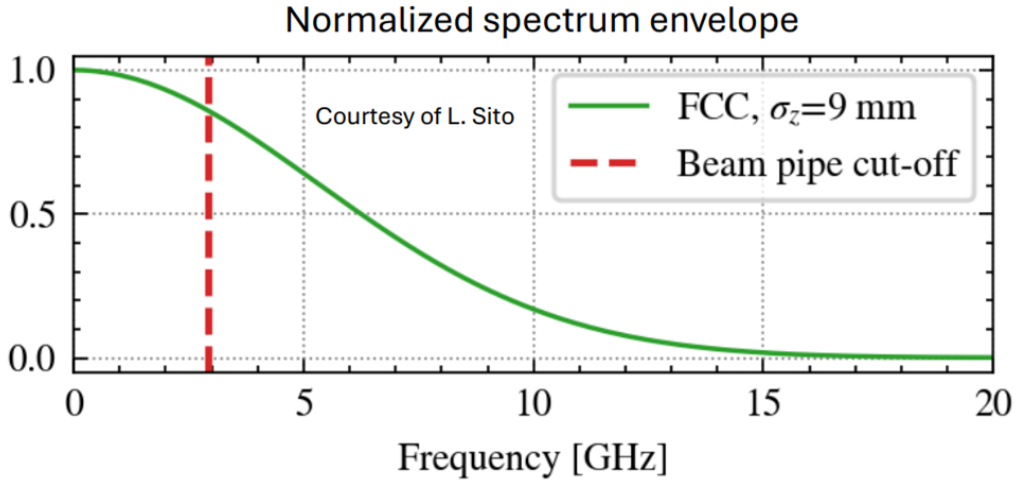

FCC-ee main ring impedance model

Identify main impedance contributors

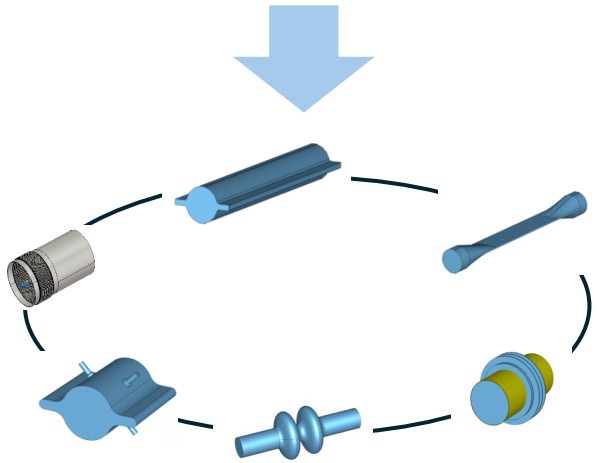

Updated elements in the FCC-ee I/W model:

- beam pipe: circular copper cross-section with a radius of 30 mm and two lateral winglets. Coated with a thin 150 nm layer of Non-Evaporable Getter (NEG)
- 41 collimators
- 132 single-cell 400 MHz RF cavities
- 10 000 BPMs
- 10 000 bellows
- tapers

FCC-ee main ring impedance model

Identify main impedance contributors → 3D EM Simulations and Analytical Model

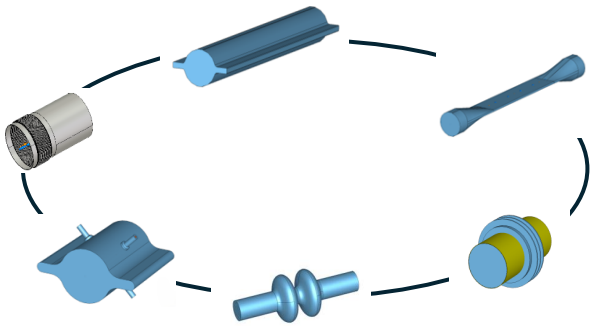

SIMULIA CST STUDIO SUITE

IRIS / IW2D · GitLab

Welcome - ECHO4D
zagorodnov/pyECHO4D

Updated elements in the FCC-ee I/W model:

- beam pipe: circular copper cross-section with a radius of 30 mm and two lateral winglets. Coated with a thin 150 nm layer of Non-Evaporable Getter (NEG)
- 41 collimators
- 132 single-cell 400 MHz RF cavities
- 10 000 BPMs
- 10 000 bellows
- tapers

FCC-ee main ring impedance model

Identify main impedance contributors → 3D EM Simulations and Analytical Model → Accelerator I/W Model

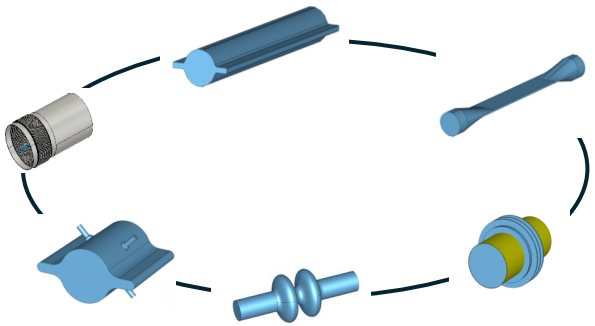

Updated elements in the FCC-ee I/W model:

- beam pipe: circular copper cross-section with a radius of 30 mm and two lateral winglets. Coated with a thin 150 nm layer of Non-Evaporable Getter (NEG)
- 41 collimators
- 132 single-cell 400 MHz RF cavities
- 10 000 BPMs
- 10 000 bellows
- tapers

SIMULIA CST STUDIO SUITE

IRIS / IW2D · GitLab

Welcome - ECHO4D

zagorodnov/pyECHO4D

Beta function for the ith element

$$Z_\perp(f) = \sum_{i=1}^{N} Z_\perp^i(f) \frac{\beta_\perp^i}{\langle \beta_\perp \rangle}$$

Transverse impedance for the ith element

Average beta function

FCC-ee main ring impedance model

Identify main impedance contributors → 3D EM Simulations and Analytical Model → Accelerator I/W Model

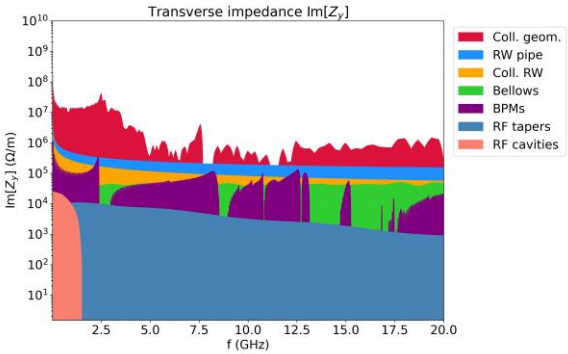

Beta function for the ith element

$$Z_\perp(f) = \sum_{i=1}^{N} Z_\perp^i(f) \frac{\beta_\perp^i}{\langle \beta_\perp \rangle}$$

Transverse impedance for the ith element

Average beta function

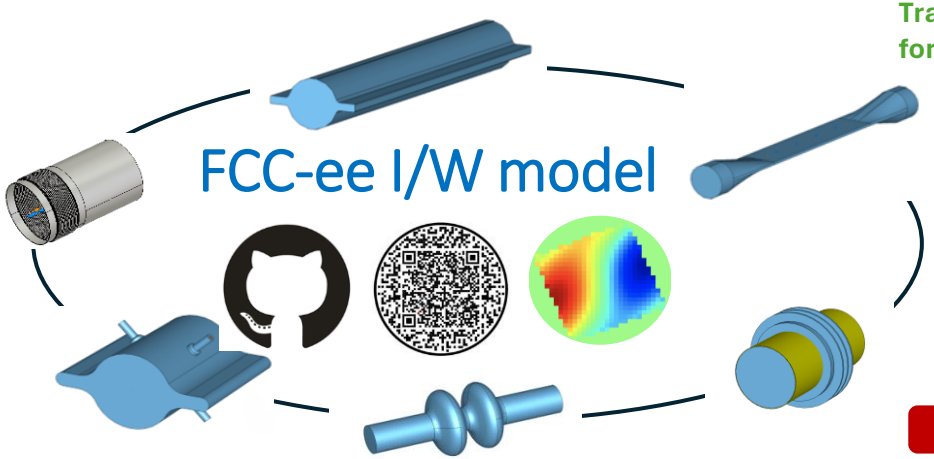

Modular and flexible

FCC-ee main ring impedance model

Identify main impedance contributors → 3D EM Simulations and Analytical Model → Accelerator I/W Model

↓

Beam Dynamics Simulations

↓

Xsuite

FCC-ee main ring impedance model

Identify main impedance contributors → 3D EM Simulations and Analytical Model → Accelerator I/W Model → Beam Dynamics Simulations → Output: Assessment of beam stability → Identify main impedance contributors

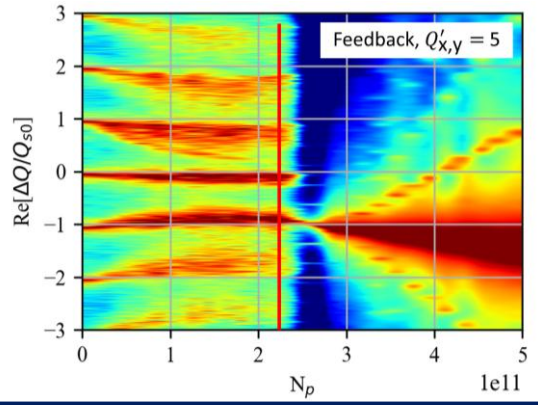

Collimation system: study process

Collimators were simulated in CST Studio Suite, initially using a simplified model ➔ step-by-step approach.

Schematic design

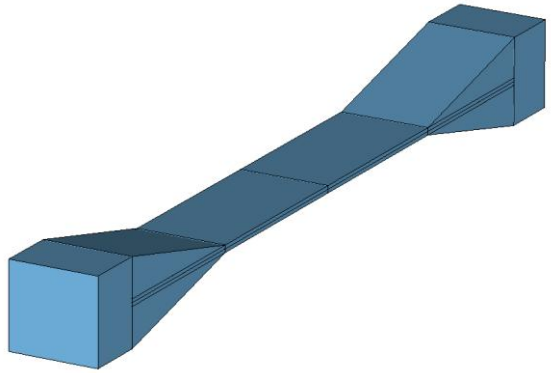

SIMULIA CST STUDIO SUITE

Despite its simplicity the model accurately reproduces the actual **jaw lengths** and **apertures** and effectively highlights critical parameters that can be optimized to mitigate impedance

By enabling the isolation of geometric effects, this model served as a baseline for next refinements

Collimation system: study process

Design based on collimators for SuperKEKB.

Schematic design | Super KEKB design

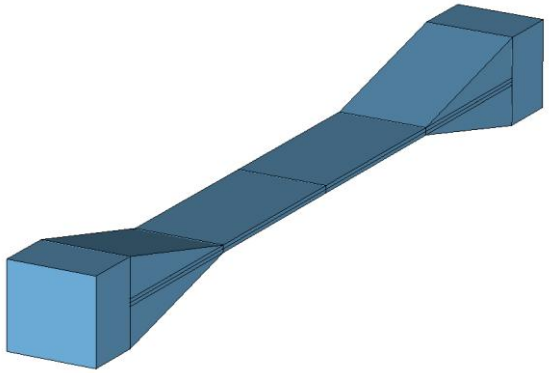

SIMULIA CST STUDIO SUITE

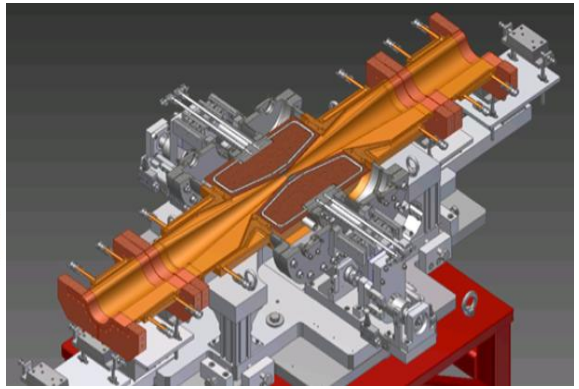

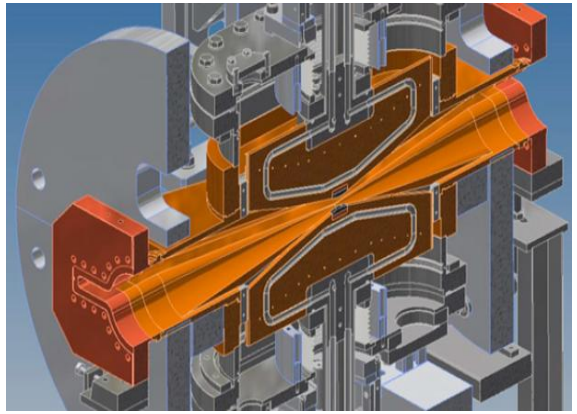

Collimation system: study process

Design based on collimators for SuperKEKB.

Schematic design | Winglets design

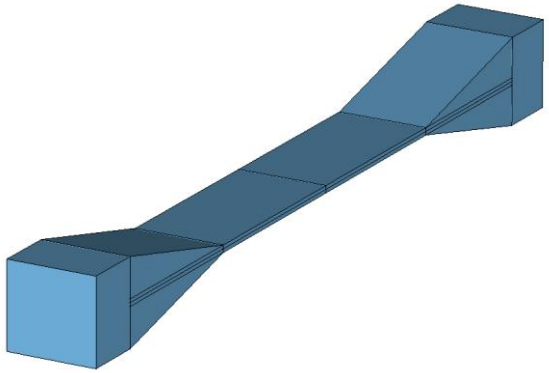

SIMULIA CST STUDIO SUITE

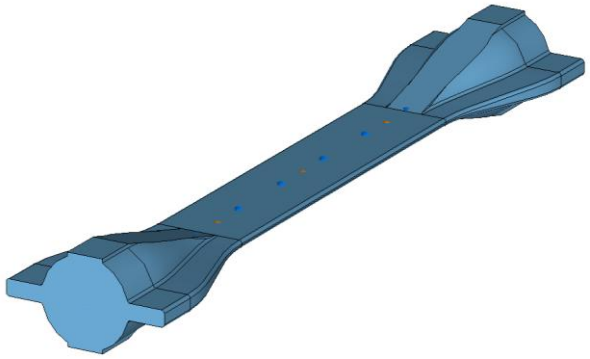

SIMULIA CST STUDIO SUITE

Collimation system: study process

Non- winglets design with round section.

Schematic design | Winglets design | Non-winglets design

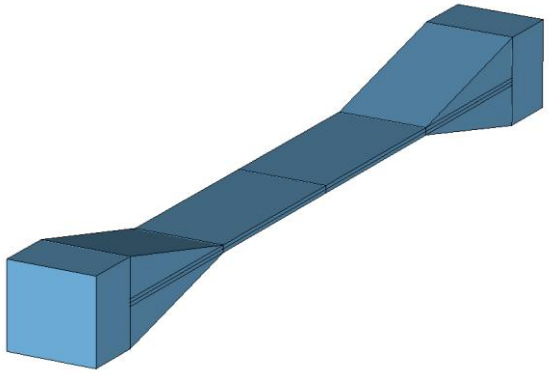

SIMULIA CST STUDIO SUITE

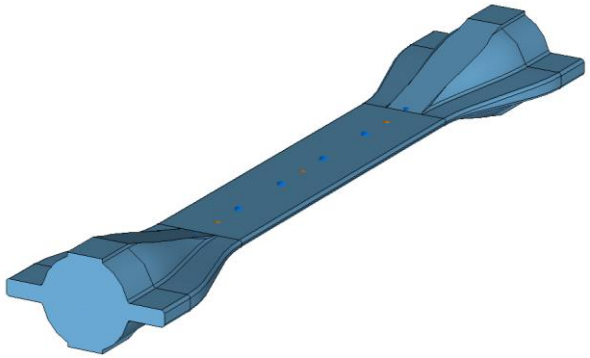

SIMULIA CST STUDIO SUITE

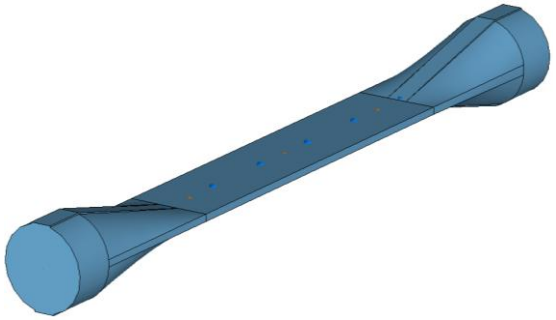

SIMULIA CST STUDIO SUITE

Collimation system: study process

Final proposed design without winglets and step taper.

Schematic design | Winglets design | Non-winglets design | Step-taper design

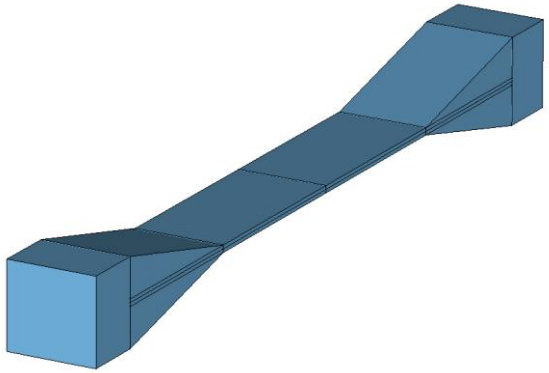

SIMULIA CST STUDIO SUITE

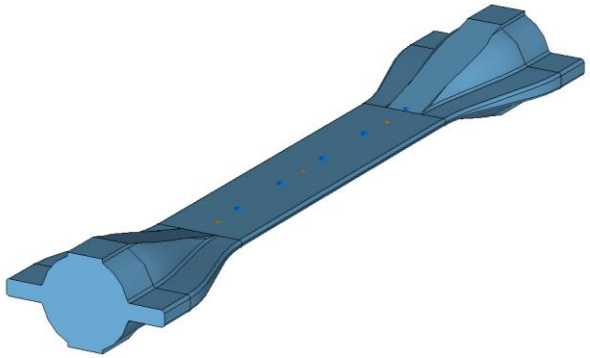

SIMULIA CST STUDIO SUITE

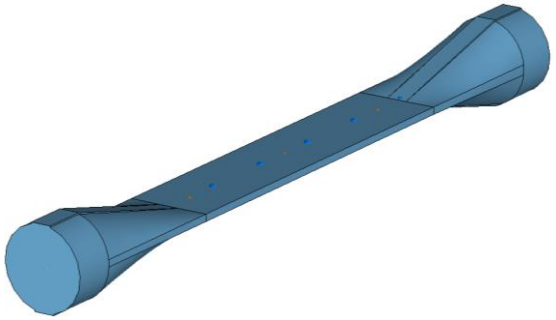

SIMULIA CST STUDIO SUITE

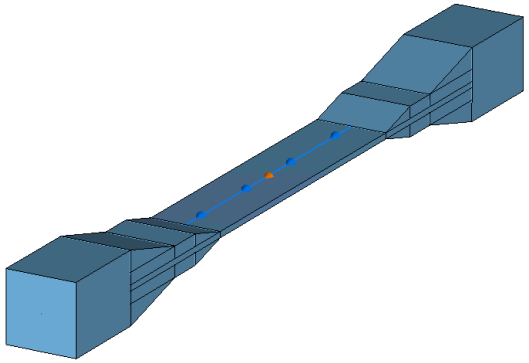

SIMULIA CST STUDIO SUITE

Criticality of the collimation system

Collimator geometrical impedance optimization

Beam dynamics simulations

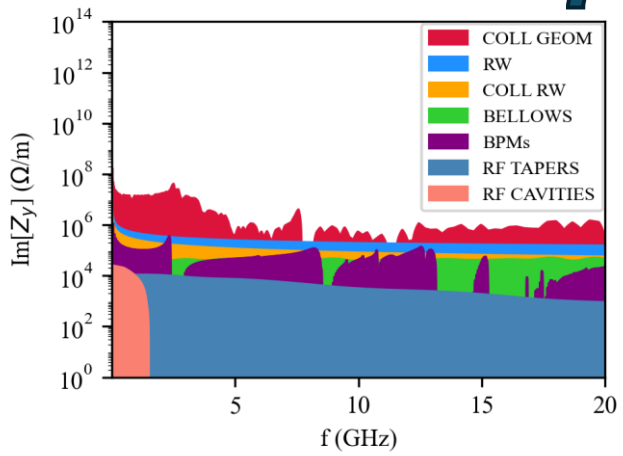

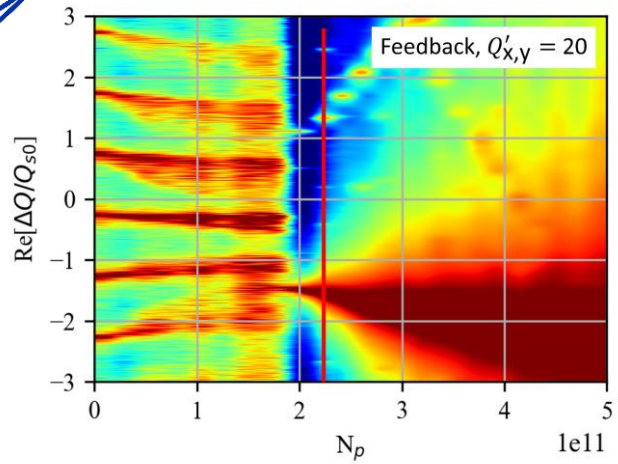

Unstable

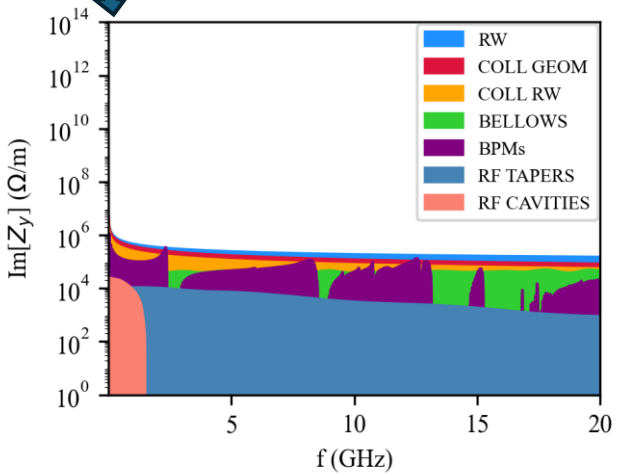

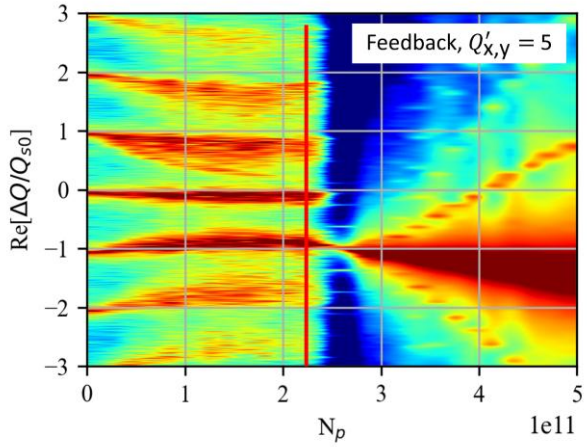

Close to stability limit

Beam dynamics simulations

Criticality of the collimation system

Collimator geometrical impedance optimization

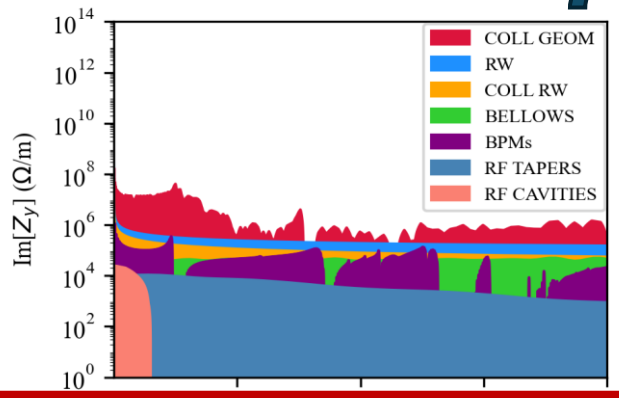

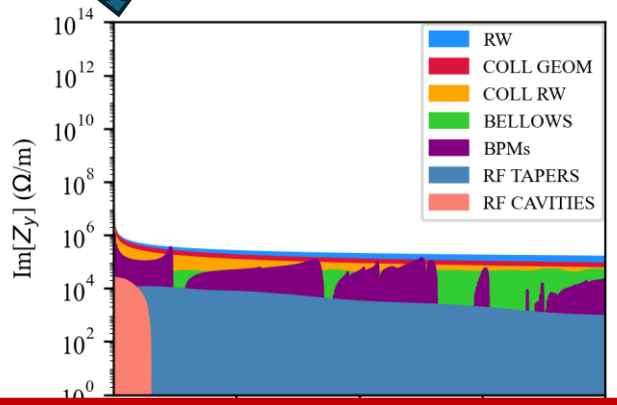

Beam dynamics simulations

Further mitigation is essential to ensure robust beam stability

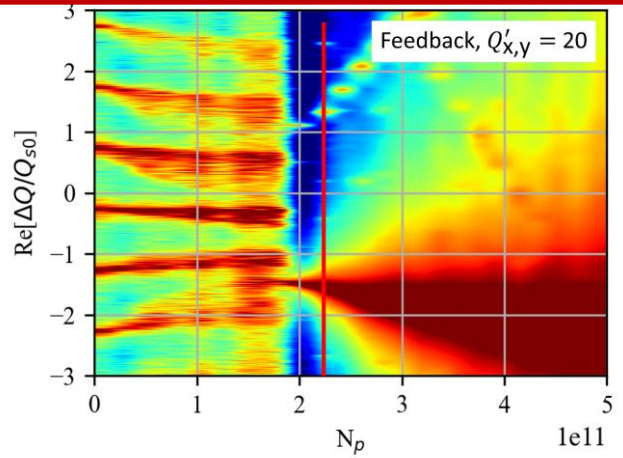

Unstable

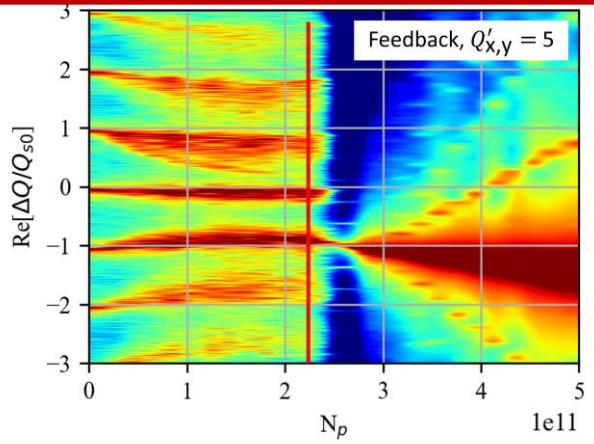

Close to stability limit

Conclusion

- **Impedance/Wake model development for critical design decisions:**
  - The extremely **short bunch length** makes impedance and wakefield simulations highly **challenging**.
  - Ensured **model flexibility** to facilitate impedance and wakefield updates in optics, material choices, coating thickness, geometries, and new machine elements.
  - Enabled **impedance assessments** of different scenarios.

- **Criticality of the collimation system:**
  - A step-by-step approach is being adopted to explore computational limits and propose optimized impedance solutions.
  - Collimators geometrical impedance:
    - **Optimization strategy** ➔ taper optimization.
      - Solutions developed in collaboration with the design and collimation groups to address spatial and mechanical constraints.
  - Collimators RW impedance:
    - Comparison between different optics layouts.
    - **Optimization strategy** ➔ optics designed to maximize the collimator aperture and favour materials with high electrical conductivity.

Next steps and ongoing activities

- I/W Model updates & implementation:
  - Finalize the full **impedance database** for the **collimation system**, including impedance estimations for
  - The new operating optics version expected by September 2025. The goal is to converge on a definitive
  - Optics layout by March 2026.
  - Establish a reliable and comprehensive methodology for evaluating the **geometric impedance** contributions of collimators, ensuring accuracy across all design variants.
  - Explore novel **collimator materials** and geometries in close collaboration with the collimation technical design teams, with a focus on reducing impedance while respecting mechanical constraints.
  - Continuous **FCC-ee I/W model updates** in line with the evolving design of components, ensuring timely integration of new elements as they are defined ➔ Ensure model **flexibility.**

- Beam dynamics simulations:
  - Investigate beam dynamics under **non-ideal feedback systems** and propose improved feedback strategies.
  - **Multi-bunch feedback system** simulations to assess beam stability with multiple bunches.
  - Integration of **advanced feedback** features from **PyHEADTAIL multi-bunch** into **Xsuite**.

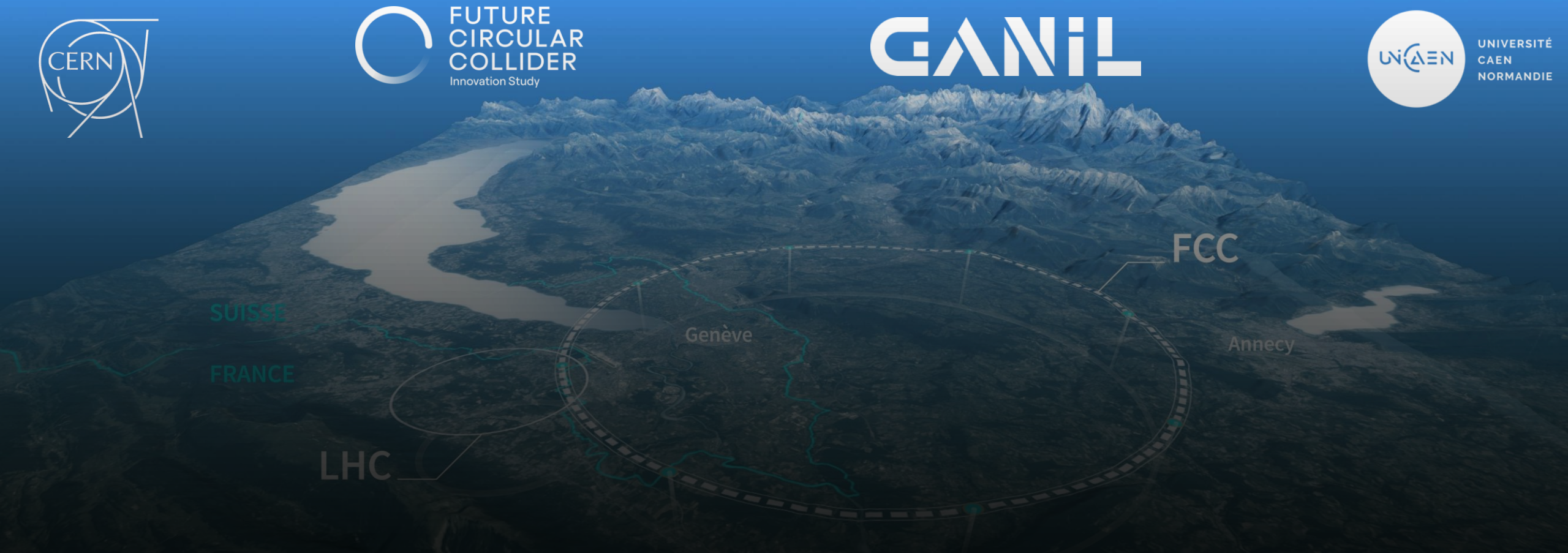

Acknowledgements

Many thanks to M. Boscolo, G. Broggi, R. Bruce, X. Buffat, C. Carli, R. J. Cowan, E. De la Fuente Garcia, A. Ghribi, L. Giacomel, S. Gilardoni, G. Iadarola, T. Ishibashi, S. Kostoglou, A. Lechner, E. Macchia, S. Marin, I. Mases Sole, M. Migliorati, K. Oide, A. Perillo-Marcone, S. Redaelli, G. Roy, G. Rumolo, R. Seidenbinder, L. Sito, R. Soos, C. Zannini, F. Zimmermann, and all CEI colleagues, as well as our colleagues from ABP and FCC-ee/FCCIS, for their valuable contributions and support.

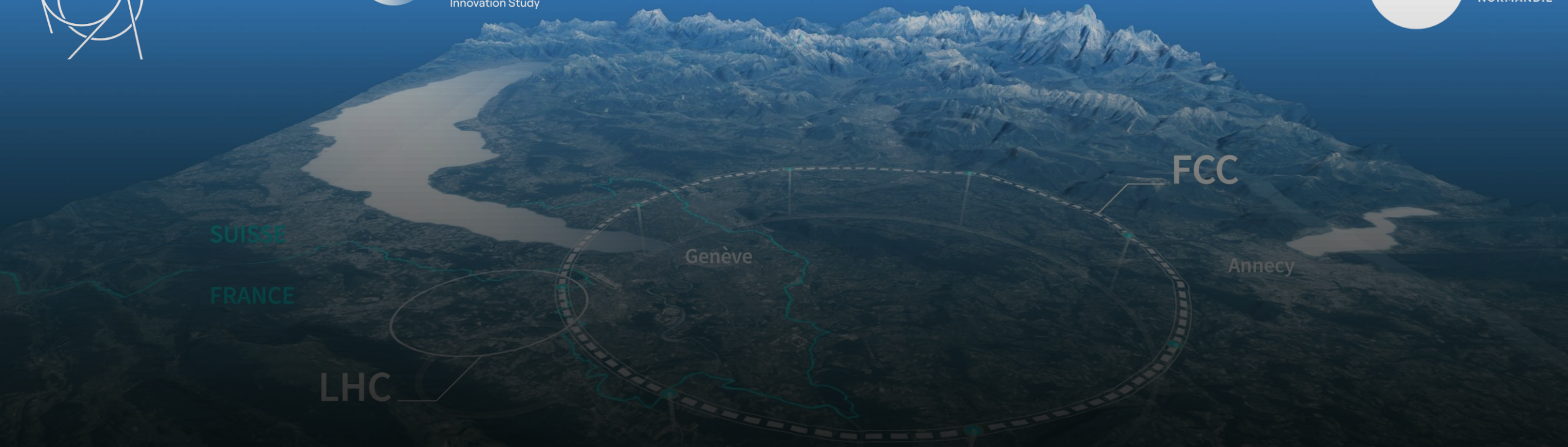

Thank you for your attention ☺

Les Journées Accélérateurs de la Société Française de Physique (SFP), 7-10 October 2025

Full paper

PALLAS

From Laser to Beam

Early Results from the PALLAS Laser Plasma Accelerator at IJCLab

Jana Serhal. October 8th Journées Accélérateurs de la Société Française de Physique (SFP)

cnrs

IJCLab Irène Joliot-Curie Laboratoire de Physique des 2 Infinis

Laser Plasma Acceleration: Concept and Mechanism

Laser Plasma Acceleration: Concept and Mechanism

- High-intensity laser beam ($\cong 1.10^{18} W/cm^2$)

Laser Plasma Acceleration: Concept and Mechanism

- High-intensity laser beam ($\cong 1.10^{18} W/cm^2$)

- Drives a plasma wakefield in a gas target.

Laser Plasma Acceleration: Concept and Mechanism

- High-intensity laser beam ($\cong 1.10^{18} W/cm^2$)

- Drives a plasma wakefield in a gas target.

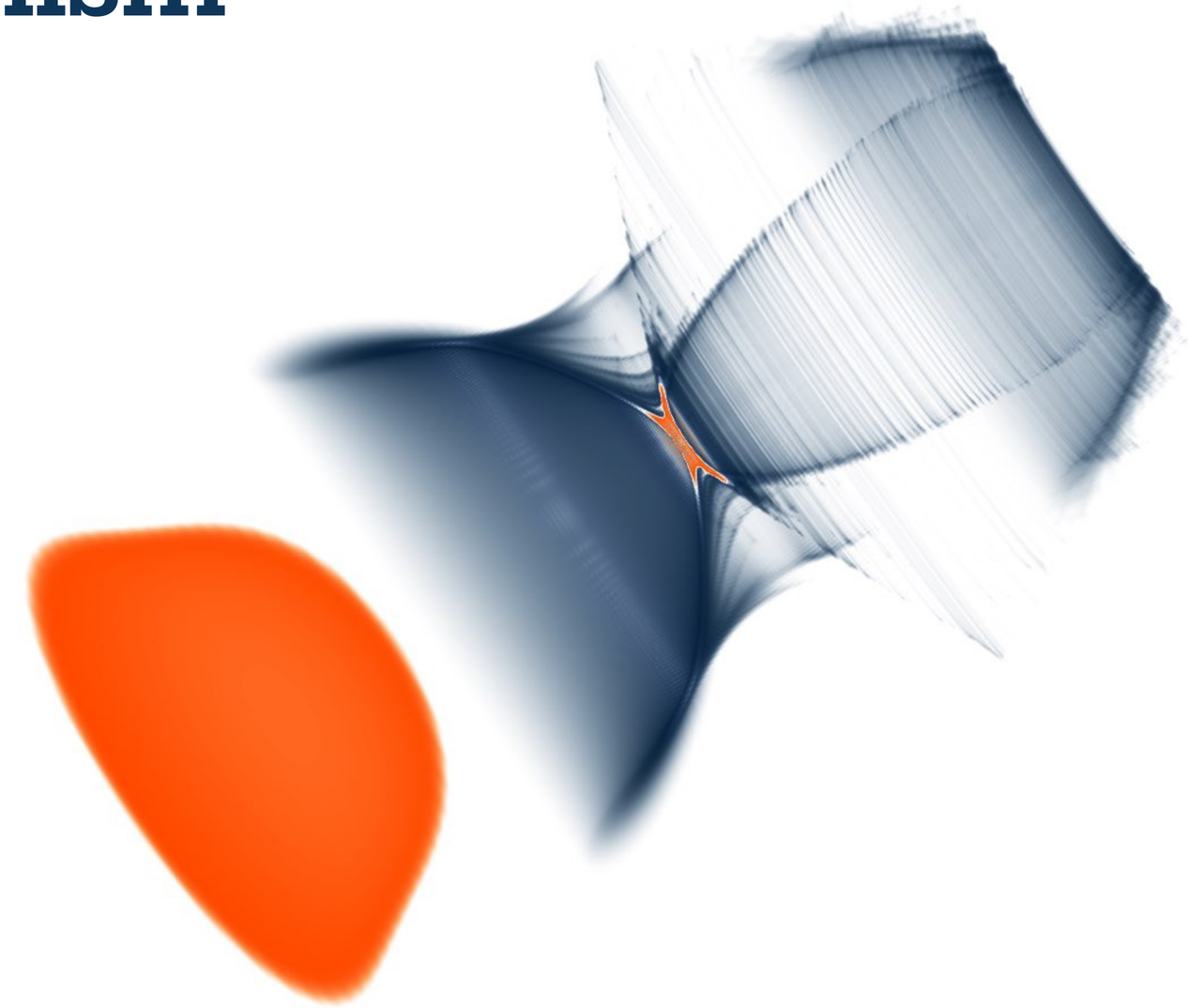

Laser Plasma Acceleration: Concept and Mechanism

- High-intensity laser beam ($\cong 1.10^{18} W/cm^2$)
- Drives a plasma wakefield in a gas target.
- Electrons can be trapped and accelerated in this wake.

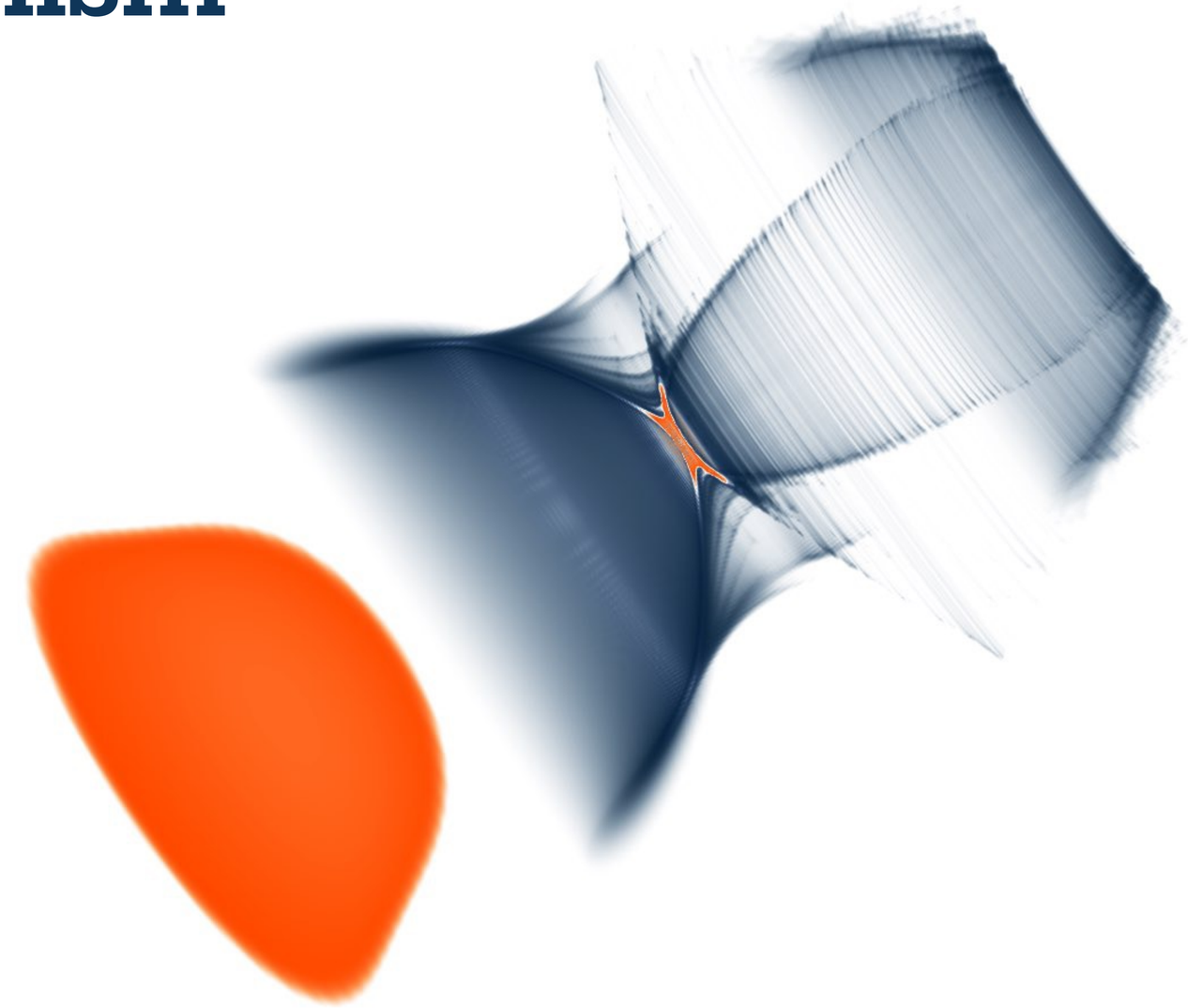

Laser Plasma Acceleration: Concept and Mechanism

- High-intensity laser beam ($\cong 1.10^{18} W/cm^2$)
- Drives a plasma wakefield in a gas target.
- Electrons can be trapped and accelerated in this wake.
- Gradient: **~100 GV/m** → 1000× convention accelerators.

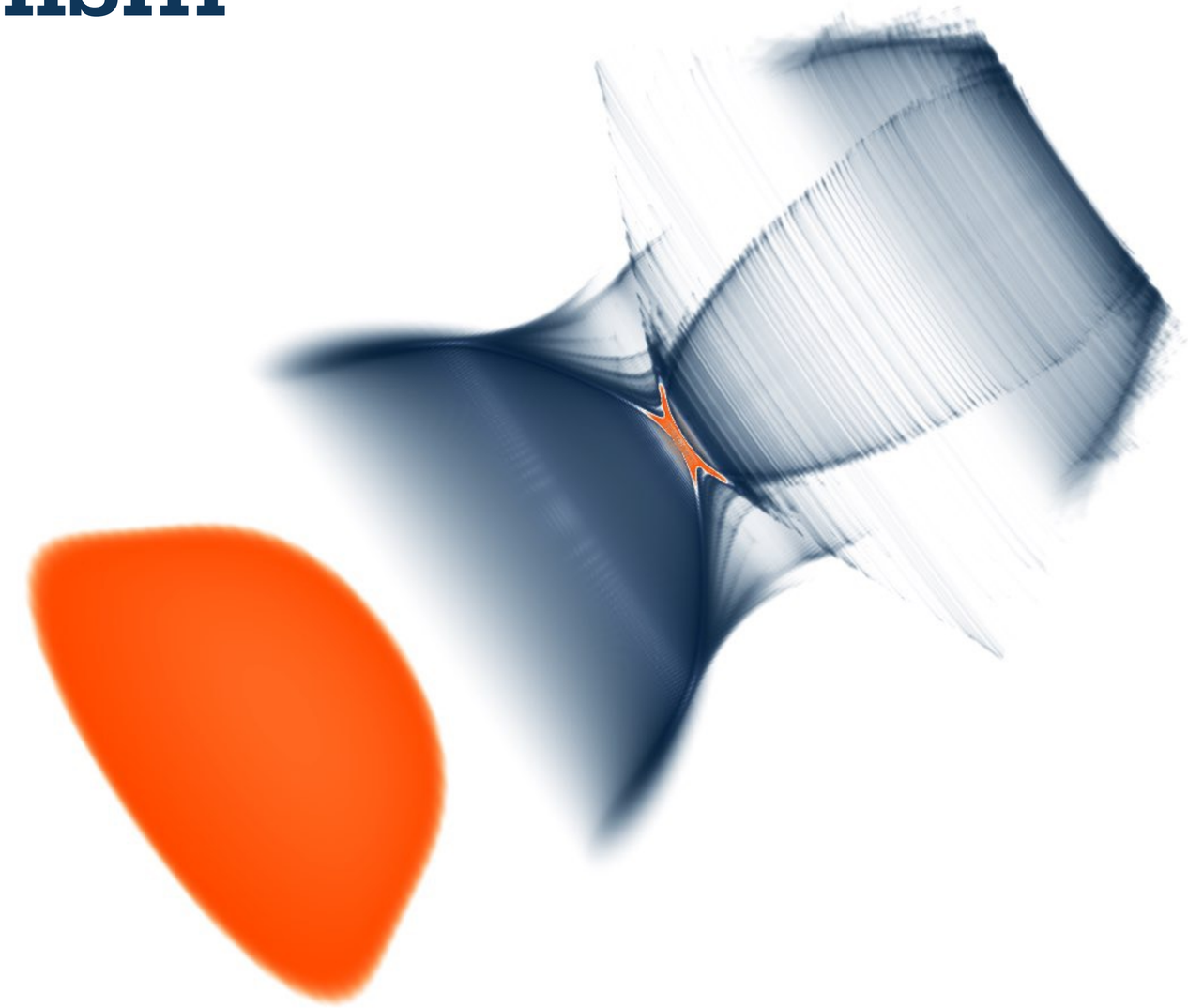

How to Inject Electrons into the Wakefield?

How to Inject Electrons into the Wakefield?

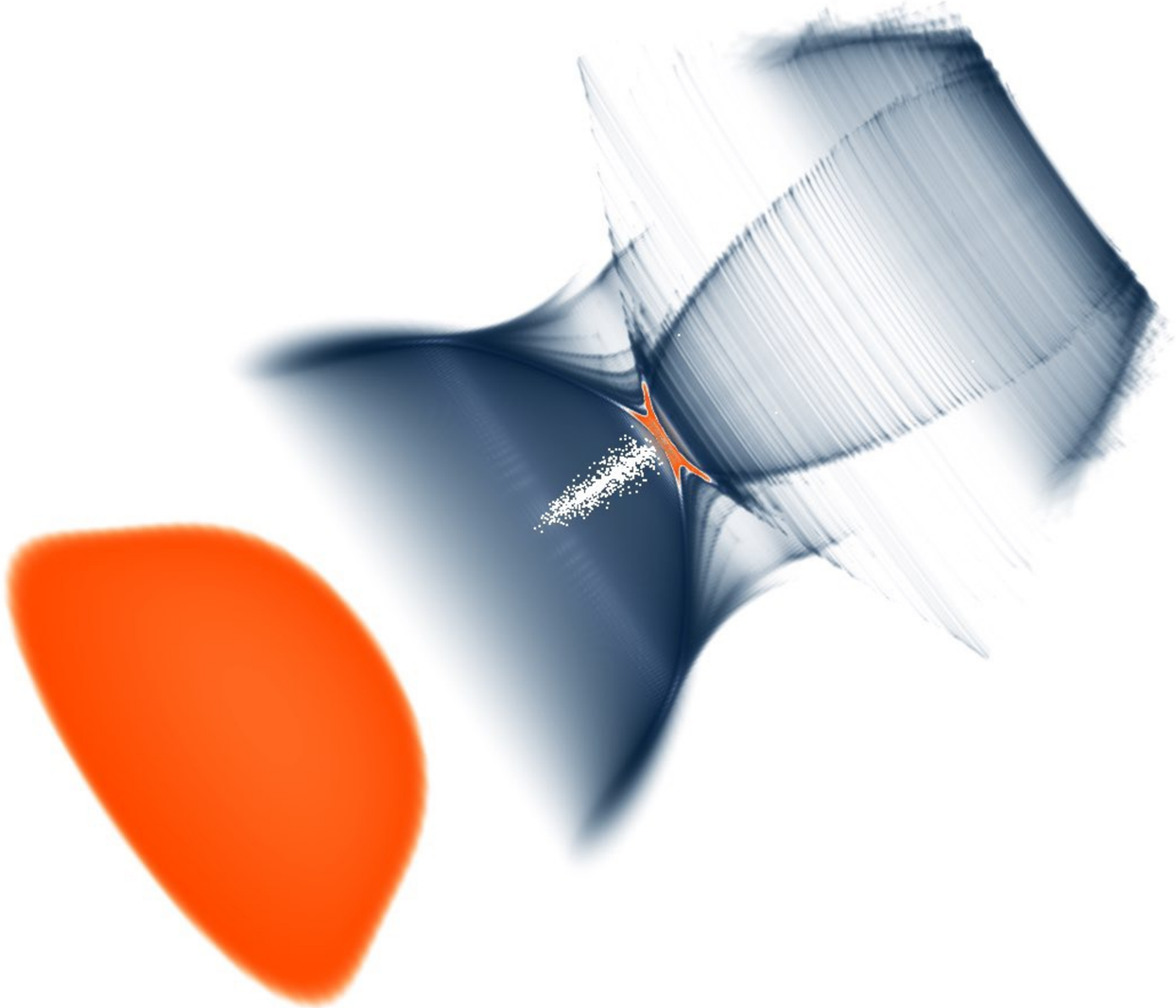

How to Inject Electrons into the Wakefield?

To be trapped, electrons must match the wakefield's phase velocity:

$$v_{electron} = v_{phase,wakefield}$$

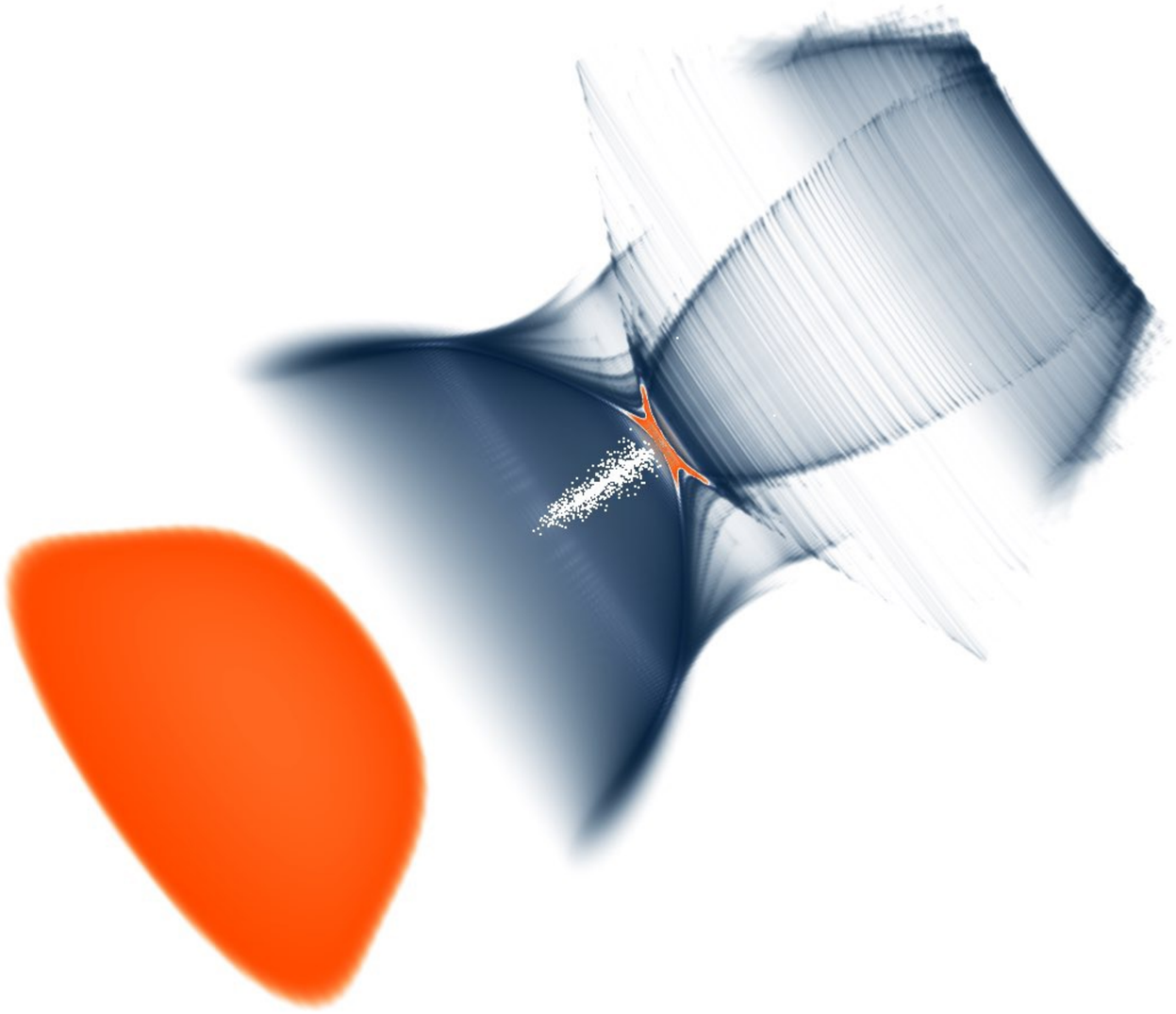

How to Inject Electrons into the Wakefield?

To be trapped, electrons must match the wakefield's phase velocity:

$$v_{electron} = v_{phase,wakefield}$$

- Ionization injection: high-Z dopant (N_2) in low-Z gas (He).
- Electrons born inside the wake are trapped and accelerated.

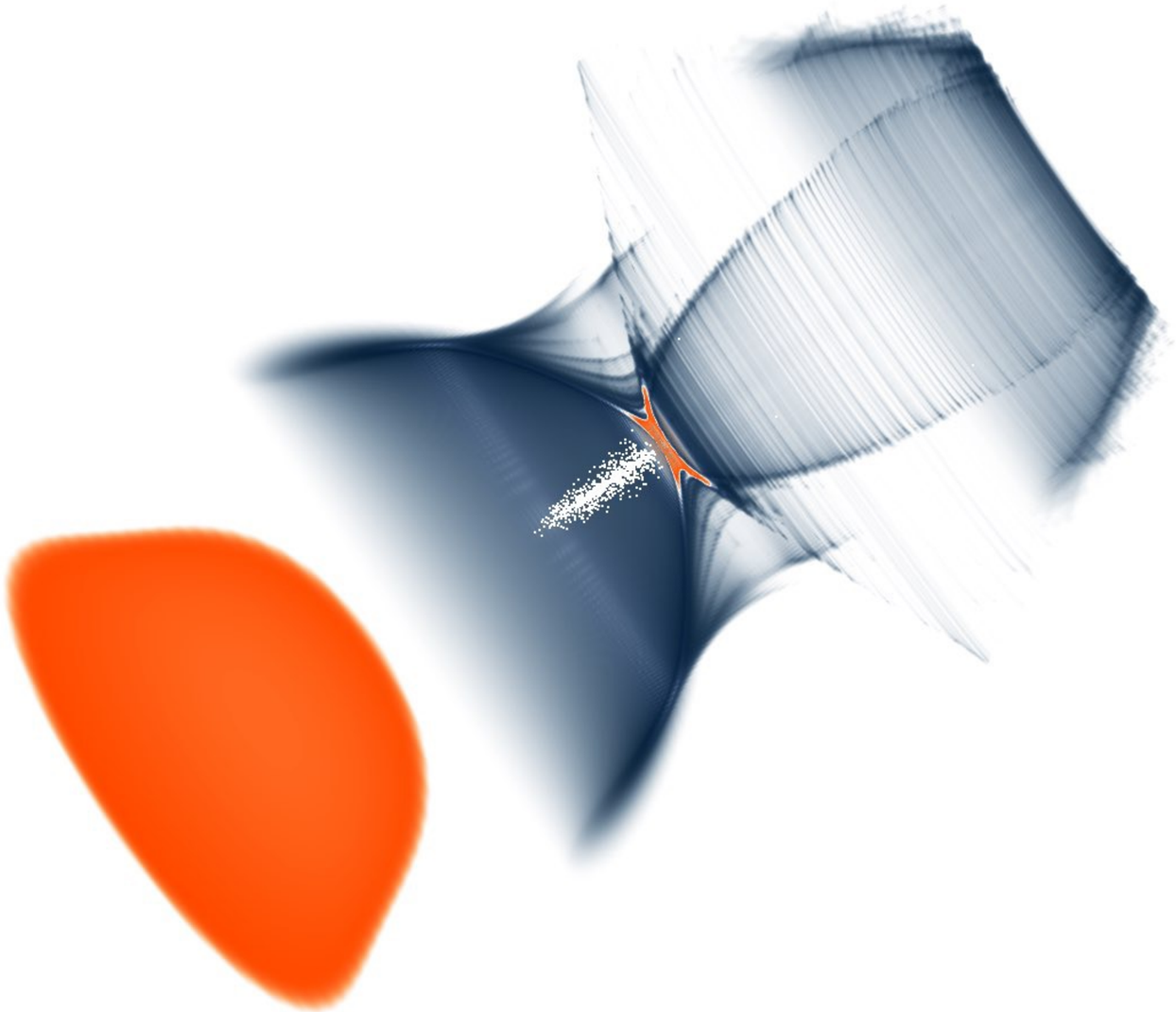

PALLAS: Laser-Plasma Injector

PALLAS: Laser-Plasma Injector

Current Laser System:

- 40 TW, 1.4–1.6 J, 45 fs
- 1 Hz rep rate
- Stability: 11–13 μrad (PV)

PALLAS: Laser-Plasma Injector

Current Laser System:

- 40 TW, 1.4–1.6 J, 45 fs
- 1 Hz rep rate
- Stability: 11–13 μrad (PV)

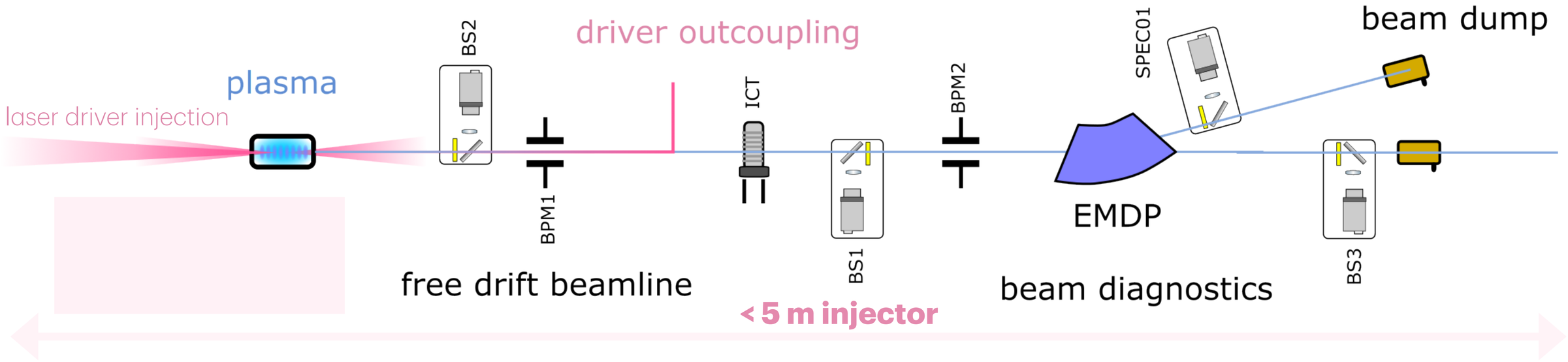

PALLAS: Laser-Plasma Injector

Current Laser System:

- 40 TW, 1.4–1.6 J, 45 fs
- 1 Hz rep rate
- Stability: 11–13 μrad (PV)

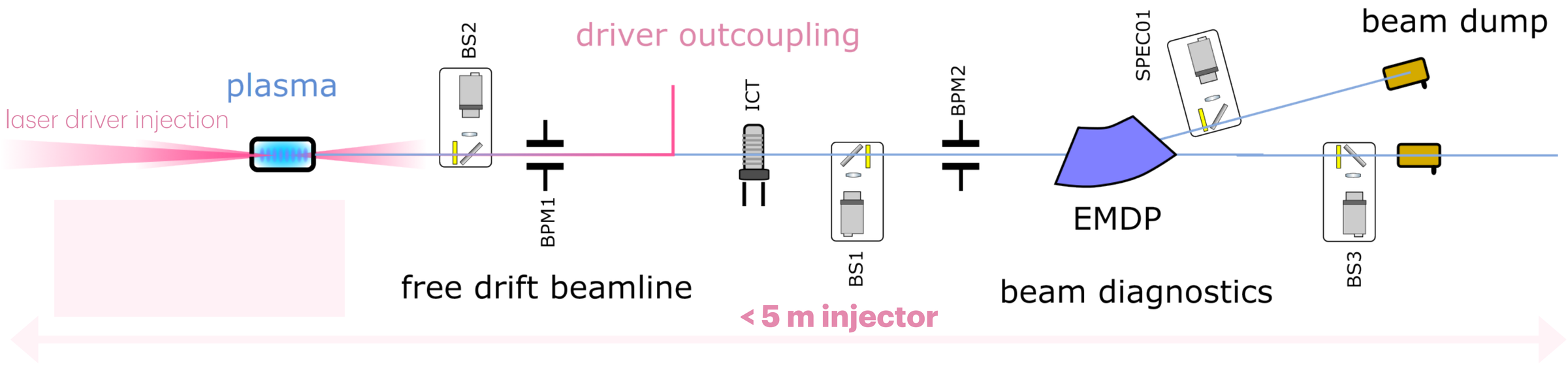

PALLAS: Laser-Plasma Injector

Current Laser System:

- 40 TW, 1.4–1.6 J, 45 fs
- 1 Hz rep rate
- Stability: 11–13 μrad (PV)

Targer Laser System:

- 3J, 40 fs
- 10 Hz rep rate
- Stability < 1 μrad (PV)

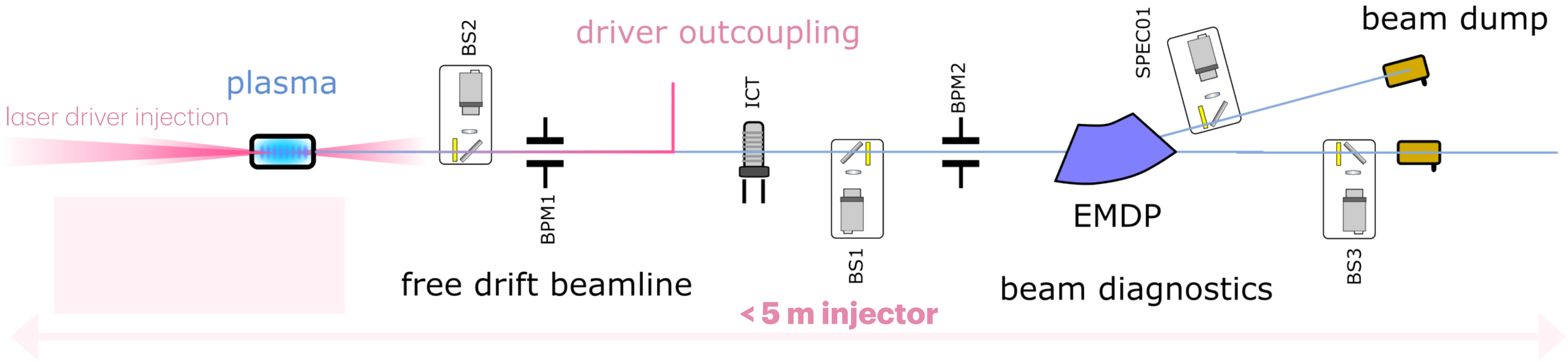

Two-Chamber Gas Cell: Injection & Acceleration

Two-Chamber Gas Cell: Injection & Acceleration

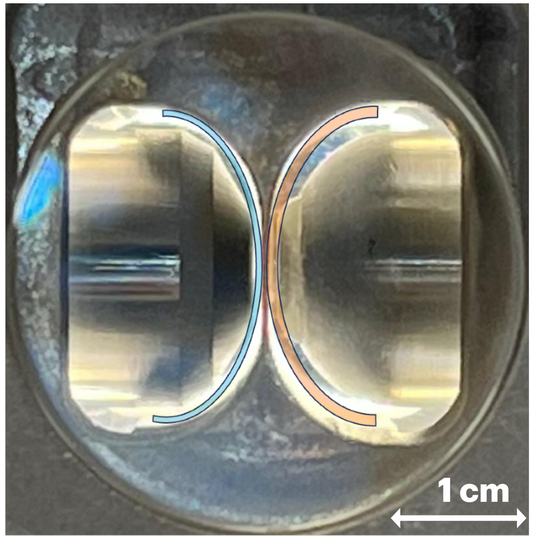

Two-Chamber Gas Cell: Injection & Acceleration

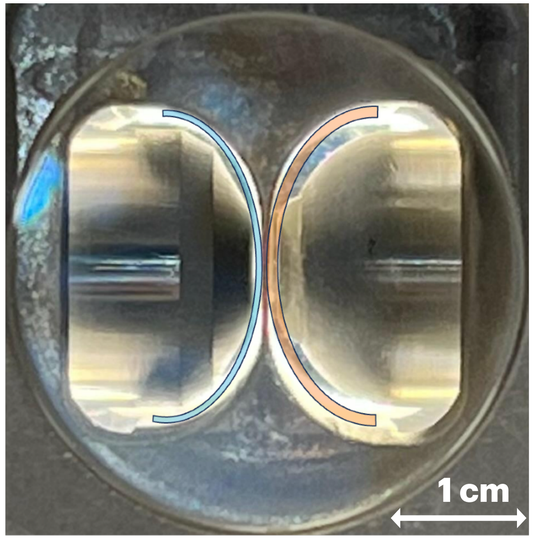

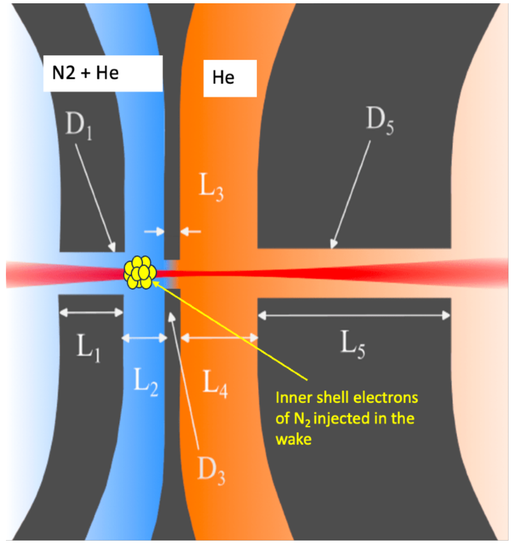

Two-Chamber Gas Cell: Injection & Acceleration

- **Injection chamber (blue)**: N_2/He mixture → ionisation injection
- **Acceleration chamber (orange):** pure He for energy gain
- **Gas profiles:** validated with computational fluid dynamics simulations

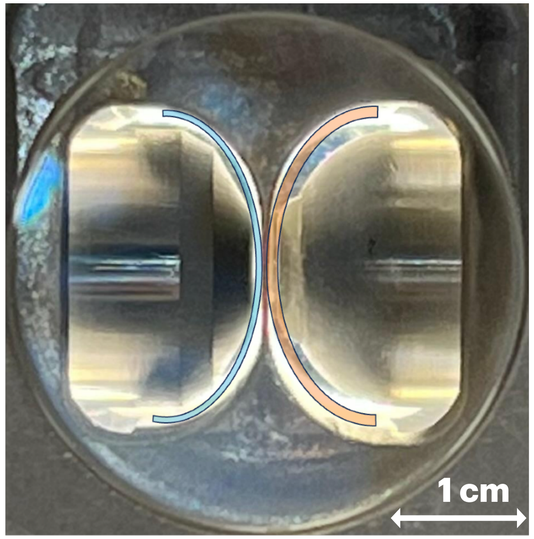

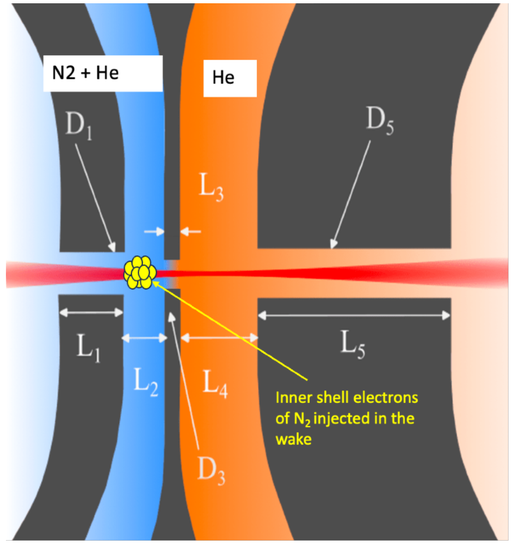

Two-Chamber Gas Cell: Injection & Acceleration

- **Injection chamber (blue)**: N_2/He mixture → ionisation injection
- **Acceleration chamber (orange):** pure He for energy gain
- **Gas profiles:** validated with computational fluid dynamics simulations

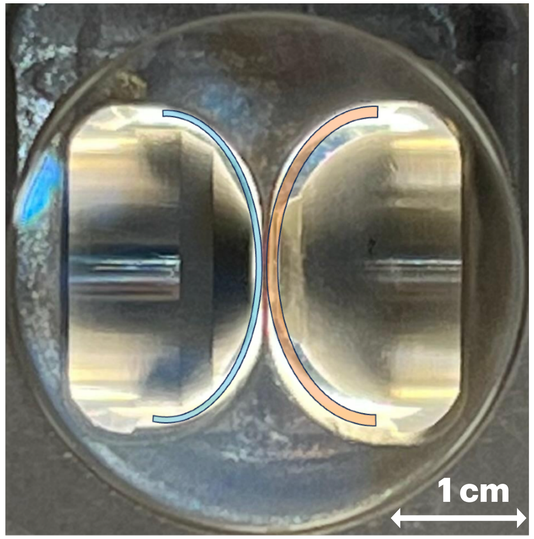

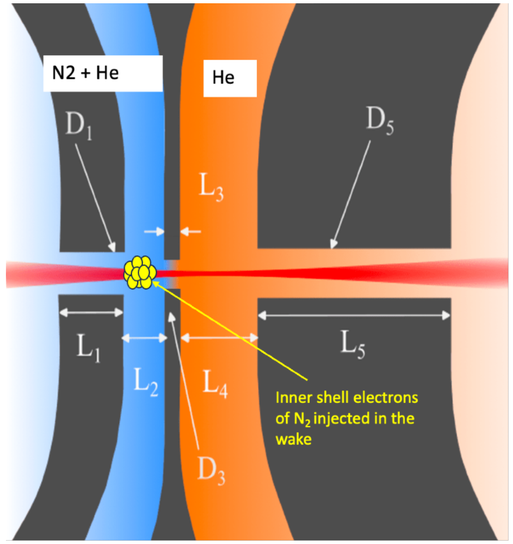

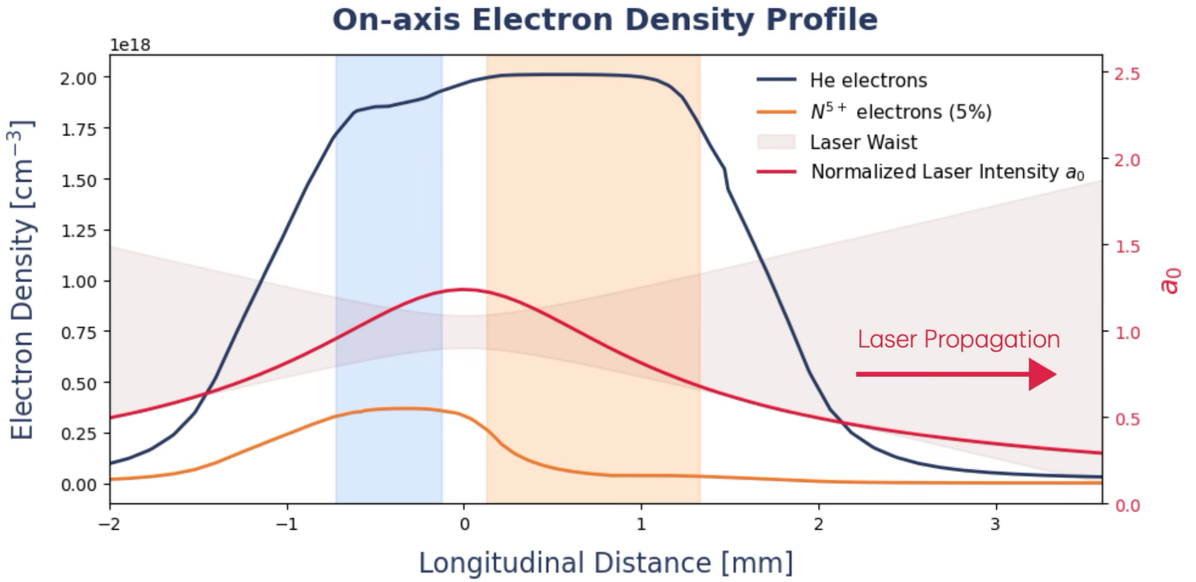

Two-Chamber Gas Cell: Injection & Acceleration

- **Injection chamber (blue)**: N_2/He mixture → ionisation injection
- **Acceleration chamber (orange):** pure He for energy gain
- **Gas profiles:** validated with computational fluid dynamics simulations

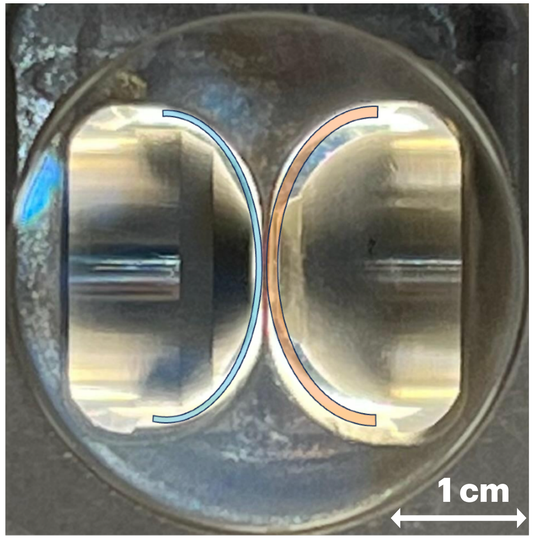

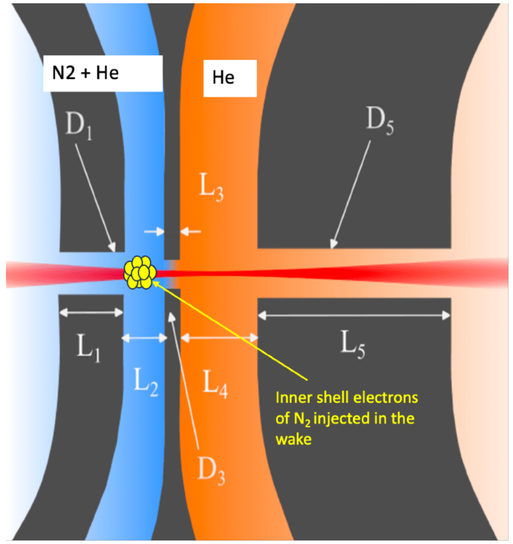

Plasma diagnostics:

- Probe beam for electron density
- Spectral diagnostics for dopant localisation via spectral emission lines

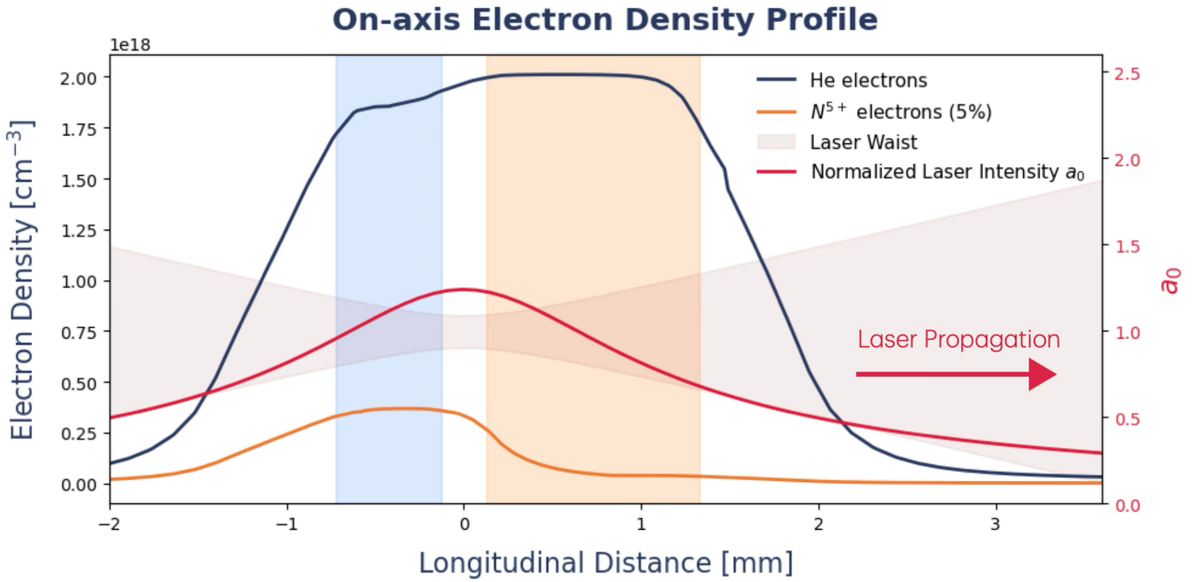

Electron Beam: First Results

Electron Beam: First Results

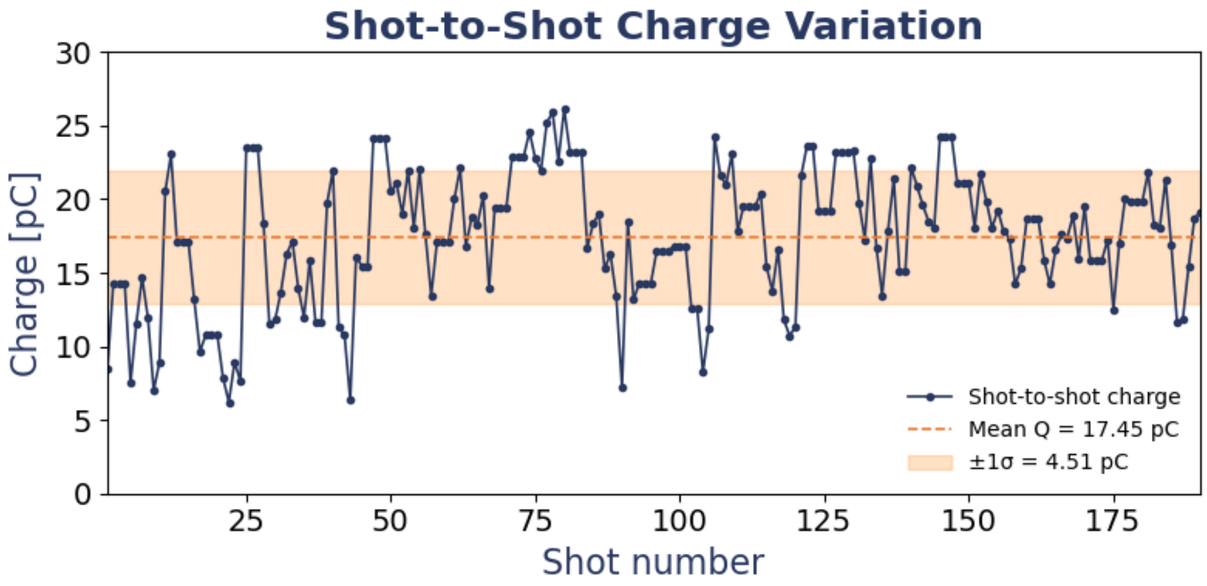

Electron Beam: First Results

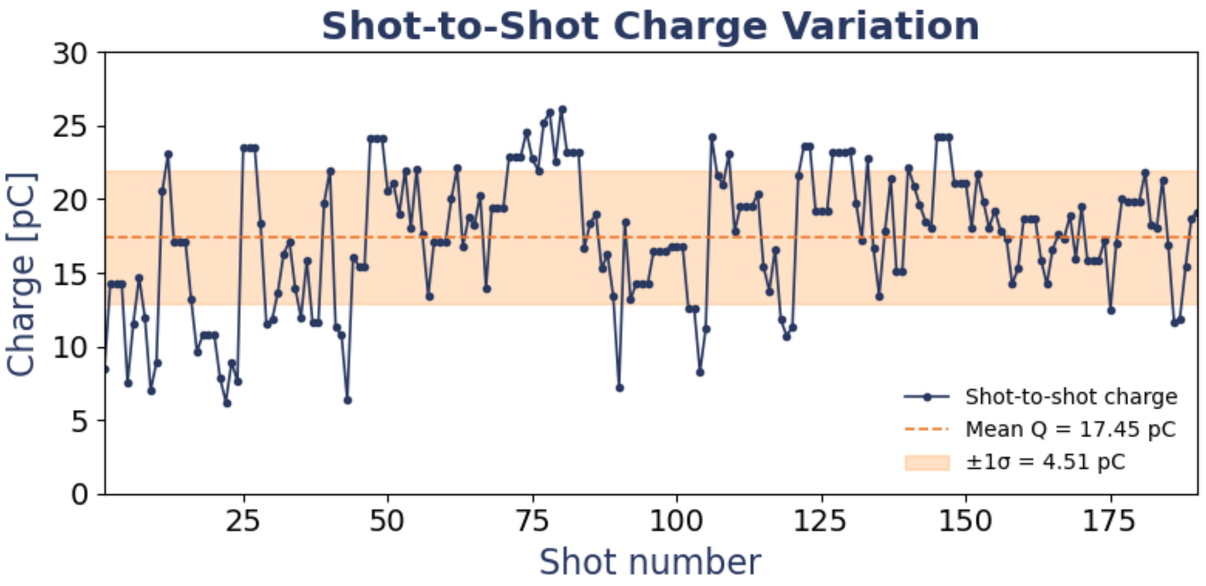

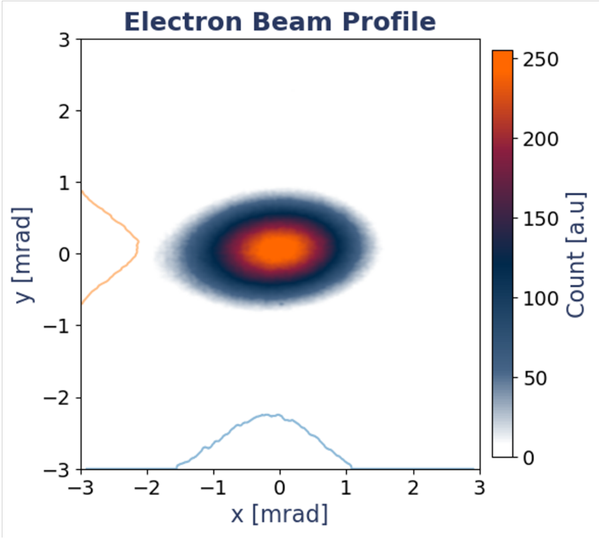

Electron Beam: First Results

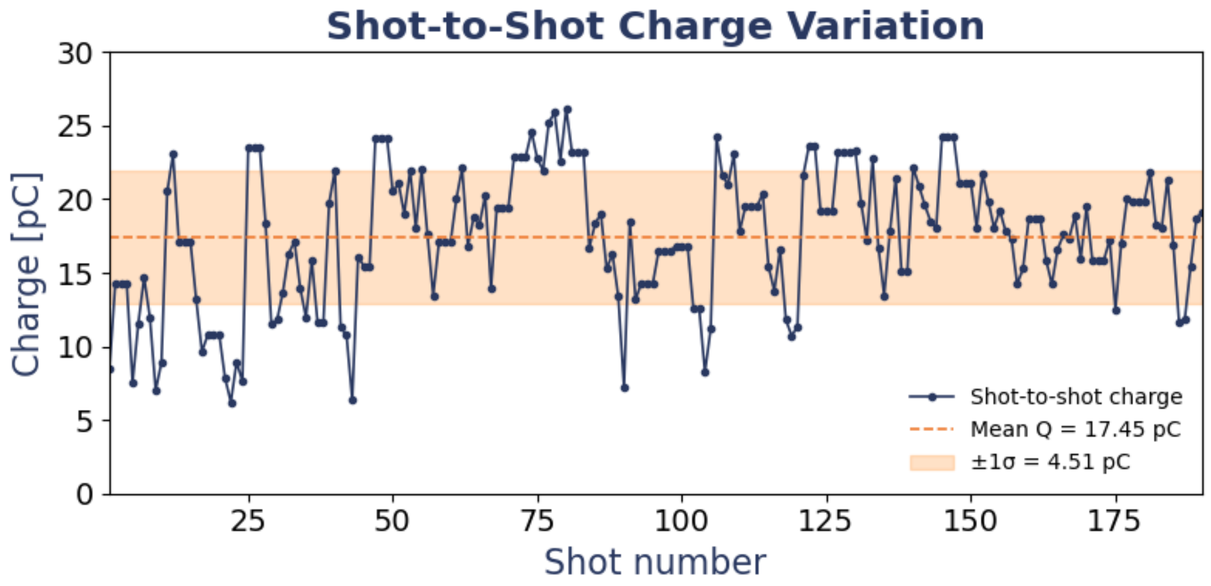

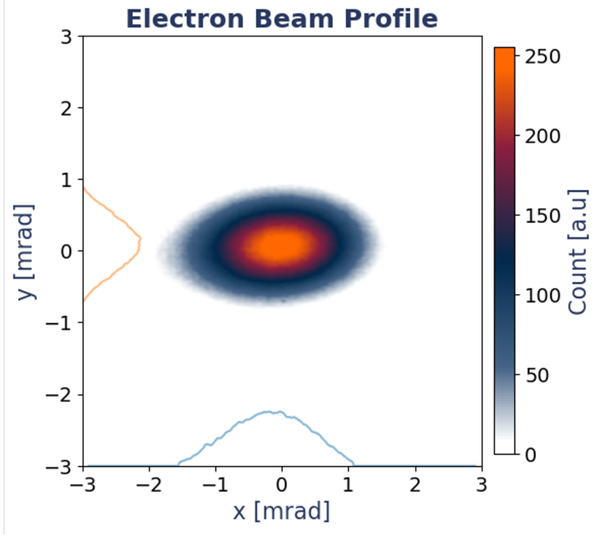

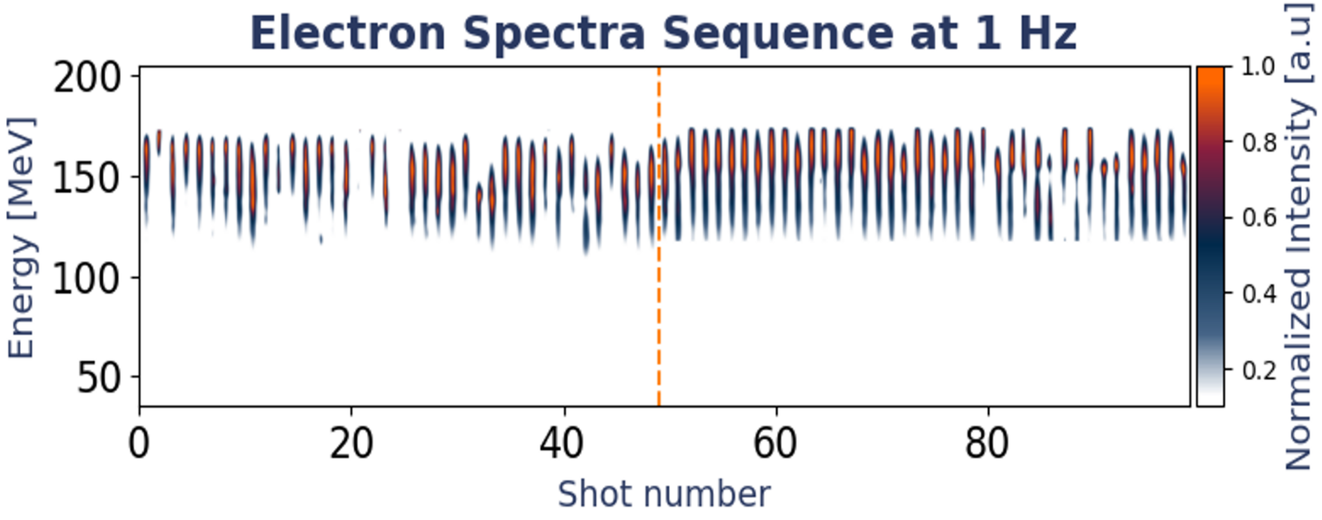

Electron Beam: First Results

Parameter		Goal	Achieved
Energy (E_{med})	[MeV]	150	140-160
Energy Spread (σ_E)	[MeV]	<7.5	18-100 (+)
Charge (Q)	[pC]	15-30	10 -25
Divergence (θ)	[mrad]	<5	0.8 x 1.2
Stability	[%]	5	15 -23

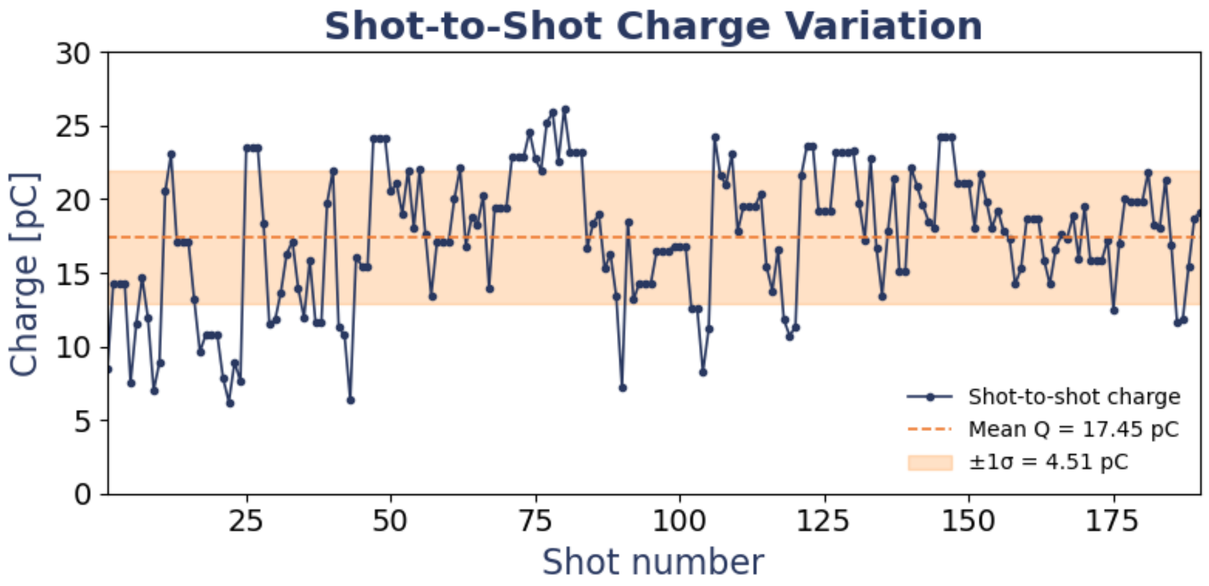

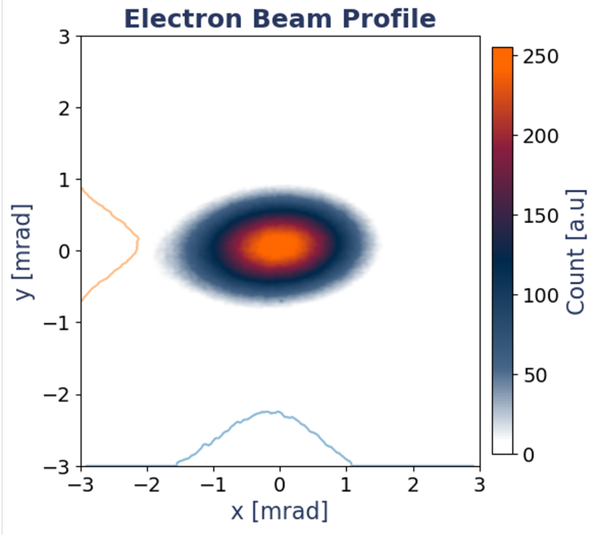

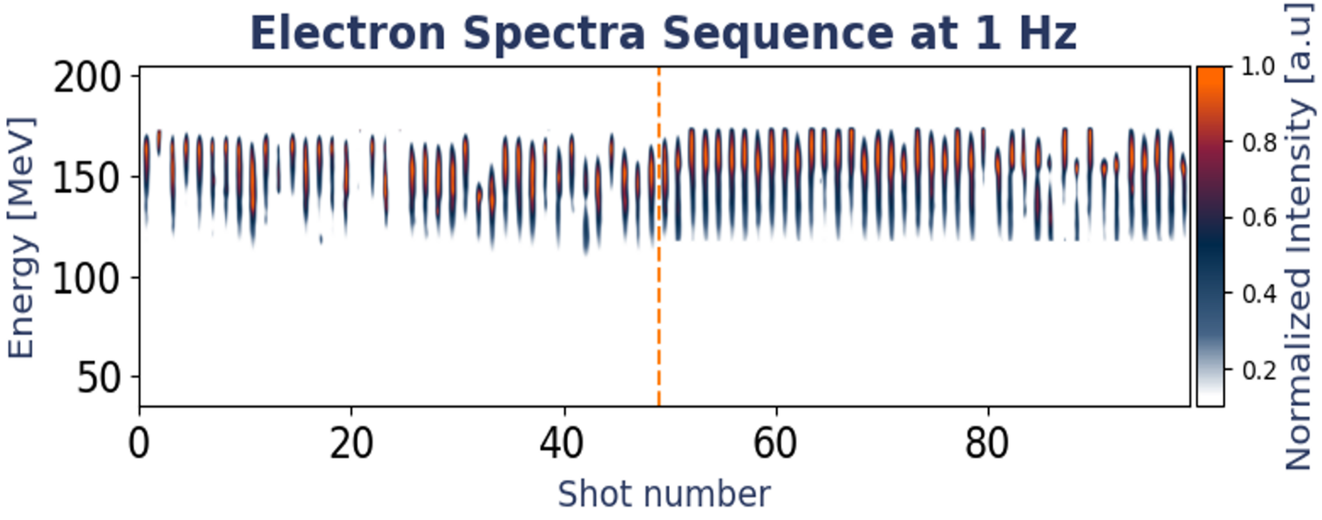

Electron Beam: First Results

Parameter		Goal	Achieved
Energy (E_{med})	[MeV]	150	140-160
Energy Spread (σ_E)	[MeV]	<7.5	18-100 (+)
Charge (Q)	[pC]	15-30	10 -25
Divergence (θ)	[mrad]	<5	0.8 x 1.2
Stability	[%]	5	15 -23

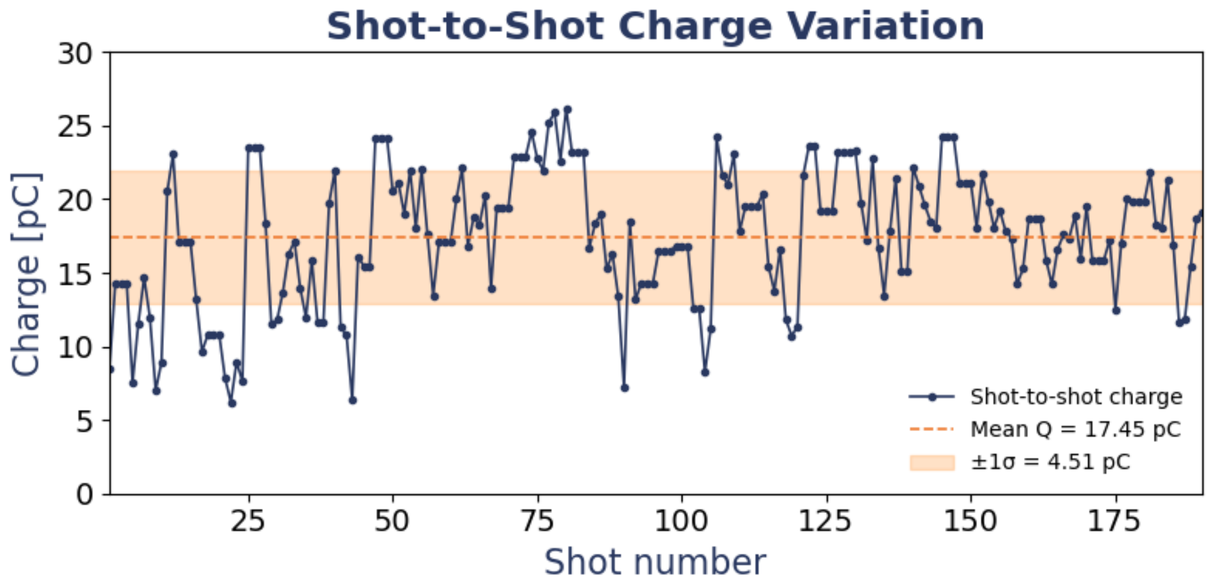

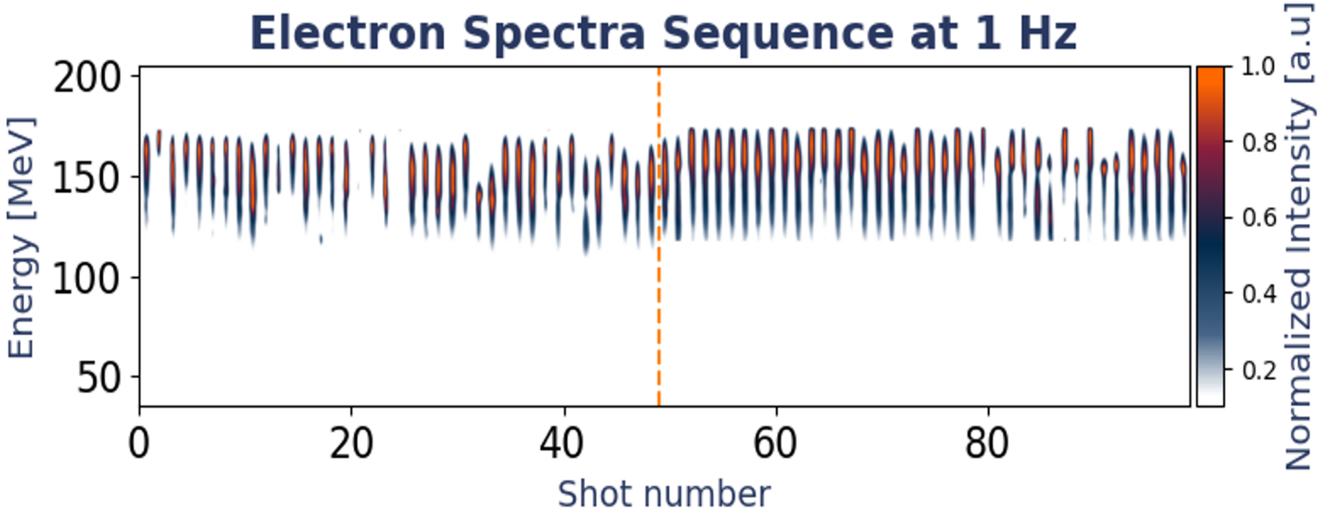

Summary:

- Good energy and charge achieved, <2 mrad divergence.
- Stability needs improvement.

The Accelerator

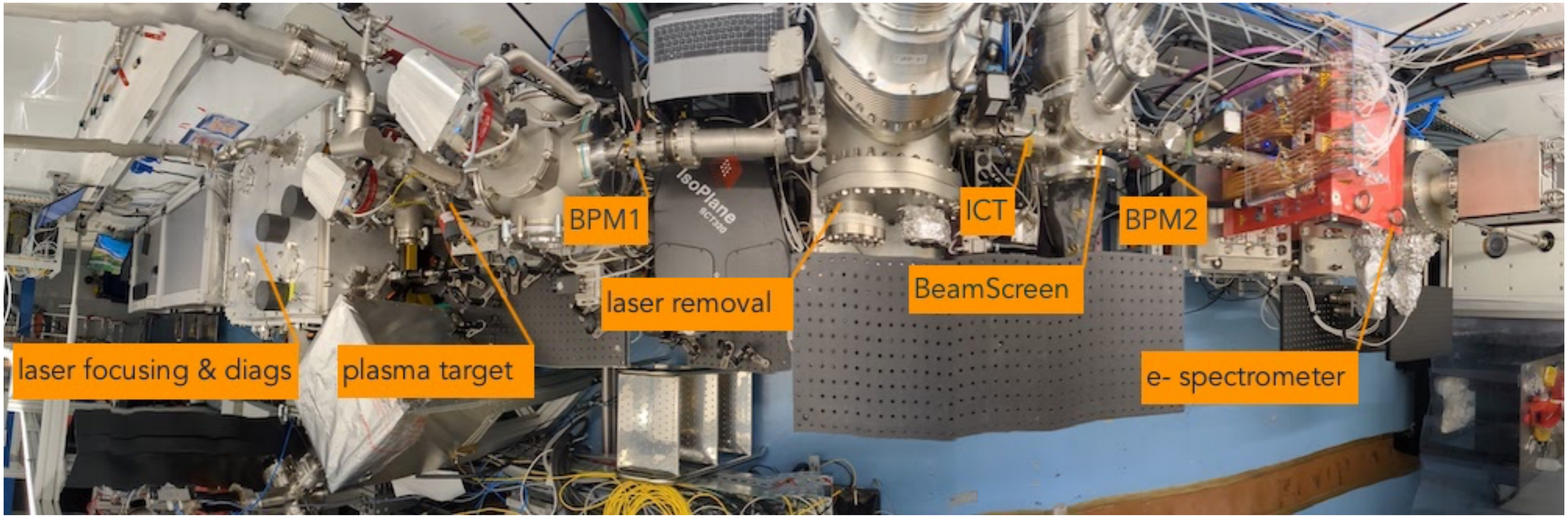

The Team